UCSF
UC San Francisco Electronic Theses and Dissertations

Title
Targeting MYCN in Pediatric Solid Tumors

Permalink
https://escholarship.org/uc/item/4155s2hz

Author
Meyerowitz, Justin Gabriel

Publication Date
2014

Peer reviewed|Thesis/dissertation

Targeting MYCN in Pediatric Solid Tumors

by

Justin Gabriel Meyerowitz

DISSERTATION

Submitted in partial satisfaction of the requirements for the degree of

DOCTOR OF PHILOSOPHY

in

Chemistry and Chemical Biology

in the

GRADUATE DIVISION

of the

UNIVERSITY OF CALIFORNIA, SAN FRANCISCO

Acknowledgments

When I look back at my experience through graduate school, it's hard to believe that I only started at UCSF 5 years ago—not because it has felt like a long time, but because I feel that I've learned and changed so much more than I ever would have expected. To this I owe the incredible people—mentors, teachers, colleagues—from whom I've learned. At the top of the list are my two co-mentors, Bill Weiss and Kevan Shokat. Their guidance regarding the science as well as grant-writing, getting through administrative red tape, interacting with editors and reviewers, and all of the other non-science things that seem to take up more time than the science, has transformed me over the last few years and prepared me well for the next steps of my career. I would also like to thank Natalia Jura, whose enthusiasm, insight and suggestions always made me look forward to thesis committee meetings.

This project happened because of the suggestion of Clay Gustafson, on a fateful shuttle ride on my way to the first day of my Shokat lab rotation. Since then, Clay has been an important mentor, role model, colleague, and friend. Working closely on this project with Clay has been the best part of graduate school for so many reasons. Among those is the fact that I could talk about this project every single day with someone who cares exactly as much about it as I do. To top it off, Clay is truly a great guy to work with. Also critical to this project has been Erin Nekritz, a great friend as well as colleague, and I have been lucky to work with someone as passionate about this project as her. I would also like to thank Nicole Nasholm, the newest member of Team Aurora, as well as the crucial lab managers of the Weiss and Shokat labs—past and present—Elise Charron, Robyn Wong, and Lauren McHenry; Delaney Lynch and Valerie Ohman. Valerie, you are missed. I would also like to thank the MSTP leadership, including Kevin Shannon, Jana Toutolmin, and Catherine Norton. UCSF is an incredible institution, and as such is built on a foundation of incredible individuals—as a consequence, I've had quite a few mentors, teachers, and role models here, including Kevin Shannon, Davide Ruggero, Martin McMahon, Daphne

Chapter-specific contributions

Chapter 1

Portions of the neuroblastoma and medulloblastoma sections of this chapter were published in *Nature Reviews Cancer* March 6, 2014 in an article entitled "The prenatal origins of cancer" co-authored with Marshall GM, Carter DR, Cheung BB, Liu T, Mateos MK, and Weiss WA. Figure 1.2 was conceptualized by co-authors Cheung and Carter. *MYC* and *MYCN* mRNA expression levels and histological classifications in Figure 1.4 were published in Swartling *et al.*, 2010; transcriptomal subgroup matching was later performed by the MD Taylor lab. Illustration of MYC-MAX-DNA complex on first page was drawn using PyMOL 1.5.0 and PDB entry 1NKP.

Chapter 2

At the time of this writing, this chapter is currently undergoing revisions at a peer-reviewed journal. This chapter is co-authored with W. Clay Gustafson, Erin A. Nekritz, Justin Chen, Cyril Benes, Elise Charron, Erin F. Simonds, Robert Seeger, Katherine Matthay, Nicholas T. Hertz, Martin Eilers, Kevan M. Shokat, and William A. Weiss. Clay Gustafson contributed equally to this work—he was the first to start on this project, guided its direction, and performed many experiments, particularly the earlier immunoblots and some of the *in vivo* data. Erin Nekritz is another main contributor in this project, as she performed a large number of the western blots and virtually all of the flow cytometry and has been invested and actively involved in this project from its conception. Justin Chen performed the quantitative analysis on the cell line profiling data (Figure 2.12). This cell line profiling data was generated by Cyril Benes as part of the Genomics of Drug Sensitivity Project at Massachusetts General Hospital. Elise Charron performed much of the cloning and other work critical to these experiments. Erin Simonds skillfully guided both design and analysis of flow cytometry. Nicholas Hertz synthesized, for a different project, some of the compounds in the initial screen, including CD532. And, of course, none of this would be possible without the incredible ideas and support of my mentors Bill Weiss and Kevan Shokat.

Chapter 3

Small selections of this chapter will be published in a book chapter focused on brain tumors in a book commissioned by Springer entitled Translation and Its Control in Cancer Biology and Medicine, edited by Armen Parsyan, MD, PhD, MPH and co-authored with Parsyan A and Weiss WA. Illustration of mTOR-mLST8 bound to ADP was drawn using PyMOL 1.5.0 and PDB entry 4JSV.

Abstract

Targeting MYCN in Pediatric Solid Tumors

MYC proteins are critical drivers of a wide range of cancers, and as transcription factors are generally considered undruggable. MYCN is the neuroblastoma-derived isoform of MYC and is a driving oncogene in neuroblastoma and medulloblastoma, two deadly solid tumors of childhood. Here we describe, in three chapters, (1) MYC proteins and their role in neuroblastoma and medulloblastoma, and (2, 3) two strategies for MYC-directed therapeutics using ATP-competitive small-molecule inhibitors of kinases.

This first strategy entails targeting MYCN for proteolysis through inhibition of Aurora Kinase A (Aurora A). MYCN is ubiquitinated and degraded by the proteasome, and Aurora A physically interacts with ubiquitinated MYCN to prevent its degradation. However, this MYCN-stabilizing function is completely independent of its kinase activity, as conventional Aurora A inhibitors have no effect on MYCN degradation. In chapter 2 we describe a new class of conformation-disrupting (CD) inhibitors of Aurora A that bind the ATP binding pocket and sufficiently alter the conformation of Aurora A as to prevent this physical interaction with ubiquitinated MYCN. This new class of compounds effects potent and rapid loss of MYCN protein in MYCN-expressing neuroblastoma and medulloblastoma, both in cell lines as well as *in vivo*, and reduces tumor burden and extends survival in an animal model. Furthermore, cell line profiling demonstrates that this new strategy for targeting MYCN is both a MYC- and MYCN-directed therapy, as MYC-like expression signature and MYC family overexpression predicts sensitivity to Aurora A conformation-disrupting inhibitors. These CD compounds represent a new strategy for targeting MYCN by way of inducing its degradation.

The second strategy for targeting MYCN, described in Chapter 3, is through the reliance of MYCN on mTOR signaling through 4EBP, the latter a main regulator of cap-dependent translation. 4EBP and c-MYC have been shown to cooperate in oncogenesis, through c-MYC

inhibition of the senescence induced by 4EBP and 4EBP inhibition of the apoptosis promoted by c-MYC. Here we show that rapamycin, an allosteric inhibitor of mTOR, blocks signaling through rpS6 but not 4EBP, whereas MLN0128, an ATP-competitive inhibitor of mTOR, blocks signaling through both rpS6 and 4EBP. Accordingly, in MYCN-driven medulloblastoma, MLN0128 but not rapamycin promotes apoptosis, and this apoptosis is consistent with loss of 4EBP phosphorylation but not loss of phosphorylation of other mTOR targets. We also show that the efficacy of mTOR kinase inhibitors is unrelated to any change in MYCN protein levels, and that MLN0128 can reduce mTOR signaling in a mouse model of MYCN-driven medulloblastoma.

CONTENTS

CHAPTER 1   Background: MYCN in Pediatric Solid Tumors

CHAPTER 2   Drugging MYCN Through an Allosteric Transition in Aurora Kinase

CHAPTER 3   Targeting the Translational Apparatus in MYCN-driven Medulloblastoma

List of Figures

Chapter 1

Chapter 2

Chapter 3

List of Tables

Chapter 2

Chapter 1

MYCN in Pediatric Solid Tumors

1.1   The MYCN transcription factor

MYCN was initially identified as a gene amplified in neuroblastoma that was homologous yet distinct from *MYC*.[1,2] It has since been implicated in retinoblastoma,[1,3-5] small cell lung carcinoma,[6] medulloblastoma,[7-9] Wilm's tumor,[7] and neuroendocrine prostate cancer.[10] The cellular-myelocytomatosis (c-MYC, or MYC) protein and the closely related neuroblastoma-derived MYC (MYCN human, NMYC mouse) are basic helix-loop-helix leucine zipper transcription factors that have long been of the most important oncoproteins across cancers. They localize to the nucleus and form heterodimers with the protein Max, which binds to DNA at specific "E-box" sequences to drive transcription of targets important for proliferation.[11,12] Consistent with their highly homologous coding regions and structures, MYC and MYCN proteins both heterodimerize with MAX to bind to E-box sequences (CANNTG) (reviewed in [13]).

MYC also heterodimerizes with MIZ1 to effect trans-repression; however, much less is known about the role of MYCN in trans-repression.[14,15]

There is a fair amount of developmental redundancy between MYC and MYCN. *MYCN* can compensate for knockout of *MYC*, and loss of either *MYC* or *MYCN* is embryonic lethal at E10.5-11.5.[16-18] Homozygous deletion of either *MYC* or *MYCN* in mouse embryonic fibroblasts does not interfere with normal proliferation, morphology, or differentiation, suggesting that MYC and MYCN can compensate for each other.[19,20]

Despite these similarities between MYC and MYCN, their functional differences in both normal development and tumorigenesis are clear. Given the similarity between MYC and MYCN in their DNA-binding and heterodimerization domains, these functional differences likely arise from distinct spatiotemporal expression patterns and their divergent regulation at transcriptional, translational, and post-translational levels. Expression of *MYC* is fairly ubiquitous and is detected in a broad spectrum of tissues in newborn mice, and is persistent in adrenal and thymic tissue of adult mice. In contrast, *MYCN* is expressed in the forebrain, kidney, and hindbrain of newborn mice and is virtually absent in the adult mouse.[21] In the cerebellum, conditional deletion of *MYCN* in neural stem and progenitor cells reduce proliferation of granule neural precursors (GNPs), whereas this effect is not seen with deletion of *MYC*.[22] Although constitutional and brain-specific deletion of MYCN causes embryonic lethality and cerebellar hypoplasia, respectively,[16,23] expression of MYCN in adult animals is restricted to a subset of lymphocytes.[21,24,25]

While both *MYC* and *MYCN* possess an internal ribosome entry sites (IRES) in their 5' untranslated regions, their substantially different sequences allow the *MYCN* IRES to possess ~7-fold greater activity than that of *MYC*.[26] Further emphasizing their differences in translational regulation, the *MYCN* IRES requires components of the translational initiation machinery that are distinct from those of the *MYC* IRES.[27] Furthermore, oncogenic Ras signaling promotes MYC accumulation by slowing its degradation; in contrast, H-Ras^{G12V} promotes accumulation of MYCN by increasing its translation despite also increasing its degradation.[28]

Our understanding of the post-translational regulation of the *MYC* family of oncogenes is primarily through studies of MYC, although several differences between MYC and MYCN have been described in this context. One mechanism of MYC degradation requires sequential phosphorylation and dephosphorylation of two residues, T58 and S62, in the MYC homology box I domain (Figure 1.1; reviewed in [29]). MYC is transiently stabilized by phosphorylation at S62 by extracellular signal-regulated kinase (ERK). When growth factor signals diminish, activation of glycogen synthase kinase-3β recognizes phosphorylated S62 as a priming site for subsequent phosphorylation of T58.[30] This doubly phosphorylated MYC is recognized by the peptidylprolyl isomerase Pin1 and protein phosphatase 2A, which direct dephosphorylation of S62. Finally, MYC protein that is singly phosphorylated at T58 is targeted for ubiquitination and proteasomal-mediated degradation by the E3 ubiquitin ligase Fbw7.[31,32]
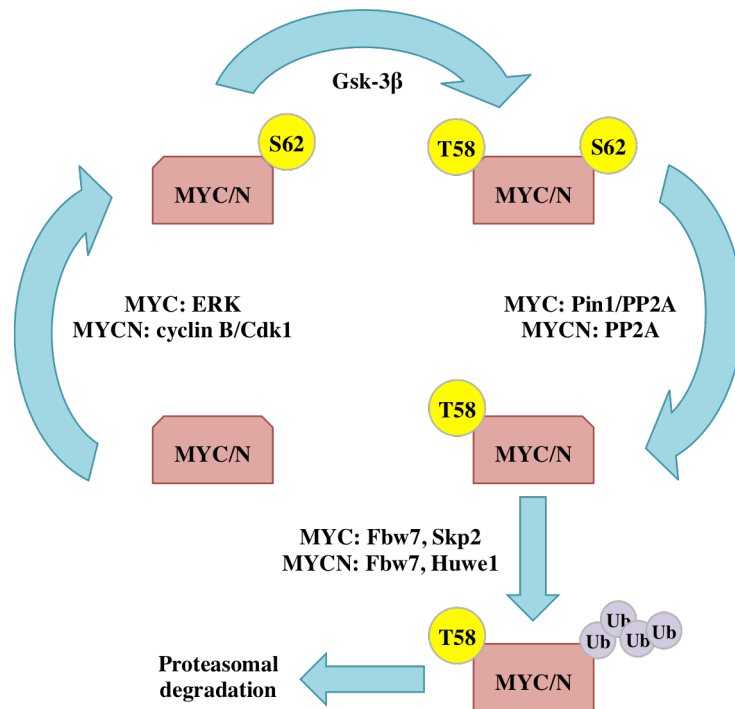
Figure 1.1: MYC and MYCN undergo a series of phosphorylation and dephosphorylation events before ubiquitination and proteasomal degradation. MYC and MYCN are phosphorylated at S62 by ERK and cyclin B/Cdk1 complex, respectively, before additional phosphorylation at T58 by Gsk-3β. Dephosphorylation of S62 by PP2A then primes MYC/MYCN for ubiquitination by E3 ubiquitin ligases Fbw7, Skp2, or Huwe1. MYC/N – MYC or MYCN; ERK – extracellular signal-regulated kinase; Gsk-3β – glycogen synthase kinase-3β; PP2A – protein phosphatase 2A; Ub – ubiquitin.

While our understanding of the mechanisms of phosphorylation, ubiquitination, and degradation of MYCN is incomplete, some key differences between MYC and MYCN are clear (reviewed in [33]). For example, while the mitotic cyclin B/Cdk1 complex phosphorylates S62 in MYCN, a modification critical for ubiquitination of both MYC and MYCN, MAP kinases are responsible for phosphorylation of S62 in MYC.[34,35] In addition, Fbw7-dependent degradation of MYCN does not require Pin1 despite phosphodegron that is identical to that of MYC.[34] The mechanistic complexity in the differences between MYC and MYCN is further emphasized by the activity of an additional ubiquitin ligase, Huwe1, which polyubiquitinates MYC via lysine 63 to enhance transcriptional activity of MYC without influencing protein turnover.[36] In contrast, Huwe1 polyubiquitination of MYCN at lysine 48 catalyzes MYCN turnover.[37] Another ubiquitin ligase implicated in MYC turnover is Skp2, which enhances MYC transcriptional activity in addition to participating in its ubiquitination and degradation.[38,39]

The wide range of MYC and MYCN transcriptional targets (cell cycle control, differentiation, multidrug resistance, and ribosome biogenesis, as well as oncogenic mRNAs) speaks to their critical role in oncogenesis.[40-43] This also speaks to the intractability of drugging downstream of MYC family proteins, particularly in light of recent evidence supporting the idea of MYC as a universal amplifier of expressed genes rather than a conventional target-specific transcription factor.[44,45] Despite this centrality of MYC in the pathogenesis of cancer, there are as yet no therapeutic approaches to modulating MYC function available to clinical oncologists. To date, the only small molecules targeting MYC are low in potency,[46-48] possess structural features at odds with medicinal chemistry,[49] and consequently lack drug-like properties to support in vivo studies in pre-clinical models.[50] Identification and characterization of small-molecule modulators of MYC function remains, therefore, a longstanding and central challenge in cancer biology and experimental therapeutics.

1.2 Origins and pathogenesis of neuroblastoma

Neuroblastoma is the most common cancer in infants and the third most common pediatric cancer overall, with 90% of cases diagnosed by age 5. The primary tumor is most frequently located in the adrenal medulla, paraspinal ganglia, or other tissues originating from the sympathetic nervous system, consistent with its neural crest origin. Almost half of all patients present with high-risk disease and have poor five-year event-free survival, characterized by relapse and death. In addition, children who survive are at significant risk for debilitating long-term toxicities as a consequence of receiving dose-intensive therapy at a young age.[51] It is therefore important to identify novel therapeutic approaches based on the biology of neuroblastoma in order to improve survival for patients, while decreasing the potential for additional toxicity.[52]

Neuroblastoma is a tumor of development that arises from a transient population of multipotent cells known as neural crest cells, which give rise to the extracranial nervous system as well as melanocytes, smooth muscle, and adrenal glands. Sympathoadrenal cells from the neural crest in the trunk region of the embryo follow a ventral migratory pathway from the neural crest and neural tube, receiving signals from somites, ventral neural tube, notochord and dorsal aorta.[53] During normal sympathoadrenal development, expression of the proto-oncogene *MYCN* is high in the early post-migratory neural crest where it regulates the ventral migration and expansion of neural crest cells.[21] MYCN protein levels gradually reduce in differentiating sympathetic neurons, suggesting that sympathoadrenal maturation requires low or absent MYCN expression.[21,54,55] Consistent with this finding is the observation that *MYCN* transduction into quiescent rat sympathetic neurons reactivates cell cycling and blocks cell death induced by nerve growth factor (NGF) withdrawal.[54,55]

After sympathoadrenal specification and expansion of the primary sympathetic ganglia, sympathoadrenal precursor development diverges into neuronal or chromaffin cell fates.[53] Based

on expression patterns of differentiation markers, the earliest cell of origin for neuroblastoma is thought to be a neural crest cell specified to the sympathoadrenal lineage, which has not received or responded to cues that determine neuronal or chromaffin cell fate (Figure 1.2). Excess neural precursors undergo apoptotic cell death at the final stage of sympathoadrenal maturation, a process catalysed by local NGF deprivation.[56] In zebrafish, persistent MYCN expression in sympathoadrenal precursor cells dramatically blocks development toward a chromaffin cell fate, leading to neuroblastoma.[57] Overexpression of human MYCN under the control of the rat tyrosine hydroxylase (*Th*) promoter in *Th-MYCN* transgenic mice is sufficient to recapitulate neuroblastoma rest disease (discussed in humans below) and tumorigenesis.[54,58-60] Transformation from a rest cell to a malignant neuroblast in *Th-MYCN* mice requires even higher levels of MYCN than are provided by the transgene. This can occur via transgene amplification and feed forward loops between MYCN and increased levels of NAD-dependent deacetylases, sirtuins 1 and 2, which increase MYCN stability. [60,61]

ALK has a key role in early sympathoadrenal development to protect neuroblast growth in utero against nutrient deprivation.[62,63] Germline and somatic mutations in *ALK* causing constitutive kinase activation are present in 8-10% of neuroblastoma cases and correlate with poor prognosis.[64-67] The most common and aggressive activating mutation of ALK, F1174L, is sufficient for tumor formation on neural crest-specific expression in transgenic mice[68] and on expression in neural crest cells transplanted into nude mice.[69] ALK-F1174L has been associated with *MYCN* amplification in human tumors and co-expression of ALK-F1174L and MYCN synergistically promotes tumor formation *in vivo* suggesting these may be co-operating events in tumor initiation.[68]

Risk in neuroblastoma correlates with age, extent of disease, unfavorable pathology and amplification of *MYCN*, the best-characterized single-gene alteration linked to aggressive tumor formation. Occurring in one third of high-risk neuroblastomas, amplification of *MYCN* is also

independently predictive of death from progression.[70-73] The fundamental roles played by MYCN in tumor biology, the restricted pattern of expression after embryogenesis, the fact that amplification of MYCN in high-risk patients represents a common and unique marker present at diagnosis and throughout the evolution of these tumors, and the failure of genome-wide sequencing efforts to identify additional targets mutated at over 5% frequency in this disease,[74-77] position MYCN as among the most attractive therapeutic targets for neuroblastoma.
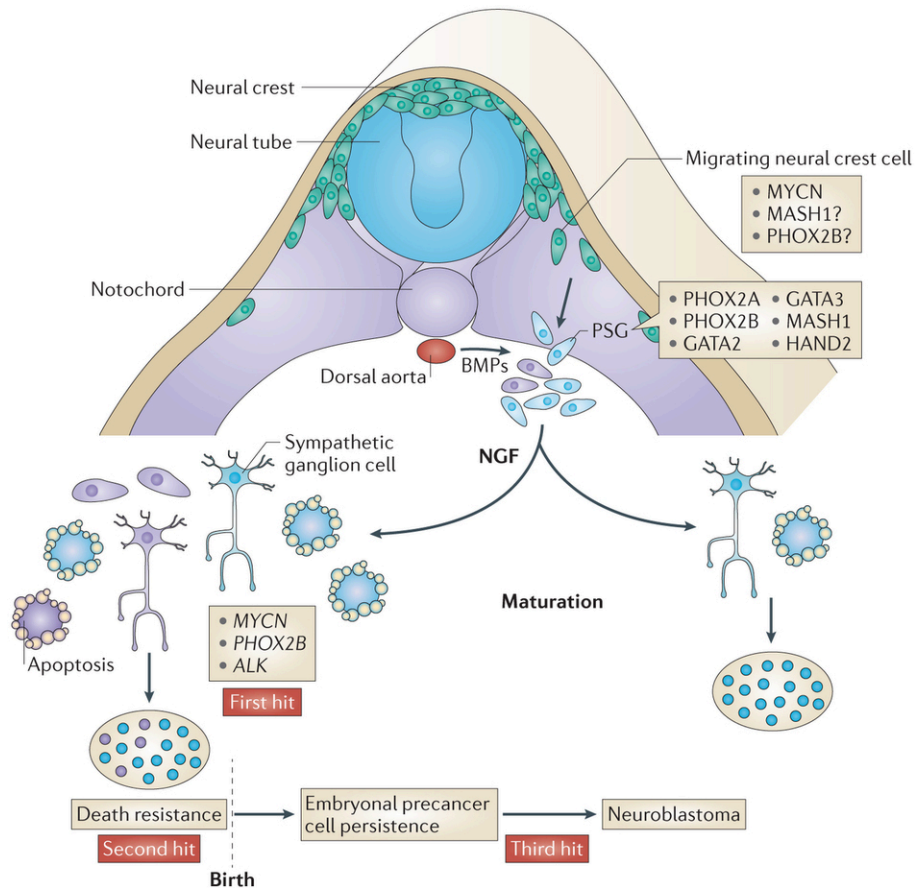
Figure 1.2: Neural crest development and the origins of neuroblastoma. Under the influence of MYCN and bone morphogenetic proteins (BMPs), neuroblast progenitors migrate from the neural crest to a region lateral to the notochord and dorsal aorta. At this site, the cells undergo specification as the primary sympathetic ganglia (PSG) before divergence into neural cells of the mature sympathetic ganglia or chromaffin cells (not shown). *MYCN* is a 'first hit', whereas mutations in anaplastic lymphoma kinase (*ALK*) and paired-like homeobox 2B (*PHOX2B*) are germline mutations. Local access to nerve growth factor (NGF) determines whether a normal sympathetic ganglion cell (blue) matures into a terminal ganglion cell or undergoes apoptotic cell death. A relatively common pathological state is postnatal survival of neuroblast precancer cells (purple). HAND2, heart and neural crest derivatives expressed 2; MASH1, murine achaete-scute homologue 1.

1.3   Origins and pathogenesis of medulloblastoma

Medulloblastoma arises from the developing cerebellum and adjoining structures, and is the most common malignant brain tumor of childhood. It represents four distinct disease entities: the sonic hedgehog (SHH) and wingless-related integration site (WNT) subgroups are named based on the predominant signaling pathway driving tumorigenesis, whereas group 3 and group 4 medulloblastoma exhibit a more pleiotropic etiology and do not have an easily identifiable oncogenic driver pathway.

The fully developed cerebellum comprises an outer cell-sparse cortical layer (molecular layer), a Purkinje cell layer (PCL), and an internal granular layer (IGL), the latter comprised of cerebellar granule cells (GCs) that form excitatory connections with Purkinje neurons (Figure 1.3).[78] Developmentally, the cerebellar anlage arises from the dorsal part of the anterior hindbrain, delineated by expression of the homeobox proteins orthodenticle homologue 2 (*OTX2*) anteriorly and *HOXA2* posteriorly.[79,80] *OTX2* is a candidate driver for some group 3 medulloblastomas as it is amplified in 20% of these tumors, and is frequently overexpressed in SHH-independent subgroups.[81] Expression of OTX2 is abundant in the developing brain and silenced in the adult brain. OTX2 has recently been shown to repress differentiation in medulloblastoma cells, suggesting that amplification of *OTX2* could generate a premalignant disease.[82] The observation that OTX2 also drives proliferation and can upregulate MYC, suggests that OTX2 might also be important in transforming premalignant cells into medulloblastoma.[81,83]

The first germinal centre of the developing cerebellum initiates along the fourth ventricle in the dorsomedial ventricular zone (VZ), and gives rise to Purkinje cells and several other types of cerebellar interneurons.[84] Neural tube closure forms the rhombic lip, the anterior portion of which provides a second germinal zone of rapidly proliferating cells that express radial glial markers and gives rise to protein atonal homologue 1 (or MATH1)-positive granule cell progenitors (GCPs).[85,86] From 24 to 40 weeks gestation in humans, the volume of the developing
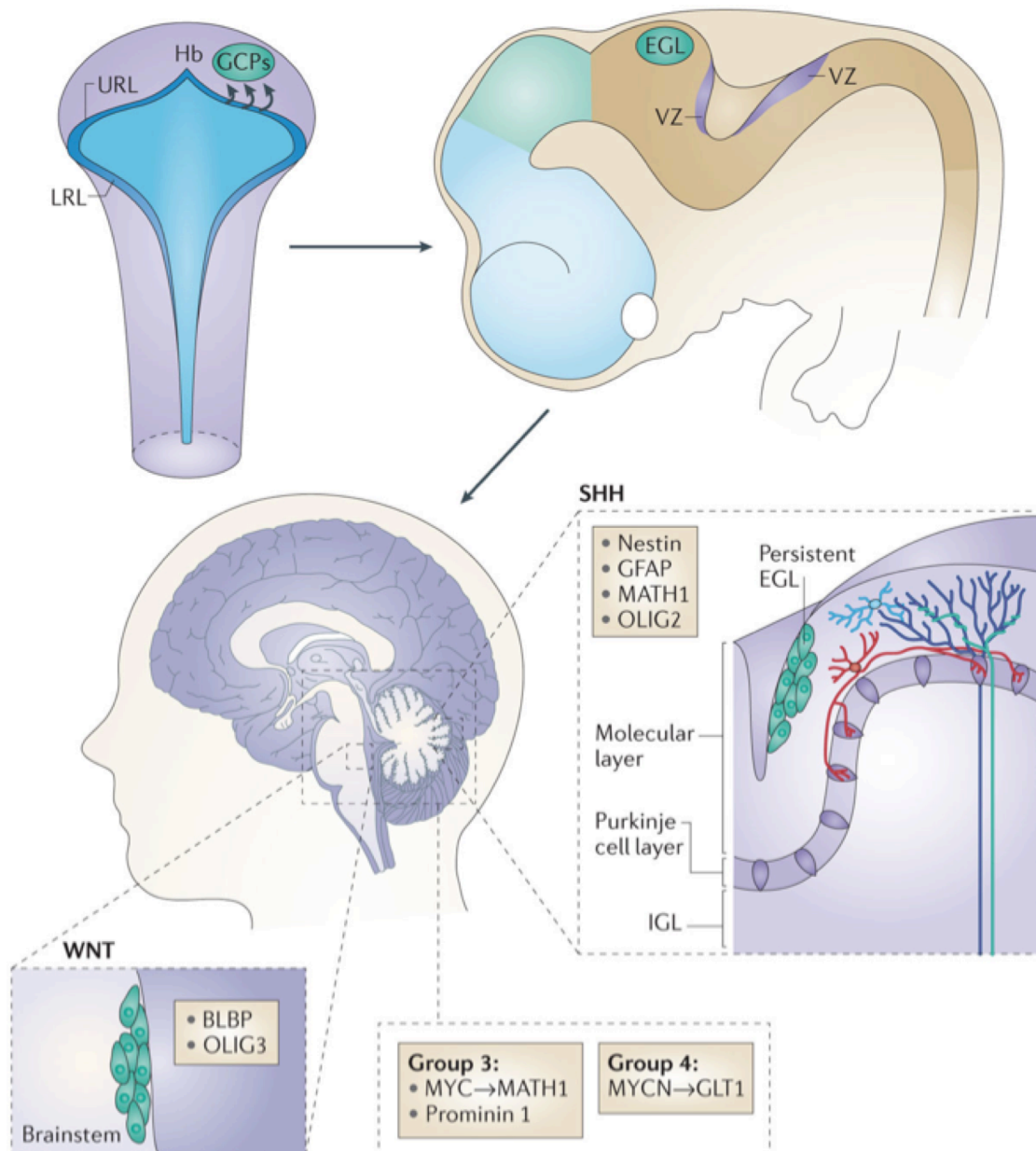
Figure 1.3: Cerebellar development and the origins of medulloblastoma. The upper (anterior) rhombic lip (URL) is a germinal zone of proliferating granule cell precursors (GCPs) that migrate rostrally to form the external granular layer (EGL). A second germinal centre is the ventricular zone (VZ), which gives rise to Purkinje cells and several other types of cerebellar interneurons. Sonic hedgehog (SHH) medulloblastoma-subgroup tumours might arise from persistent cells of the EGL that have not migrated to the internal granular layer (IGL), whereas WNT-subgroup tumours probably originate from the lower rhombic lip (LRL) and embryonic dorsal brainstem. Group 3 and 4 medulloblastomas might arise from neural stem cells of the hindbrain or the brainstem. Beige boxes indicate the identity of the originating cell in mouse models. *MYC* and *MYCN* are driving oncogenes for group 3 and group 4 tumour models, respectively. GFAP, glial fibrillary acidic protein; Hb, hindbrain; Mb, midbrain; OLIG, oligodendrocyte transcription factor.

9

cerebellum enlarges 5-fold, corresponding to more than a 30-fold increase in cerebellar cortex surface area.[87,88] This expansion is largely imparted by the rapid proliferation of GCPs that give rise to cerebellar GCs and almost all cerebellar cortical neurons.[84,89] Proliferation of these neuronal progenitors depends on SHH produced by Purkinje neurons: inhibiting SHH signalling blocks the proliferation and migration of GCPs.[90] GCPs migrate rostrally along the surface of the developing cerebellum to form the external granule layer (EGL), where they continue to divide and eventually migrate inward to form the IGL, with consequent depletion of the EGL.[91,92] This process of GCP maturation and concurrent spontaneous cell death of excess GCPs is complete by the postnatal age of 20 months in children.[93]

The connection between SHH signaling and medulloblastoma was initially made in the context of Gorlin syndrome, an autosomal dominant disorder that causes developmental defects and predisposes individuals to several cancers, including medulloblastoma.[94] Fine mapping revealed the putative gene to be highly homologous to the Drosophila gene *Patched* (*PTCH1*).[95] Loss of chromosome 9q, which contains *PTCH1*, occurs in ~30% of all SHH tumors.[96] The PTCH1 protein is an essential negative regulator of SHH signaling, thus mice heterozygous for *Ptch1* develop cerebellar medulloblastoma.[97] Other germline mutations that predispose children to SHH medulloblastoma occur due to loss-of-function mutation in Suppressor of fused homolog (*SUFU*), a negative regulator of the SHH signaling.[98] Amplification of GLI family zinc finger 2 (*GLI2*), a positive regulator of the SHH signal, is also implicated in medulloblastoma development.[99] In a mouse model of SHH-induced medulloblastoma, tumor formation was preceded by GCP hyperplasia in the first week of life which regressed before later emerging as a malignant tumor.[100] However, in vivo labeling studies following a rest cell to tumor transformation have not yet been performed in either model. *In vitro*, the murine GCPs were resistant to SHH withdrawal and this feature was partially MYCN-dependent.[100] Neural stem cells

(NSCs) and GCPs have repeatedly been shown to be the cell of origin for SHH medulloblastoma.[101-105]

WNT signaling has many roles in neural development and aberrant WNT signaling in NSCs of the cerebellar ventricular zone induces transient proliferation and impaired differentiation.[112] Individuals with Familiar Adenomatous Polyposis (FAP) and WNT pathway-driven colorectal cancer also have an increased risk of developing medulloblastoma.[113] Mutations that increase WNT signaling in members of the WNT signaling pathway have been described in sporadic medulloblastomas.[114-116] Recent data from the Medulloblastoma Advanced Genomics International Consortium showed that β-catenin (*CTNNB1*) displayed canonical exon 3 deletion in the vast majority (70-80%) of WNT-subgroup medulloblastoma.[99,115,117]

Insight into the cell of origin for WNT medulloblastomas comes from two mouse models, both involving the conditional expression of degradation-resistant β-catenin under the control of fatty acid binding protein 7 (*Fabp7*; also known as *Blbp*) in the context of *Trp53* deletion (*Blbp-cre:Ctnnb1:Trp53*). The addition of MYC expression increased penetrance from 4% (*Trp53*$^{+/-}$) and 15% (*Trp53*$^{-/-}$) to 83%, suggesting that activation of β-catenin and WNT signaling alone are only weak oncogenic events.[118,119] These MYC-driven medulloblastomas were evident in young mice and were formed from BLBP$^+$, OLIG3$^+$ mossy-fibre neuron precursors that are present in the brainstem between E11.5 and E15.5, consistent with the radiological observation that WNT medulloblastomas are frequently located within the fourth ventricle and infiltrate the dorsal surface of the brainstem.[108,119,120] This observation was consistent with the model of OLIG3$^+$ neural precursors representing a brain stem premalignant disease preceding WNT medulloblastoma.

The pathogenesis of group 3 and group 4 medulloblastoma is less clear, yet they account for over 60% of all medulloblastoma cases.[121] Targeted inducible expression of MYCN to the postnatal cerebellum using the glial high affinity glutamate transporter (*Glt1*) promoter (*Glt1-tTA:TRE-MYCN-Luc,* or GTML mice) leads to tumors with a transcriptional profile of group 3

medulloblastoma.[108] GTML mice had a normal EGL, suggesting that group 3 medulloblastoma could originate from a cellular population that is distinct from SHH medulloblastoma. However, proliferating GCPs isolated from cyclin-dependent kinase inhibitor 2C (*Cdkn2c*)[-/-], *Trp53*^{-/-}, *Math1-GFP* mice generate group 3 medulloblastoma when transformed with MYC, but not MYCN.[109] Furthermore, group 3 tumors have been modeled through MYC transformation of postnatal cerebellar stem cells marked by the expression of prominin 1 (also known as CD133) and lack of neuronal or glial markers.[110] Thus, it appears that a single oncogene can give rise to multiple different medulloblastoma tumor subtypes, depending on the developmental age and anatomical origin of the transformed cell, indicating that susceptibility to medulloblastoma is highly dependent on embryonal site and stage.[122]
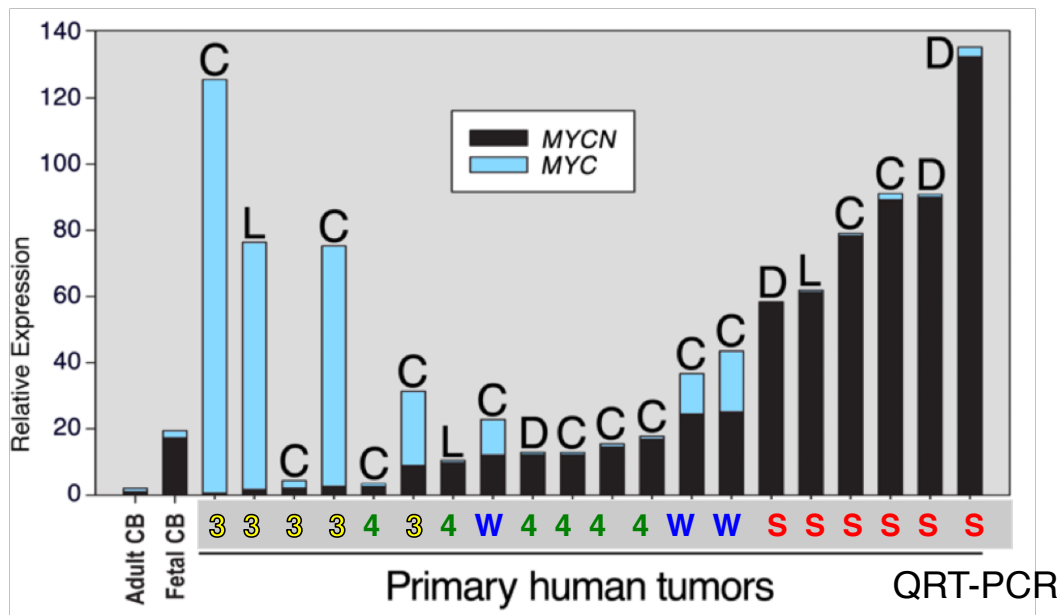
Figure 1.4: *MYC* and *MYCN* are expressed across all medulloblastoma subtypes. Expression of *MYC* or *MYCN* normalized to adult cerebellum (CB) with indications of medulloblastoma subtype and histological classification. W – Wnt, S – SHH, 3 – Group 3, 4 – Group 4, C – Classic, L – Large cell/Anaplastic, D – Desmoplastic.

MYCN and its homologue *MYC* have crucial roles in all medulloblastoma subgroups. Brain-specific germline deletion of mouse *Mycn* results in cerebellar dysplasia.[23] Expression of

12

MYCN is essential for SHH medulloblastoma in mouse models[106] and amplification of *MYCN* marks a subset of poor-outcome SHH-driven human tumors.[107] Moreover, tumorigenic SHH signaling markedly increases MYCN expression in GCP cells due to effects on MYCN protein stability.[100] MYCN is also expressed in WNT and group 4 tumors, with targeted expression of MYCN or MYC driving SHH-independent medulloblastoma in transgenic mice.[108-110] Group 3 tumors express MYC and have amplification of *MYC* rather than *MYCN*.[111] Expression of *MYC* or *MYCN* mRNA is elevated across all subgroups and histological classes, although their expression is typically mutually exclusive (Figure 1.4).

1.4 Chapter 1 References

(1)   Kohl, N. E.; Kanda, N.; Schreck, R. R.; Bruns, G.; Latt, S. A.; Gilbert, F.; Alt, F. W. Transposition and Amplification of Oncogene-Related Sequences in Human Neuroblastomas. *Cell* **1983**, *35*, 359–367.

(2)   Schwab, M.; Alitalo, K.; Klempnauer, K. H.; Varmus, H. E.; Bishop, J. M.; Gilbert, F.; Brodeur, G.; Goldstein, M.; Trent, J. Amplified DNA with Limited Homology to Myc Cellular Oncogene Is Shared by Human Neuroblastoma Cell Lines and a Neuroblastoma Tumour. *Nature* **1983**, *305*, 245–248.

(3)   Lee, W. H.; Murphree, A. L.; Benedict, W. F. Expression and Amplification of the N-Myc Gene in Primary Retinoblastoma. *Nature* **1984**, *309*, 458–460.

(4)   Kohl, N. E.; Gee, C. E.; Alt, F. W. Activated Expression of the N-Myc Gene in Human Neuroblastomas and Related Tumors. *Science* **1984**, *226*, 1335–1337.

(5)   Rushlow, D. E.; Mol, B. M.; Kennett, J. Y.; Yee, S.; Pajovic, S.; Thériault, B. L.; Prigoda-Lee, N. L.; Spencer, C.; Dimaras, H.; Corson, T. W.; et al. Characterisation of Retinoblastomas Without RB1 Mutations: Genomic, Gene Expression, and Clinical Studies. *The Lancet Oncology* **2013**, *14*, 327–334.

(6)   Nau, M. M.; Brooks, B. J.; Carney, D. N.; Gazdar, A. F.; Battey, J. F.; Sausville, E. A.; Minna, J. D. Human Small-Cell Lung Cancers Show Amplification and Expression of the N-Myc Gene. *Proceedings of the National Academy of Sciences of the United States of America* **1986**, *83*, 1092–1096.

(7)   Nisen, P. D.; Zimmerman, K. A.; Cotter, S. V.; Gilbert, F.; Alt, F. W. Enhanced Expression of the N-Myc Gene in Wilms' Tumors. *Cancer Res* **1986**, *46*, 6217–6222.

(8)   Aldosari, N.; Bigner, S. H.; Burger, P. C.; Becker, L.; Kepner, J. L.; Friedman, H. S.; McLendon, R. E. MYCC and MYCN Oncogene Amplification in Medulloblastoma. *archivesofpathology.org*.

(9)   Frühwald, M. C.; O'Dorisio, M. S.; Rush, L. J.; Reiter, J. L.; Smiraglia, D. J.; Wenger, G.; Costello, J. F.; White, P. S.; Krahe, R.; Brodeur, G. M.; et al. Gene Amplification in PNETs/Medulloblastomas: Mapping of a Novel Amplified Gene Within the MYCN Amplicon. *J. Med. Genet.* **2000**, *37*, 501–509.

(10)   Mosquera, J. M.; Beltran, H.; Park, K.; MacDonald, T. Y.; Robinson, B. D.; Tagawa, S. T.; Perner, S.; Bismar, T.; Erbersdobler, A.; Dhir, R.; et al. Concurrent AURKA and MYCN Gene Amplifications Are Harbingers of Lethal Treatment-Related Neuroendocrine Prostate Cancer. *Neoplasia* **2013**, *15*, 1.

(11)   Blackwell, T. K.; Kretzner, L.; Blackwood, E. M.; Eisenman, R. N.; Weintraub, H. Sequence-Specific DNA Binding by the C-Myc Protein. *Science* **1990**, *250*, 1149–1151.

(12)   Blackwood, E. M.; Eisenman, R. N. Max: a Helix-Loop-Helix Zipper Protein That Forms a Sequence-Specific DNA-Binding Complex with Myc. *Science* **1991**, *251*, 1211–1217.

(13)   Huang, M.; Weiss, W. A. Neuroblastoma and MYCN. *Cold Spring Harb Perspect Med* **2013**, *3*, a014415.

(14)   Iraci, N.; Diolaiti, D.; Papa, A.; Porro, A.; Valli, E.; Gherardi, S.; Herold, S.; Eilers, M.; Bernardoni, R.; Valle, Della, G.; et al. A SP1/MIZ1/MYCN Repression Complex Recruits HDAC1 at the TRKA and p75NTR Promoters and Affects Neuroblastoma Malignancy by Inhibiting the Cell Response to NGF. *Cancer Res* **2011**, *71*, 404–412.

(15)   Akter, J.; Takatori, A.; Hossain, M. S.; Ozaki, T.; Nakazawa, A.; Ohira, M.; Suenaga, Y.; Nakagawara, A. Expression of NLRR3 Orphan Receptor Gene Is Negatively Regulated by MYCN and Miz-1, and Its Downregulation Is Associated with Unfavorable Outcome in Neuroblastoma. *Clin Cancer Res* **2011**, *17*, 6681–6692.

(16)   Charron, J.; Malynn, B. A.; Fisher, P.; Stewart, V.; Jeannotte, L.; Goff, S. P.; Robertson, E. J.; Alt, F. W. Embryonic Lethality in Mice Homozygous for a Targeted Disruption of the N-Myc Gene. *Genes Dev* **1992**, *6*, 2248–2257.

(17)   Sawai, S.; Shimono, A.; Wakamatsu, Y.; Palmes, C.; Hanaoka, K.; Kondoh, H. Defects of Embryonic Organogenesis Resulting From Targeted Disruption of the N-Myc Gene in the Mouse. … **1993**.

(18)   Davis, A. C.; Wims, M.; Spotts, G. D.; Hann, S. R.; Bradley, A. A Null C-Myc Mutation Causes Lethality Before 10.5 Days of Gestation in Homozygotes and Reduced Fertility in Heterozygous Female Mice. *Genes Dev* **1993**, *7*, 671–682.

(19)   Yancopoulos, G. D.; Nisen, P. D.; Tesfaye, A.; Kohl, N. E.; Goldfarb, M. P.; Alt, F. W. N-Myc Can Cooperate with Ras to Transform Normal Cells in Culture. *Proceedings of the …* **1985**.

(20)   Schwab, M.; Varmus, H. E.; Bishop, J. M. Human N-Myc Gene Contributes to Neoplastic Transformation of Mammalian Cells in Culture. *Nature* **1985**, *316*, 160–162.

(21)   Zimmerman, K. A.; Yancopoulos, G. D.; Collum, R. G.; Smith, R. K.; Kohl, N. E.; Denis, K. A.; Nau, M. M.; Witte, O. N.; Toran-Allerand, D.; Gee, C. E. Differential Expression of Myc Family Genes During Murine Development. *Nature* **1986**, *319*, 780–783.

(22)   Hatton, B. A.; Knoepfler, P. S.; Kenney, A. M.; Rowitch, D. H.; de Albarán, I. M.; Olson, J. M.; Eisenman, R. N. N-Myc Is an Essential Downstream Effector of Shh Signaling During Both Normal and Neoplastic Cerebellar Growth. *Cancer Res* **2006**, *66*, 8655–8661.

(23)   Knoepfler, P. S.; Cheng, P. F.; Eisenman, R. N. N-Myc Is Essential During Neurogenesis for the Rapid Expansion of Progenitor Cell Populations and the Inhibition of Neuronal Differentiation. *Genes Dev* **2002**, *16*, 2699–2712.

(24)   Semsei, I.; Ma, S. Y.; Cutler, R. G. Tissue and Age Specific Expression of the Myc Proto-Oncogene Family Throughout the Life Span of the C57BL/6J Mouse Strain. *Oncogene* **1989**, *4*, 465–471.

(25)   Stanton, B. R.; Parada, L. F. The N-Myc Proto-Oncogene: Developmental Expression and in Vivo Site-Directed Mutagenesis. *Brain Pathol* **1992**, *2*, 71–83.

(26)   Jopling, C. L.; Willis, A. E. N-Myc Translation Is Initiated via an Internal Ribosome Entry Segment That Displays Enhanced Activity in Neuronal Cells. *Oncogene* **2001**, *20*, 2664–2670.

(27)   Spriggs, K. A.; Cobbold, L. C.; Jopling, C. L.; Cooper, R. E.; Wilson, L. A.; Stoneley, M.; Coldwell, M. J.; Poncet, D.; Shen, Y. C.; Morley, S. J.; et al. Canonical Initiation Factor Requirements of the Myc Family of Internal Ribosome Entry Segments. *Mol Cell Biol* **2009**, *29*, 1565–1574.

(28)   Kapeli, K.; Hurlin, P. J. Differential Regulation of N-Myc and C-Myc Synthesis, Degradation, and Transcriptional Activity by the Ras/Mitogen-Activated Protein Kinase Pathway. *J Biol Chem* **2011**, *286*, 38498–38508.

(29)   Sears, R. C. The Life Cycle of C-Myc: From Synthesis to Degradation. *Cell Cycle* **2004**, *3*, 1133–1137.

(30)   Yeh, E.; Cunningham, M.; Arnold, H.; Chasse, D.; Monteith, T.; Ivaldi, G.; Hahn, W. C.; Stukenberg, P. T.; Shenolikar, S.; Uchida, T.; et al. A Signalling Pathway Controlling C-Myc Degradation That Impacts Oncogenic Transformation of Human Cells. *Nat Cell Biol* **2004**, *6*, 308–318.

(31)   Yada, M.; Hatakeyama, S.; Kamura, T.; Nishiyama, M.; Tsunematsu, R.; Imaki, H.; Ishida, N.; Okumura, F.; Nakayama, K.; Nakayama, K. I. Phosphorylation-Dependent Degradation of C-Myc Is Mediated by the F-Box Protein Fbw7. *EMBO J* **2004**, *23*, 2116–2125.

(32)   Welcker, M.; Orian, A.; Jin, J.; Grim, J. E.; Grim, J. A.; Harper, J. W.; Eisenman, R. N.; Clurman, B. E. The Fbw7 Tumor Suppressor Regulates Glycogen Synthase Kinase 3 Phosphorylation-Dependent C-Myc Protein Degradation. *Proceedings of the National Academy of Sciences of the United States of America* **2004**, *101*, 9085–9090.

(33)   Müller, J.; Eilers, M. Ubiquitination of Myc: Proteasomal Degradation and Beyond. In *link.springer.com*; Ernst Schering Foundation Symposium Proceedings; Springer Berlin Heidelberg: Berlin, Heidelberg, 2008; Vol. 2008/1, pp. 99–113.

(34)   Sjostrom, S. K.; Finn, G.; Hahn, W. C.; Rowitch, D. H.; Kenney, A. M. The Cdk1 Complex Plays a Prime Role in Regulating N-Myc Phosphorylation and Turnover in Neural Precursors. *Dev. Cell* **2005**, *9*, 327–338.

(35)   Benassi, B.; Fanciulli, M.; Fiorentino, F.; Porrello, A.; Chiorino, G.; Loda, M.; Zupi, G.; Biroccio, A. C-Myc Phosphorylation Is Required for Cellular Response to Oxidative Stress. *Molecular Cell* **2006**, *21*, 509–519.

(36)   Adhikary, S.; Marinoni, F.; Hock, A.; Hulleman, E.; Popov, N.; Beier, R.; Bernard, S.; Quarto, M.; Capra, M.; Goettig, S.; et al. The Ubiquitin Ligase HectH9 Regulates Transcriptional Activation by Myc and Is Essential for Tumor Cell Proliferation. *Cell* **2005**, *123*, 409–421.

(37)   Zhao, X.; Heng, J. I.-T.; Guardavaccaro, D.; Jiang, R.; Pagano, M.; Guillemot, F.; Iavarone, A.; Lasorella, A. The HECT-Domain Ubiquitin Ligase Huwe1 Controls Neural Differentiation and Proliferation by Destabilizing the N-Myc Oncoprotein. *Nat Cell Biol* **2008**, *10*, 643–653.

(38)   Kim, S. Y.; Herbst, A.; Tworkowski, K. A.; Salghetti, S. E.; Tansey, W. P. Skp2 Regulates Myc Protein Stability and Activity. *Molecular Cell* **2003**, *11*, 1177–1188.

(39)   Lehr, von der, N.; Johansson, S.; Wu, S.; Bahram, F.; Castell, A.; Cetinkaya, C.; Hydbring, P.; Weidung, I.; Nakayama, K.; Nakayama, K. I.; et al. The F-Box Protein Skp2 Participates in C-Myc Proteosomal Degradation and Acts as a Cofactor for C-Myc-Regulated Transcription. *Molecular Cell* **2003**, *11*, 1189–1200.

(40)   Manohar, C. F.; Bray, J. A.; Salwen, H. R.; Madafiglio, J.; Cheng, A.; Flemming, C.; Marshall, G. M.; Norris, M. D.; Haber, M.; Cohn, S. L. MYCN-Mediated Regulation of the MRP1 Promoter in Human Neuroblastoma. *Oncogene* **2004**, *23*, 753–762.

(41)   Bell, E.; Lunec, J.; Tweddle, D. A. Cell Cycle Regulation Targets of MYCN Identified by Gene Expression Microarrays. *Cell Cycle* **2007**, *6*, 1249–1256.

(42)   Berwanger, B.; Hartmann, O.; Bergmann, E.; Bernard, S.; Nielsen, D.; Krause, M.; Kartal, A.; Flynn, D.; Wiedemeyer, R.; Schwab, M.; et al. Loss of a FYN-Regulated Differentiation and Growth Arrest Pathway in Advanced Stage Neuroblastoma. *Cancer Cell* **2002**, *2*, 377–386.

(43)   Gustafson, W. C.; Weiss, W. A. Myc Proteins as Therapeutic Targets. *Oncogene* **2010**, *29*, 1249–1259.

(44)   Nie, Z.; Hu, G.; Wei, G.; Cui, K.; Yamane, A.; Resch, W.; Wang, R.; Green, D. R.; Tessarollo, L.; Casellas, R.; et al. C-Myc Is a Universal Amplifier of Expressed Genes in Lymphocytes and Embryonic Stem Cells. **2012**, *151*, 68–79.

(45)   Lin, C. Y.; Lovén, J.; Rahl, P. B.; Paranal, R. M.; Burge, C. B.; Bradner, J. E.; Lee, T. I.; Young, R. A. Transcriptional Amplification in Tumor Cells with Elevated C-Myc. *Cell* **2012**, *151*, 56–67.

(46)   Hammoudeh, D. I.; Follis, A. V.; Prochownik, E. V.; Metallo, S. J. Multiple Independent Binding Sites for Small-Molecule Inhibitors on the Oncoprotein C-Myc. *J Am Chem Soc* **2009**, *131*, 7390–7401.

(47)   Wang, H.; Hammoudeh, D. I.; Follis, A. V.; Reese, B. E.; Lazo, J. S.; Metallo, S. J.; Prochownik, E. V. Improved Low Molecular Weight Myc-Max Inhibitors. *Molecular cancer therapeutics* **2007**, *6*, 2399–2408.

(48)   Yin, X.; Giap, C.; Lazo, J. S.; Prochownik, E. V. Low Molecular Weight Inhibitors of

Myc-Max Interaction and Function. *Oncogene* **2003**, *22*, 6151–6159.

(49)   Baell, J. B.; Holloway, G. A. New Substructure Filters for Removal of Pan Assay Interference Compounds (PAINS) From Screening Libraries and for Their Exclusion in Bioassays. *J Med Chem* **2010**, *53*, 2719–2740.

(50)   Clausen, D. M.; Guo, J.; Parise, R. A.; Beumer, J. H.; Egorin, M. J.; Lazo, J. S.; Prochownik, E. V.; Eiseman, J. L. In Vitro Cytotoxicity and in Vivo Efficacy, Pharmacokinetics, and Metabolism of 10074-G5, a Novel Small-Molecule Inhibitor of C-Myc/Max Dimerization. *J. Pharmacol. Exp. Ther.* **2010**, *335*, 715–727.

(51)   Maris, J. M. Recent Advances in Neuroblastoma. *N Engl J Med* **2010**, *362*, 2202–2211.

(52)   Modak, S.; Cheung, N.-K. V. Neuroblastoma: Therapeutic Strategies for a Clinical Enigma. *Cancer Treat. Rev.* **2010**, *36*, 307–317.

(53)   Huber, K. The Sympathoadrenal Cell Lineage: Specification, Diversification, and New Perspectives. *Dev. Biol.* **2006**, *298*, 335–343.

(54)   Hansford, L. M. Mechanisms of Embryonal Tumor Initiation: Distinct Roles for MycN Expression and MYCN Amplification. *Proceedings of the National Academy of Sciences* **2004**, *101*, 12664–12669.

(55)   Wartiovaara, K.; Barnabe-Heider, F.; Miller, F. D.; Kaplan, D. R. N-Myc Promotes Survival and Induces S-Phase Entry of Postmitotic Sympathetic Neurons. *J. Neurosci.* **2002**, *22*, 815–824.

(56)   Yuan, J.; Yankner, B. A. Apoptosis in the Nervous System. *Nature* **2000**, *407*, 802–809.

(57)   Zhu, S.; Lee, J.-S.; Guo, F.; Shin, J.; Perez-Atayde, A. R.; Kutok, J. L.; Rodig, S. J.; Neuberg, D. S.; Helman, D.; Feng, H.; et al. Activated ALK Collaborates with MYCN in Neuroblastoma Pathogenesis. *Cancer Cell* **2012**, *21*, 362–373.

(58)   Calao, M.; Sekyere, E. O.; Cui, H. J.; Cheung, B. B.; Thomas, W. D.; Keating, J.; Chen, J. B.; Raif, A.; Jankowski, K.; Davies, N. P.; et al. Direct Effects of Bmi1 on P53 Protein Stability Inactivates Oncoprotein Stress Responses in Embryonal Cancer Precursor Cells at Tumor Initiation. *Oncogene* **2013**, *32*, 3616–3626.

(59)   Weiss, W. A. Targeted Expression of MYCN Causes Neuroblastoma in Transgenic Mice. *EMBO J* **1997**, *16*, 2985–2995.

(60)   Marshall, G. M.; Liu, P. Y.; Gherardi, S.; Scarlett, C. J.; Bedalov, A.; Xu, N.; Iraci, N.; Valli, E.; Ling, D.; Thomas, W.; et al. SIRT1 Promotes N-Myc Oncogenesis Through a Positive Feedback Loop Involving the Effects of MKP3 and ERK on N-Myc Protein Stability. *PLoS Genet* **2011**, *7*, e1002135.

(61)   Liu, P. Y.; Xu, N.; Malyukova, A.; Scarlett, C. J.; Sun, Y. T.; Zhang, X. D.; Ling, D.; Su, S.-P.; Nelson, C.; Chang, D. K.; et al. The Histone Deacetylase SIRT2 Stabilizes Myc Oncoproteins. *Cell Death Differ.* **2013**, *20*, 503–514.

(62)   Cheng, L. Y.; Bailey, A. P.; Leevers, S. J.; Ragan, T. J.; Driscoll, P. C.; Gould, A. P. Anaplastic Lymphoma Kinase Spares Organ Growth During Nutrient Restriction in Drosophila. *Cell* **2011**, *146*, 435–447.

(63)   Reiff, T.; Huber, L.; Kramer, M.; Delattre, O.; Janoueix-Lerosey, I.; Rohrer, H. Midkine and Alk Signaling in Sympathetic Neuron Proliferation and Neuroblastoma Predisposition. *Development* **2011**, *138*, 4699–4708.

(64)   Mosse, Y. P.; Laudenslager, M.; Longo, L.; Cole, K. A.; Wood, A.; Attiyeh, E. F.; Laquaglia, M. J.; Sennett, R.; Lynch, J. E.; Perri, P.; et al. Identification of ALK as a Major Familial Neuroblastoma Predisposition Gene. *Nature* **2008**, *455*, 930–935.

(65)   Janoueix-Lerosey, I.; Lequin, D.; Brugières, L.; Ribeiro, A.; de Pontual, L.; Combaret, V.; Raynal, V.; Puisieux, A.; Schleiermacher, G.; Pierron, G.; et al. Somatic and Germline Activating Mutations of the ALK Kinase Receptor in Neuroblastoma. *Nature* **2008**, *455*, 967–970.

(66)   Chen, Y.; Takita, J.; Choi, Y. L.; Kato, M.; Ohira, M.; Sanada, M.; Wang, L.; Soda, M.; Kikuchi, A.; Igarashi, T.; et al. Oncogenic Mutations of ALK Kinase in Neuroblastoma. *Nature* **2008**, *455*, 971–974.

(67)   De Brouwer, S.; De Preter, K.; Kumps, C.; Zabrocki, P.; Porcu, M.; Westerhout, E. M.; Lakeman, A.; Vandesompele, J.; Hoebeeck, J.; Van Maerken, T.; et al. Meta-Analysis of Neuroblastomas Reveals a Skewed ALK Mutation Spectrum in Tumors with MYCN Amplification. *Clin Cancer Res* **2010**, *16*, 4353–4362.

(68)   Heukamp, L. C.; Thor, T.; Schramm, A.; De Preter, K.; Kumps, C.; De Wilde, B.; Odersky, A.; Peifer, M.; Lindner, S.; Spruessel, A.; et al. Targeted Expression of Mutated ALK Induces Neuroblastoma in Transgenic Mice. *Sci Transl Med* **2012**, *4*, 141ra91.

(69)   Schulte, J. H.; Lindner, S.; Bohrer, A.; Maurer, J.; De Preter, K.; Lefever, S.; Heukamp, L.; Schulte, S.; Molenaar, J.; Versteeg, R.; et al. MYCN and ALKF1174L Are Sufficient to Drive Neuroblastoma Development From Neural Crest Progenitor Cells. *Oncogene* **2012**, *32*, 1059–1065.

(70)   Brodeur, G. M.; Seeger, R. C.; Schwab, M.; Varmus, H. E.; Bishop, J. M. Amplification of N-Myc in Untreated Human Neuroblastomas Correlates with Advanced Disease Stage. *Science* **1984**, *224*, 1121–1124.

(71)   Seeger, R. C.; Brodeur, G. M.; Sather, H.; Dalton, A.; Siegel, S. E.; Wong, K. Y.; Hammond, D. Association of Multiple Copies of the N-Myc Oncogene with Rapid Progression of Neuroblastomas. *N Engl J Med* **1985**, *313*, 1111–1116.

(72)   Matthay, K. K.; Villablanca, J. G.; Seeger, R. C.; Stram, D. O.; Harris, R. E.; Ramsay, N. K.; Swift, P.; Shimada, H.; Black, C. T.; Brodeur, G. M.; et al. Treatment of High-Risk Neuroblastoma with Intensive Chemotherapy, Radiotherapy, Autologous Bone Marrow Transplantation, and 13-Cis-Retinoic Acid. Children's Cancer Group. *N Engl J Med* **1999**, *341*, 1165–1173.

(73)   Schmidt, M. L.; Lukens, J. N.; Seeger, R. C.; Brodeur, G. M.; Shimada, H.; Gerbing, R. B.; Stram, D. O.; Perez, C.; Haase, G. M.; Matthay, K. K. Biologic Factors Determine Prognosis in Infants with Stage IV Neuroblastoma: a Prospective Children's Cancer Group Study. *J. Clin. Oncol.* **2000**, *18*, 1260–1268.

(74)   Pugh, T. J.; Morozova, O.; Attiyeh, E. F.; Asgharzadeh, S.; Wei, J. S.; Auclair, D.; Carter, S. L.; Cibulskis, K.; Hanna, M.; Kiezun, A.; et al. The Genetic Landscape of High-Risk Neuroblastoma. *Nature genetics* **2013**, *45*, 279–284.

(75)   Cheung, N.-K. V.; Zhang, J.; Lu, C.; Parker, M.; Bahrami, A.; Tickoo, S. K.; Heguy, A.; Pappo, A. S.; Federico, S.; Dalton, J.; et al. Association of Age at Diagnosis and Genetic Mutations in Patients with Neuroblastoma. *JAMA: The Journal of the American Medical Association* **2012**, *307*, 1062–1071.

(76)   Molenaar, J. J.; Koster, J.; Zwijnenburg, D. A.; van Sluis, P.; Valentijn, L. J.; van der Ploeg, I.; Hamdi, M.; van Nes, J.; Westerman, B. A.; van Arkel, J.; et al. Sequencing of Neuroblastoma Identifies Chromothripsis and Defects in Neuritogenesis Genes. *Nature* **2012**, *483*, 589–593.

(77)   Sausen, M.; Leary, R. J.; Jones, S.; Wu, J.; Reynolds, C. P.; Liu, X.; Blackford, A.; Parmigiani, G.; Diaz, L. A.; Papadopoulos, N.; et al. Integrated Genomic Analyses Identify ARID1A and ARID1B Alterations in the Childhood Cancer Neuroblastoma. *Nature genetics* **2013**, *45*, 12–17.

(78)   Ito, M. Control of Mental Activities by Internal Models in the Cerebellum. *Nat. Rev. Neurosci.* **2008**, *9*, 304–313.

(79)   Simeone, A.; Acampora, D.; Gulisano, M.; Stornaiuolo, A.; Boncinelli, E. Nested Expression Domains of Four Homeobox Genes in Developing Rostral Brain. *Nature* **1992**, *358*, 687–690.

(80)   Wingate, R. J.; Hatten, M. E. The Role of the Rhombic Lip in Avian Cerebellum

Development. *Development* **1999**, *126*, 4395–4404.

(81)   Adamson, D. C.; Shi, Q.; Wortham, M.; Northcott, P. A.; Di, C.; Duncan, C. G.; Li, J.; McLendon, R. E.; Bigner, D. D.; Taylor, M. D.; et al. OTX2 Is Critical for the Maintenance and Progression of Shh-Independent Medulloblastomas. *Cancer Res* **2010**, *70*, 181–191.

(82)   Bai, R. Y.; Staedtke, V.; Lidov, H. G.; Eberhart, C. G.; Riggins, G. J. OTX2 Represses Myogenic and Neuronal Differentiation in Medulloblastoma Cells. *Cancer Res* **2012**, *72*, 5988–6001.

(83)   Bunt, J.; Hasselt, N. E.; Zwijnenburg, D. A.; Hamdi, M.; Koster, J.; Versteeg, R.; Kool, M. OTX2 Directly Activates Cell Cycle Genes and Inhibits Differentiation in Medulloblastoma Cells. *Int. J. Cancer* **2011**, *131*, E21–E32.

(84)   Hatten, M. E.; Heintz, N. Mechanisms of Neural Patterning and Specification in the Developing Cerebellum. *Annu. Rev. Neurosci.* **1995**, *18*, 385–408.

(85)   Morales, D.; Hatten, M. E. Molecular Markers of Neuronal Progenitors in the Embryonic Cerebellar Anlage. *J. Neurosci.* **2006**, *26*, 12226–12236.

(86)   Spassky, N.; Han, Y.-G.; Aguilar, A.; Strehl, L.; Besse, L.; Laclef, C.; Ros, M. R.; García-Verdugo, J. M.; Alvarez-Buylla, A. Primary Cilia Are Required for Cerebellar Development and Shh-Dependent Expansion of Progenitor Pool. *Dev. Biol.* **2008**, *317*, 246–259.

(87)   Chang, C. H.; Chang, F. M.; Yu, C. H.; Ko, H. C.; Chen, H. Y. Assessment of Fetal Cerebellar Volume Using Three-Dimensional Ultrasound. *Ultrasound Med Biol* **2000**, *26*, 981–988.

(88)   Volpe, J. J. Cerebellum of the Premature Infant: Rapidly Developing, Vulnerable, Clinically Important. *J. Child Neurol.* **2009**, *24*, 1085–1104.

(89)   Andersen, B. B.; Korbo, L.; Pakkenberg, B. A Quantitative Study of the Human Cerebellum with Unbiased Stereological Techniques. *J. Comp. Neurol.* **1992**, *326*, 549–560.

(90)   Dahmane, N.; Ruiz i Altaba, A. Sonic Hedgehog Regulates the Growth and Patterning of the Cerebellum. *Development* **1999**, *126*, 3089–3100.

(91)   Lee, A.; Kessler, J. D.; Read, T.-A.; Kaiser, C.; Corbeil, D.; Huttner, W. B.; Johnson, J. E.; Wechsler-Reya, R. J. Isolation of Neural Stem Cells From the Postnatal Cerebellum. *Nat Neurosci* **2005**, *8*, 723–729.

(92)   Wang, V. Y.; Rose, M. F.; Zoghbi, H. Y. Math1 Expression Redefines the Rhombic Lip Derivatives and Reveals Novel Lineages Within the Brainstem and Cerebellum. *Neuron* **2005**, *48*, 31–43.

(93)   Raaf, J.; Kernohan, J. W. A Study of the External Granular Layer in the Cerebellum. the Disappearance of the External Granular Layer and the Growth of the Molecular and Internal Granular Layers in the Cerebellum. *Am. J. Anat.* **1944**, *75*, 151–172.

(94)   Gailani, M. R.; Bale, S. J.; Leffell, D. J.; DiGiovanna, J. J.; Peck, G. L.; Poliak, S.; Drum, M. A.; Pastakia, B.; McBride, O. W.; Kase, R. Developmental Defects in Gorlin Syndrome Related to a Putative Tumor Suppressor Gene on Chromosome 9. *Cell* **1992**, *69*, 111–117.

(95)   Hahn, H.; Wicking, C.; Zaphiropoulous, P. G.; Gailani, M. R.; Shanley, S.; Chidambaram, A.; Vorechovsky, I.; Holmberg, E.; Unden, A. B.; Gillies, S.; et al. Mutations of the Human Homolog of Drosophila Patched in the Nevoid Basal Cell Carcinoma Syndrome. *Cell* **1996**, *85*, 841–851.

(96)   Northcott, P. A.; Hielscher, T.; Dubuc, A.; Mack, S.; Shih, D.; Remke, M.; Al-Halabi, H.; Albrecht, S.; Jabado, N.; Eberhart, C. G.; et al. Pediatric and Adult Sonic Hedgehog Medulloblastomas Are Clinically and Molecularly Distinct. *Acta Neuropathol* **2011**.

(97)   Goodrich, L. V.; Milenković, L.; Higgins, K. M.; Scott, M. P. Altered Neural Cell

Fates and Medulloblastoma in Mouse Patched Mutants. *Science* **1997**, *277*, 1109–1113.

(98)   Brugières, L.; Pierron, G.; Chompret, A.; Paillerets, B. B.-D.; Di Rocco, F.; Varlet, P.; Pierre-Kahn, A.; Caron, O.; Grill, J.; Delattre, O. Incomplete Penetrance of the Predisposition to Medulloblastoma Associated with Germ-Line SUFU Mutations. *J. Med. Genet*. **2010**, *47*, 142–144.

(99)   Northcott, P. A.; Shih, D. J. H.; Peacock, J.; Garzia, L.; Morrissy, A. S.; Zichner, T.; Stütz, A. M.; Korshunov, A.; Reimand, J.; Schumacher, S. E.; et al. Subgroup-Specific Structural Variation Across 1,000 Medulloblastoma Genomes. *Nature* **2012**, *488*, 49–56.

(100)   Thomas, W. D.; Chen, J.; Gao, Y. R.; Cheung, B.; Koach, J.; Sekyere, E.; Norris, M. D.; Haber, M.; Ellis, T.; Wainwright, B.; et al. Patched1 Deletion Increases N-Myc Protein Stability as a Mechanism of Medulloblastoma Initiation and Progression. *Oncogene* **2009**, *28*, 1605–1615.

(101)   Hallahan, A. R.; Pritchard, J. I.; Hansen, S.; Benson, M.; Stoeck, J.; Hatton, B. A.; Russell, T. L.; Ellenbogen, R. G.; Bernstein, I. D.; Beachy, P. A.; et al. The SmoA1 Mouse Model Reveals That Notch Signaling Is Critical for the Growth and Survival of Sonic Hedgehog-Induced Medulloblastomas. *Cancer Res* **2004**, *64*, 7794–7800.

(102)   Mao, J.; Ligon, K. L.; Rakhlin, E. Y.; Thayer, S. P.; Bronson, R. T.; Rowitch, D.; McMahon, A. P. A Novel Somatic Mouse Model to Survey Tumorigenic Potential Applied to the Hedgehog Pathway. *Cancer Res* **2006**, *66*, 10171–10178.

(103)   Weiner, H. L.; Bakst, R.; Hurlbert, M. S.; Ruggiero, J.; Ahn, E.; Lee, W. S.; Stephen, D.; Zagzag, D.; Joyner, A. L.; Turnbull, D. H. Induction of Medulloblastomas in Mice by Sonic Hedgehog, Independent of Gli1. *Cancer Res* **2002**, *62*, 6385–6389.

(104)   Schüller, U.; Heine, V. M.; Mao, J.; Kho, A. T.; Dillon, A. K.; Han, Y.-G.; Huillard, E.; Sun, T.; Ligon, A. H.; Qian, Y.; et al. Acquisition of Granule Neuron Precursor Identity Is a Critical Determinant of Progenitor Cell Competence to Form Shh-Induced Medulloblastoma. *Cancer Cell* **2008**, *14*, 123–134.

(105)   Yang, Z.-J.; Ellis, T.; Markant, S. L.; Read, T.-A.; Kessler, J. D.; Bourboulas, M.; Schüller, U.; Machold, R.; Fishell, G.; Rowitch, D. H.; et al. Medulloblastoma Can Be Initiated by Deletion of Patched in Lineage-Restricted Progenitors or Stem Cells. *Cancer Cell* **2008**, *14*, 135–145.

(106)   Browd, S. R.; Kenney, A. M.; Gottfried, O. N.; Yoon, J. W.; Walterhouse, D.; Pedone, C. A.; Fults, D. W. N-Myc Can Substitute for Insulin-Like Growth Factor Signaling in a Mouse Model of Sonic Hedgehog-Induced Medulloblastoma. *Cancer Res* **2006**, *66*, 2666–2672.

(107)   Korshunov, A.; Remke, M.; Kool, M.; Hielscher, T.; Northcott, P. A.; Williamson, D.; Pfaff, E.; Witt, H.; Jones, D. T. W.; Ryzhova, M.; et al. Biological and Clinical Heterogeneity of MYCN-Amplified Medulloblastoma. *Acta Neuropathol* **2012**, *123*, 515–527.

(108)   Swartling, F. J.; Grimmer, M. R.; Hackett, C. S.; Northcott, P. A.; Fan, Q.-W.; Goldenberg, D. D.; Lau, J.; Masic, S.; Nguyen, K.; Yakovenko, S.; et al. Pleiotropic Role for MYCN in Medulloblastoma. *Genes Dev* **2010**, *24*, 1059–1072.

(109)   Kawauchi, D.; Robinson, G.; Uziel, T.; Gibson, P.; Rehg, J.; Gao, C.; Finkelstein, D.; Qu, C.; Pounds, S.; Ellison, D. W.; et al. A Mouse Model of the Most Aggressive Subgroup of Human Medulloblastoma. *Cancer Cell* **2012**, *21*, 168–180.

(110)   Pei, Y.; Moore, C. E.; Wang, J.; Tewari, A. K.; Eroshkin, A.; Cho, Y.-J.; Witt, H.; Korshunov, A.; Read, T.-A.; Sun, J. L.; et al. An Animal Model of MYC-Driven Medulloblastoma. *Cancer Cell* **2012**, *21*, 155–167.

(111)   Kool, M.; Korshunov, A.; Remke, M.; Jones, D. T. W.; Schlanstein, M.; Northcott, P. A.; Cho, Y.-J.; Koster, J.; Schouten-van Meeteren, A.; van Vuurden, D.; et al.

Molecular Subgroups of Medulloblastoma: an International Meta-Analysis of Transcriptome, Genetic Aberrations, and Clinical Data of WNT, SHH, Group 3, and Group 4 Medulloblastomas. *Acta Neuropathol* **2012**.

(112) Pei, Y.; Brun, S. N.; Markant, S. L.; Lento, W.; Gibson, P.; Taketo, M. M.; Giovannini, M.; Gilbertson, R. J.; Wechsler-Reya, R. J. WNT Signaling Increases Proliferation and Impairs Differentiation of Stem Cells in the Developing Cerebellum. *Development* **2012**, *139*, 1724–1733.

(113) Kropilak, M.; Jagelman, D. G.; Fazio, V. W.; Lavery, I. L.; McGannon, E. Brain Tumors in Familial Adenomatous Polyposis. *Cell. Mol. Life Sci.* **1989**, *32*, 778–782.

(114) Taylor, M. D.; Zhang, X.; Liu, L.; Hui, C.-C.; Mainprize, T. G.; Scherer, S. W.; Wainwright, B.; Hogg, D.; Rutka, J. T. Failure of a Medulloblastoma-Derived Mutant of SUFU to Suppress WNT Signaling. *Oncogene* **2004**, *23*, 4577–4583.

(115) Robinson, G.; Parker, M.; Kranenburg, T. A.; Lu, C.; Chen, X.; Ding, L.; Phoenix, T. N.; Hedlund, E.; Wei, L.; Zhu, X.; et al. Novel Mutations Target Distinct Subgroups of Medulloblastoma. *Nature* **2012**, *488*, 43–48.

(116) Barker, N. The Chromatin Remodelling Factor Brg-1 Interacts with Beta-Catenin to Promote Target Gene Activation. *EMBO J* **2001**, *20*, 4935–4943.

(117) Pugh, T. J.; Weeraratne, S. D.; Archer, T. C.; Pomeranz Krummel, D. A.; Auclair, D.; Bochicchio, J.; Carneiro, M. O.; Carter, S. L.; Cibulskis, K.; Erlich, R. L.; et al. Medulloblastoma Exome Sequencing Uncovers Subtype-Specific Somatic Mutations. *Nature* **2012**, *488*, 106–110.

(118) Momota, H.; Shih, A. H.; Edgar, M. A.; Holland, E. C. C-Myc and Beta-Catenin Cooperate with Loss of P53 to Generate Multiple Members of the Primitive Neuroectodermal Tumor Family in Mice. *Oncogene* **2008**, *27*, 4392–4401.

(119) Gibson, P.; Tong, Y.; Robinson, G.; Thompson, M. C.; Currle, D. S.; Eden, C.; Kranenburg, T. A.; Hogg, T.; Poppleton, H.; Martin, J.; et al. Subtypes of Medulloblastoma Have Distinct Developmental Origins. *Nature* **2010**, *468*, 1095–1099.

(120) Takebayashi, H.; Ohtsuki, T.; Uchida, T.; Kawamoto, S.; Okubo, K.; Ikenaka, K.; Takeichi, M.; Chisaka, O.; Nabeshima, Y.-I. Non-Overlapping Expression of Olig3 and Olig2 in the Embryonic Neural Tube. *Mech. Dev.* **2002**, *113*, 169–174.

(121) Taylor, M. D.; Northcott, P. A.; Korshunov, A.; Remke, M.; Cho, Y.-J.; Clifford, S. C.; Eberhart, C. G.; Parsons, D. W.; Rutkowski, S.; Gajjar, A.; et al. Molecular Subgroups of Medulloblastoma: the Current Consensus. *Acta Neuropathol* **2012**, *123*, 465–472.

(122) Swartling, F. J.; Savov, V.; Persson, A. I.; Chen, J.; Hackett, C. S.; Northcott, P. A.; Grimmer, M. R.; Lau, J.; Chesler, L.; Perry, A.; et al. Distinct Neural Stem Cell Populations Give Rise to Disparate Brain Tumors in Response to N-MYC. *Cancer Cell* **2012**, *21*, 601–613.

CHAPTER 2

Drugging MYCN through an allosteric transition in Aurora Kinase A
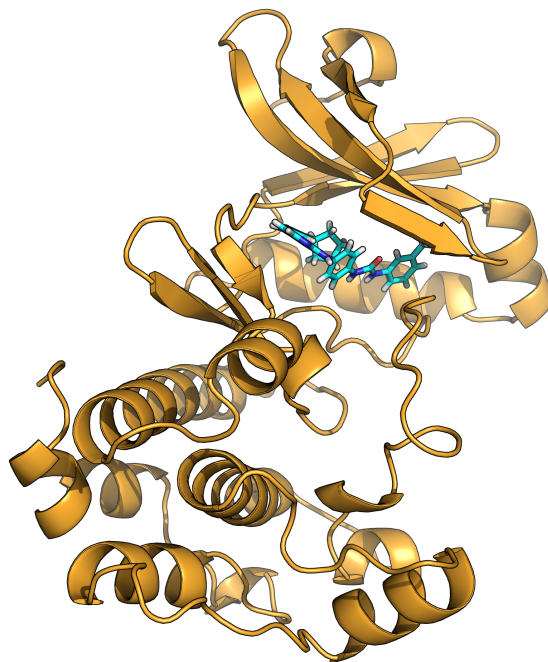
2.1 Abstract

MYC genes contribute to a range of cancers including neuroblastoma, where amplification of *MYCN* confers a poor prognosis. Proteolytic degradation of MYCN protein is regulated in part by a kinase-independent function of Aurora Kinase A. We describe a class of inhibitors that disrupts the native conformation of Aurora A and causes degradation of MYCN protein across MYCN-expressing neuroblastoma cell lines. Comparison of co-crystal structures with structure-activity relationships across multiple inhibitors and chemotypes, coupled with mechanistic studies and biochemical assays, delineates an Aurora A conformation-specific effect on proteolytic degradation of MYCN, rather than simple nanomolar-level inhibition of Aurora

Kinase A kinase activity. This new class of inhibitors, which disrupts stabilizing interactions between Aurora A and MYCN, represents candidate agents to target MYC and MYCN-driven cancers, as well as a prototype for inhibitors that induce an allosteric change to block non-enzymatic functions of enzymes.

2.2 Introduction

MYC proteins are considered undruggable, as their DNA binding domains are composed of two extended alpha helices with no apparent surfaces for small molecule binding. *MYC* also regulates as much as a third of the genome, with overexpression proposed to amplify cell-type specific gene expression rather than modulate a MYC-specific group of genes.[1,2] Both MYC and MYCN targets may be blocked through bromodomain inhibitors.[3-5] Other methods, such as synthetic lethal screens for potential targets, have revealed druggable targets that may act downstream of MYC.[6,7] Using an inducible dominant negative MYC protein, others have shown that systemic MYC inhibition is a viable cancer therapeutic strategy.[8] However, using current medicinal chemistry, direct and efficient pharmacologic targeting of MYC transcription factors has proven challenging if not impossible.[9]

MYC genes contribute to a wide range of human tumors through overexpression, amplification, translocation, or stabilizing point mutations. The normal concentration of MYC in cells is tightly regulated at the level of protein stability through canonical upstream kinase signaling pathways, including PI3K/mTOR, CDK2, and MAPK. These kinases direct sequential phosphorylation and dephosphorylation of conserved residues in MYC proteins, which target them for ubiquitination and degradation by the proteasome (reviewed in [6]).

The MYC family member MYCN, named based on its association with amplification in the childhood tumor neuroblastoma, is stabilized by Aurora Kinase A (Aurora A) in a kinase-independent fashion involving protein-protein interaction.[10] Independent of its effects on MYCN, Aurora Kinase A is an attractive cancer target, as it regulates entry into mitosis, maturation of

24

centrosomes, cytokinesis, and formation of the bipolar spindle, in part through phosphorylation of key regulators of proliferation and survival such as p53, BRCA1, and Histone H3.[11-15] Increased Aurora Kinase A expression is a negative prognostic factor in neuroblastoma,[16] and pre-clinical testing with MLN8237, a specific Aurora Kinase A inhibitor, showed significant promise in cell line xenograft experiments.[17] Furthermore, the co-crystal structure of MLN8054 (the predecessor of MLN8237) with Aurora Kinase A shows a partial shift away from the active state of the kinase, and a modest decrease in MYCN protein when treating MYCN-expressing neuroblastoma with MLN8237 or MLN8054 at high doses for prolonged periods.[18,19] This partial effect on MYCN may therefore result from the prolonged kinase inhibitory effect of these compounds, or from a partial shift in the tertiary structure of Aurora Kinase A, in response to MLN8237/MLN8054 binding, which subtly alters Aurora's affinity for the MYCN complex. Consistent with this modest effect on MYCN, early phase clinical testing has shown little efficacy in *MYCN*-amplified neuroblastoma, underscoring the need for inhibitors of Aurora A that more potently block MYCN.[20]

We hypothesized that the kinase-independent stabilization of MYCN requires a distinct conformation of this protein kinase, and that we could rationally design specific and potent conformation-disrupting inhibitors (CDs) of Aurora Kinase A that perturb these protein-protein interactions, effecting degradation of MYCN. To identify such conformation-disrupting compounds, we synthesized a set of candidate inhibitors predicted to induce a large structural shift in Aurora A, by appending a range of type II (inactive state-binding) pharmacophores to two different kinase inhibitor scaffolds. Candidate compounds were used to treat *MYCN*-amplified neuroblastoma cell lines. Levels of MYCN were assayed by immunoblot, and a lead compound, CD532, was identified. CD532 inhibited Aurora A at low nanomolar concentrations, induced potent degradation of MYCN and blockade of p-Histone H3 and p-Aurora A (the latter two measures of Aurora kinase inhibition), and disruption of the Aurora A–MYCN complex as measured by co-immunoprecipitation. Co-crystal structures of Aurora A with and without CD532

show that CD532 induced a pronounced shift of structural features in the kinase domain of Aurora A, as compared to Aurora A alone, or bound to either ATP or to the clinical inhibitors VX-680 or MLN8054. CD532 represents the first member of a class of conformation-disrupting inhibitors of Aurora Kinase A that induces an allosteric transition in the kinase to block a kinase-independent stabilizing function for MYCN protein.

2.3 Results

2.3.1 Initial screen for conformation-disrupting Aurora A inhibitors

To construct a diverse panel of inhibitors that might disrupt the native conformation of Aurora A, we started with both diaminopyrimidine (VX-680-like) and pyrazolopyrimidine (PP-1-like) scaffolds (Figure 1A, red and blue text). Derivatives of each of these scaffolds were known to bind to Aurora Kinase A. Structural data were available on both scaffolds bound to related kinases, and routes to their synthesis were tractable. To these scaffolds, we fused biphenyl urea and amide moieties predicted, based on published structures, to stabilize distinct conformations of Aurora A that might alter scaffolding functions.[21,22]

To test whether this panel of 32 putative conformation-disrupting Aurora A inhibitors would destabilize MYCN, we initially treated Kelly *MYCN*-amplified neuroblastoma cells with candidate inhibitors and measured MYCN protein by western blot. We also assessed phosphorylation of Histone H3, a known substrate for Aurora A and B and a marker for mitosis. Figures 2.1B-D show decreased levels of both MYCN protein and p-Histone H3 in response to several members of the screening panel (quantified in Figure 2.1B). CD532 and CD572 treatment decreased levels of both MYCN and p-Histone H3 proteins (Figure 2.1B). In contrast, and as predicted, known inhibitors of Aurora A, VX-680 and MLN8237, blocked Histone H3 phosphorylation at 1 μM yet demonstrated much more modest effects on levels of MYCN protein. Candidate CD compounds were subsequently screened against a second *MYCN*-amplified

neuroblastoma cell line, SK-N-BE(2) (Figure 1C), substantiating CD532 as our most active lead compound.
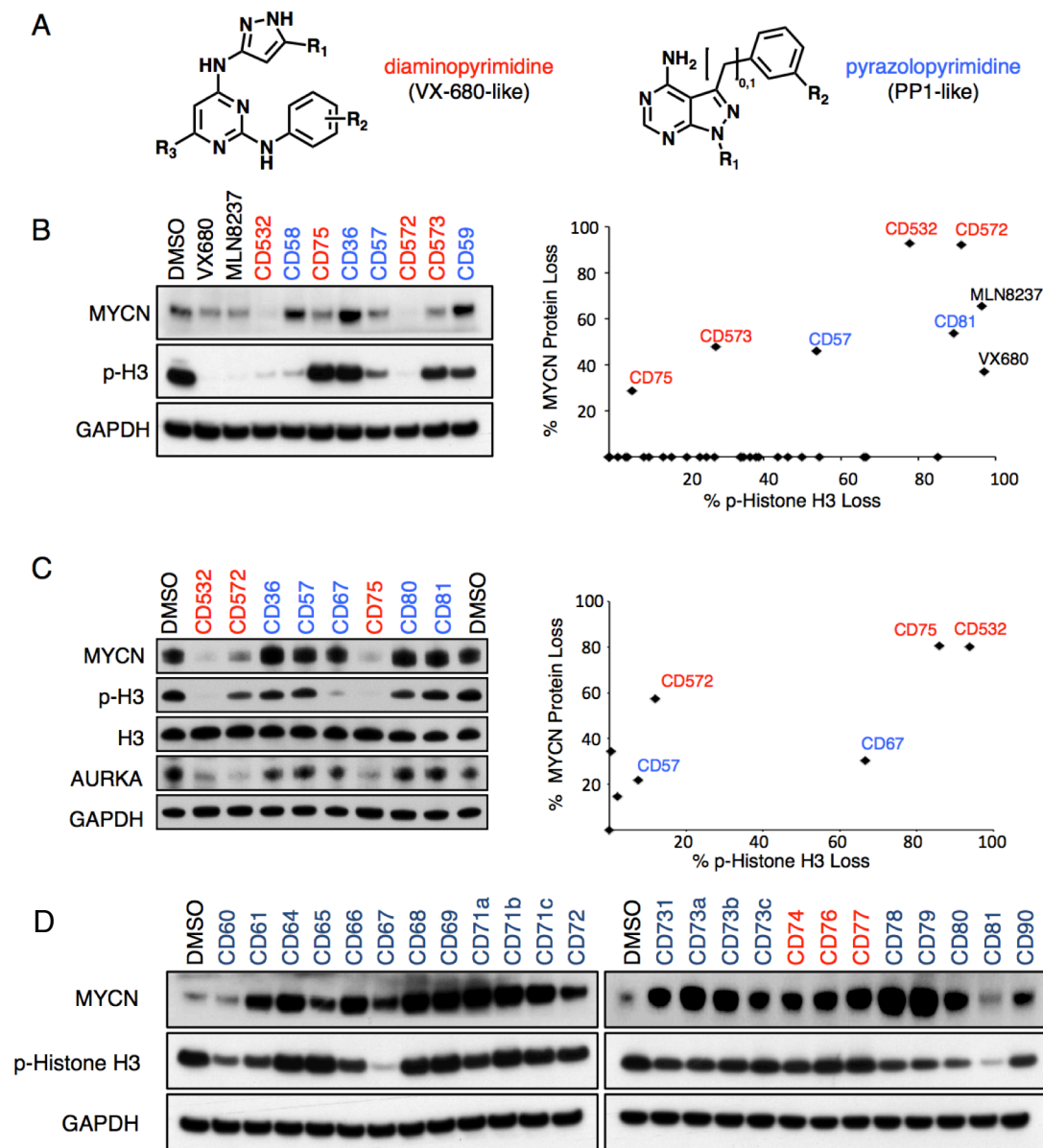
Figure 2.1: Screening of conformation disrupting Aurora A inhibitor (CD) compounds.
(A) Both VX-680-like diaminopyrimidine (red text) and a PP1-like pyrazolopyrimidine (blue text) scaffolds were used for initial screening panel. Cell lines were treated for 24hrs with 1μM of 32 different compounds predicted to bind to Aurora A and modulate tertiary structure. Extracts were examined by western blot for MYCN and phospho-histone H3 expression, in (B) Kelly cells (quantitation on the right expressed as percent of control) and (C) a selected sub-panel of compounds was tested against SK-N-BE(2) cells (quantitation on the right expressed as percent of control). (D) Additional screening of CD compounds in MYCN-amplified Kelly cells.

2.3.2 CD532 potently inhibits Aurora A, causes loss of MYCN, and is cytotoxic in *MYCN*-amplified neuroblastoma cells

To determine the biochemical potency of CD532 we measured activity against purified Aurora A protein, revealing potent Aurora A kinase inhibition with an IC_{50} of 45 nM (Figure 2.2A-B). CD532 inhibited Aurora A kinase activity in cells as measure by both p-Aurora A (T288) and p-H3 at short time points (Figure 2.2C). Treatment of multiple cell lines with CD532, MLN8237, and VX-680 showed dose-dependent loss of MYCN protein with CD532, and little or no response to high concentrations of MLN8237 (Figure 2.3A-C).
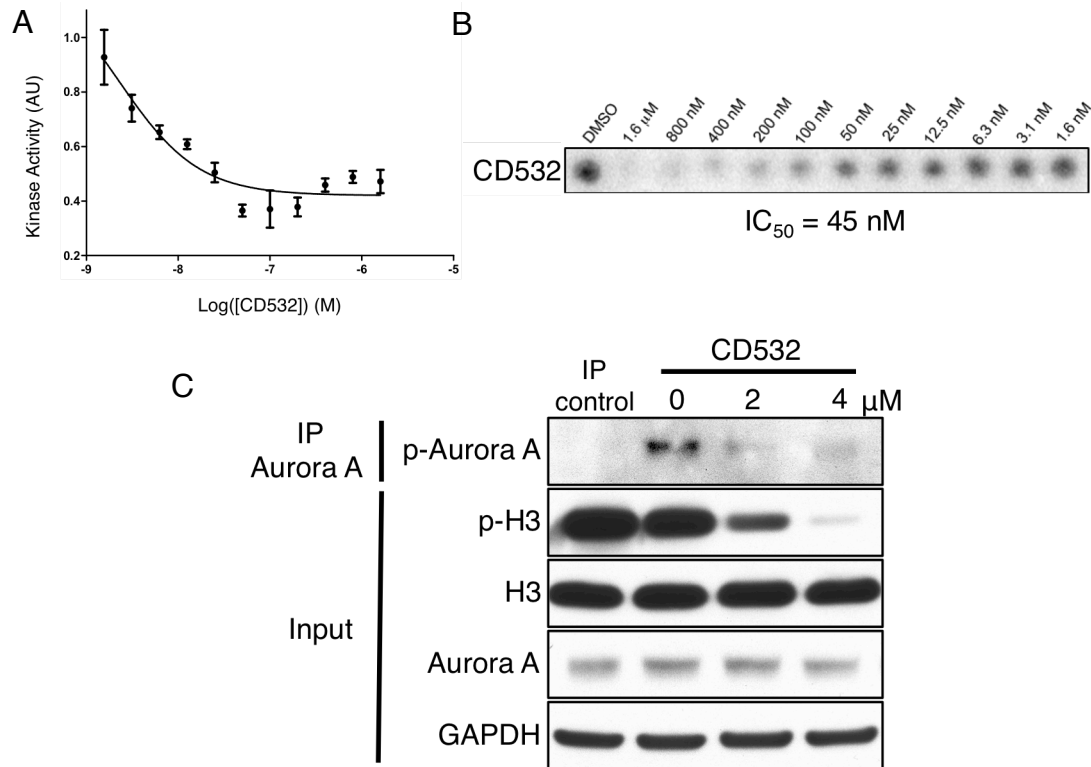
Figure 2.2: CD532 is an inhibitor of Aurora A kinase. (A) Representative sigmoidal dose response curve and (B) 32P ATP blot of CD532 against Aurora A. Enzyme was either full-length or kinase domain-only Aurora A, and substrate was either full-length purified Histone H3 or target oligopeptide. (C) Immunoprecipitation of Aurora A and immunoblot for p-Aurora A (T288) after 2 hrs treatment of IMR32 neuroblastoma cells with CD532.
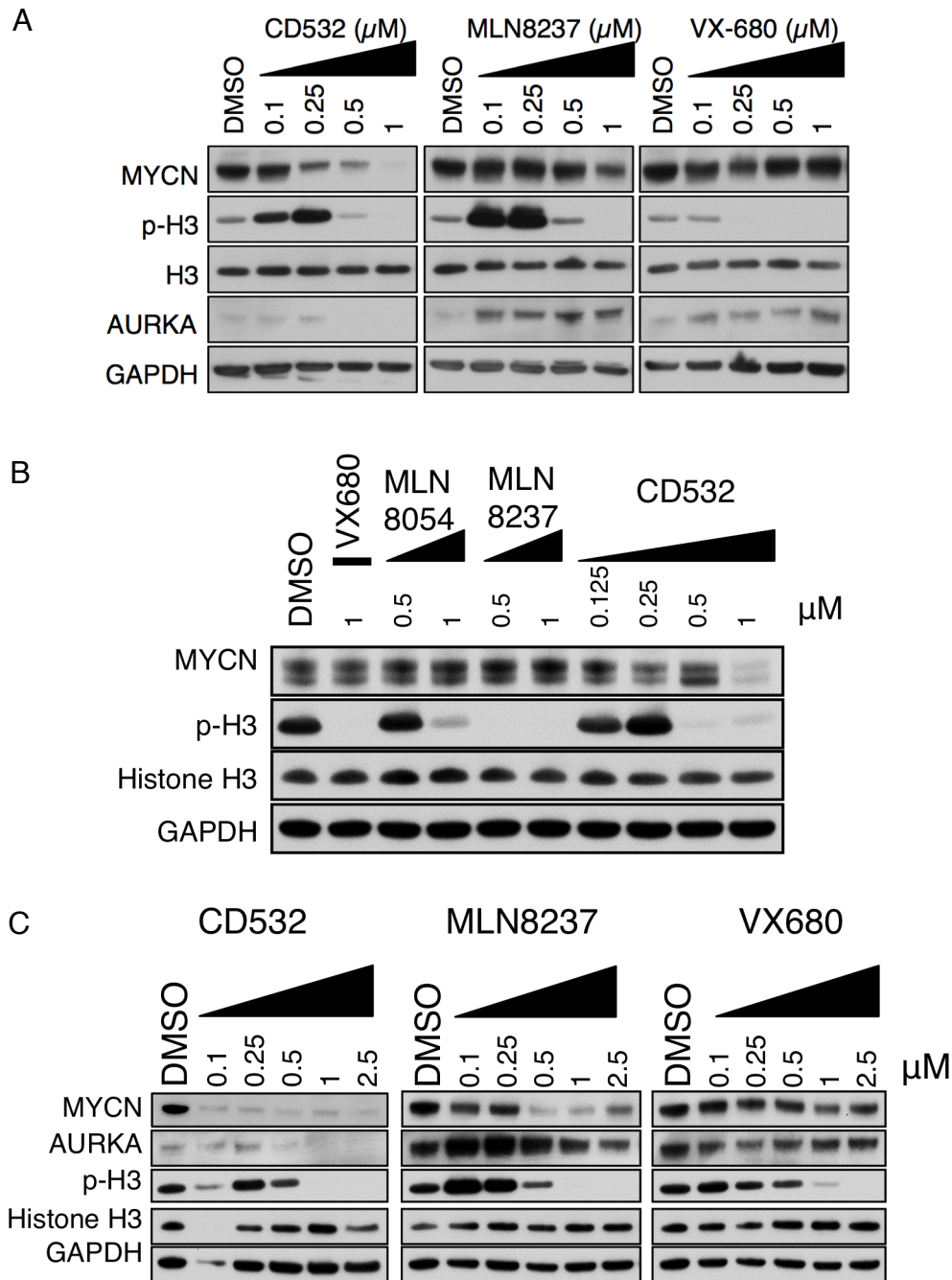
Figure 2.3: Dose response of CD532 in MYCN amplified neuroblastoma cell lines. (A) SK-N-BE(2) cells, (B) SMS-KCN cells or (C) Kelly cells were treated for 24hrs with indicated of CD532, MLN8237, MLN8054 or VX-680 and analyzed by immunoblot for the indicated proteins.

MLN8237 is a relatively selective inhibitor of Aurora A with IC_{50}s of 1.2nM and 396.5nM for Aurora A and B respectively, while VX-680 is potent against both Aurora A and Aurora B, with IC_{50}s of 0.6nM and 18nM respectively.[23] Notably, the *in vitro* (cell line) activity of CD532 against MYCN paralleled its cell-free *in vitro* IC_{50} for Aurora A by approximately 10 fold (Figures 2.2A-B and 2.3). By contrast MLN8237 and VX-680 treatment effected little loss of MYCN protein even at doses 100 to 1000 times greater than their IC_{50}s for Aurora A. MLN8237 and VX-680 upregulated or had little effect on Aurora A protein. CD532, in contrast, downregulated Aurora A protein across cell lines (at higher concentrations) consistent with distinct mechanisms of binding underlying these differential effects (Figures 2.2A-B and 2.3). At low concentrations of CD532 and short time points however, loss of MYCN was apparent while levels of Aurora A protein were unaffected (Figures 2.3A, 2.3C, and 2.5A). These observations are consistent with degradation of MYCN resulting from CD532 binding, rather than from loss of Aurora A protein.

Histone H3 is a known substrate for both Aurora A and B. Accordingly, dual inhibition of Aurora A/B with VX-680 abrogates phosphorylation of Histone H3 at S10. In contrast, MLN8237 caused an initial increase in S10 phosphorylation at lower concentrations, followed by a sharp drop at higher concentrations (Figure 2.3A-C). This increase in phosphorylation of Histone H3 in response to MLN8237 has been described previously, and results from Aurora A inhibition with feedback increase in Aurora B activity.[24,25] CD532 behaves similarly to MLN8237 with regard to Histone H3 phosphorylation, consistent with an Aurora A-specific effect.

We measured the cellular EC_{50} at 72hrs against two different *MYCN*-amplified neuroblastoma cell lines for both CD532 (223.2nM and 146.7nM) and MLN8237 (40.89nM and 33.92nM). These values are directly proportionate to the cell-free IC_{50} for Aurora A inhibition by CD532 (45nM) and MLN8237 (4nM) by ~10 fold (Figure 2.4). Additionally, the IC_{50} of CD532 for on-target MYCN knockdown in SK-N-BE(2) cells (~250nM—Figure 2.3A) is consistent with the cellular EC_{50} (223.2nM—Figure 2.4A). Notably the maximal cytotoxicity (E_{max}) for each

compound is proportionate to the degree of MYCN knockdown (and not to the degree of Aurora A inhibition) in *MYCN*-amplified neuroblastoma lines. These data argue for an Aurora A-dependent effect on inhibition of cell growth, and a MYCN-dependent effect on loss of viability.
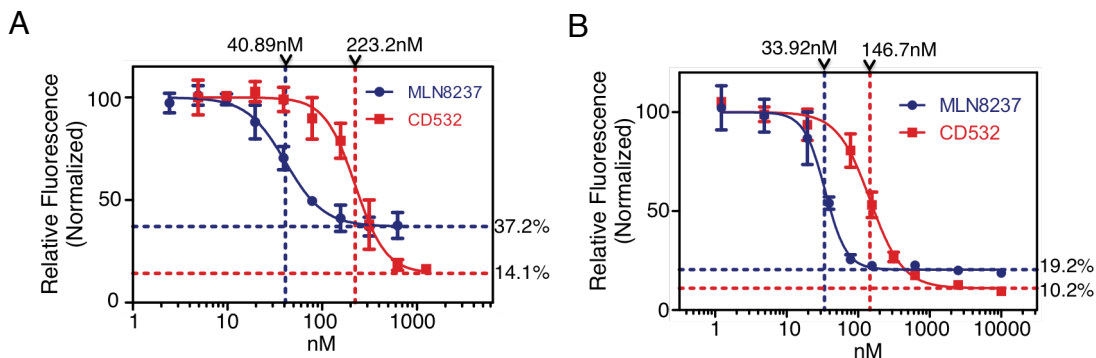
Figure 2.4: Cytotoxicity of CD532 in MYCN-amplified neuroblastoma. Dose responses of MLN8237 and CD532 at 72hrs using a cyquant assay in (A) SK- N-BE(2) and (B) Kelly MYCN-amplified neuroblastoma cells.

2.3.3 Degradation of MYCN requires phosphorylation and proteasomal degradation of MYCN

Upon loss of Aurora A scaffolding function by siRNA knockdown, MYCN is degraded through canonical ubiquitination and proteasomal degradation.[10] As such, we would expect rapid degradation of MYCN protein to occur within hours of dissociation of the MYCN-Aurora A complex. In fact, we observed a clear and time-dependent loss of MYCN protein at time points as short as 4hrs of treatment with CD532 (Figure 2.5A). In contrast, treatment with MLN8237 results in similarly rapid, but much more modest decrease in levels of MYCN protein that does not change over time (Figure 2.5A). We also treated MYCN-amplified SK-N-BE(2) and IMR32 cells with increasing concentrations of CD532 in the presence of the proteasome inhibitor MG-132. While MG-132 had no effect on inhibition of H3 phosphorylation in response to CD532, proteasomal inhibition protected MYCN from degradation in response to CD532 (Figure 2.5B).

MYCN is sequentially phosphorylated at S62/T58 before it is targeted for degradation by ubiquitination, and only phosphorylated, ubiquitinated MYCN is protected from degradation by

Aurora A.[6,10] To test whether the activity of CD532 is dependent on these phospho-residues, we treated SH-EP *MYCN*-non-amplified neuroblastoma cells, engineered to express either MYCN[WT] or a non-phosphorylatable mutant of MYCN (MYCN[T58A/S62A]) with increasing concentrations of CD532. Figure 2.5C shows a dose-dependent decrease in wild-type MYCN protein. In contrast, MYCN[T58A/S62A] was partially protected from degradation, suggesting that CD532 potentiates loss of MYCN through the canonical phosphorylation and ubiquitination pathway. Notably, even high concentrations of the conventional type I inhibitor VX-680, which stabilizes Aurora A in the active conformation,[11] had little effect on MYCN protein levels in this system (Figure 2.5C).
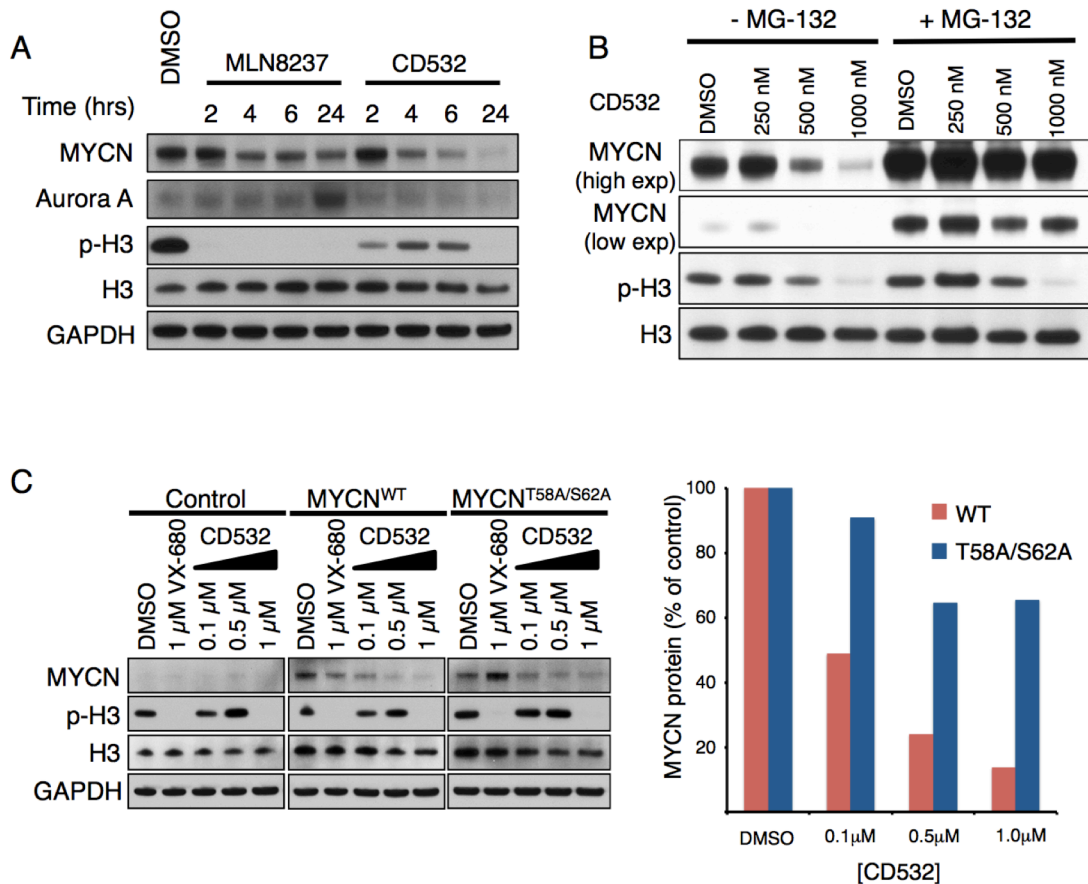
Figure 2.5: Degradation of MYCN is proteasome-dependent and requires phosphorylation of MYCN. (A) Time dependence of MYCN protein loss in SK-N-BE(2) cells due to treatment with MLN8237 or CD532 performed at 1μM. (B) CD532 dose dependence of MYCN protein loss in the absence or presence of proteasomal inhibition. (C) Immunoblot showing the effect of compounds at indicated concentrations for 24hrs on protein levels of wild-type vs. T58A/S62A degradation-resistant MYCN in SHEP cells.

2.3.4 CD532 stabilizes a DFG-in, inactive conformation of Aurora A

CD532 consists of an aminopyrazole-pyrimidine ATP-mimetic backbone, similar to VX-680, but includes a 3-trifluoromethyl-biphenyl urea as its conformation-disrupting pharmacophore (Figures 2.6A). To determine how CD532 binding affects the conformation of Aurora A, we solved the crystal structure of the catalytic domain of Aurora A (residues 123-390) both alone (Apo) and bound to CD532, to resolutions of 3.14 Å and 1.85 Å, respectively (Figure 2.6A, statistics in Table 2.1). This Apo structure is the first published structure of Aurora A without ligand. While the B-factor of the relatively disordered activation loop in both structures is high, the tracing of the polypeptide backbone was unambiguous. Electron density for CD532 within the active site was well defined (Figure 2.6B).

The ATP-binding hinge region of the Aurora A active site makes polar contacts with the aminopyrazole portion of CD532, consistent with our choice of ATP-mimetic scaffold. The catalytic D274 achieves polar contacts with the urea moiety of CD532 to stabilize the biphenyl urea in its orientation towards the N-terminal β1 and β2 strands forming part of the ATP binding pocket (Figures 2.6B-C). The polar contacts between the urea moiety and CD532 in fact allow for a ~7 Å displacement of the β1 and β2 strands in the N-terminal domain, via steric clash with the trifluoromethylphenyl moiety of CD532 (Figure 2.6D). These β1 and β2 strands form part of a β-sheet that is the core of the relatively rigid N-terminal domain. Thus displacement of these strands by CD532 disrupts the conformation of Aurora Kinase A (Apo), rotating and shifting the N-terminal domain by 6.2 Angstroms, relative to the C-terminal domain (Figure 2.6E).

The highly conserved HRD sequence across virtually all kinases is located at the lip of the active site. Coordination between this conserved HRD arginine and a phospho-threonine in the activation loop (R255 and T288 respectively, in the case of Aurora A) orients the HRD catalytic aspartic acid to be primed for catalysis. By this mechanism, the catalytic activity of HRD-containing kinases can be regulated through phosphorylation of their activation loop. In the
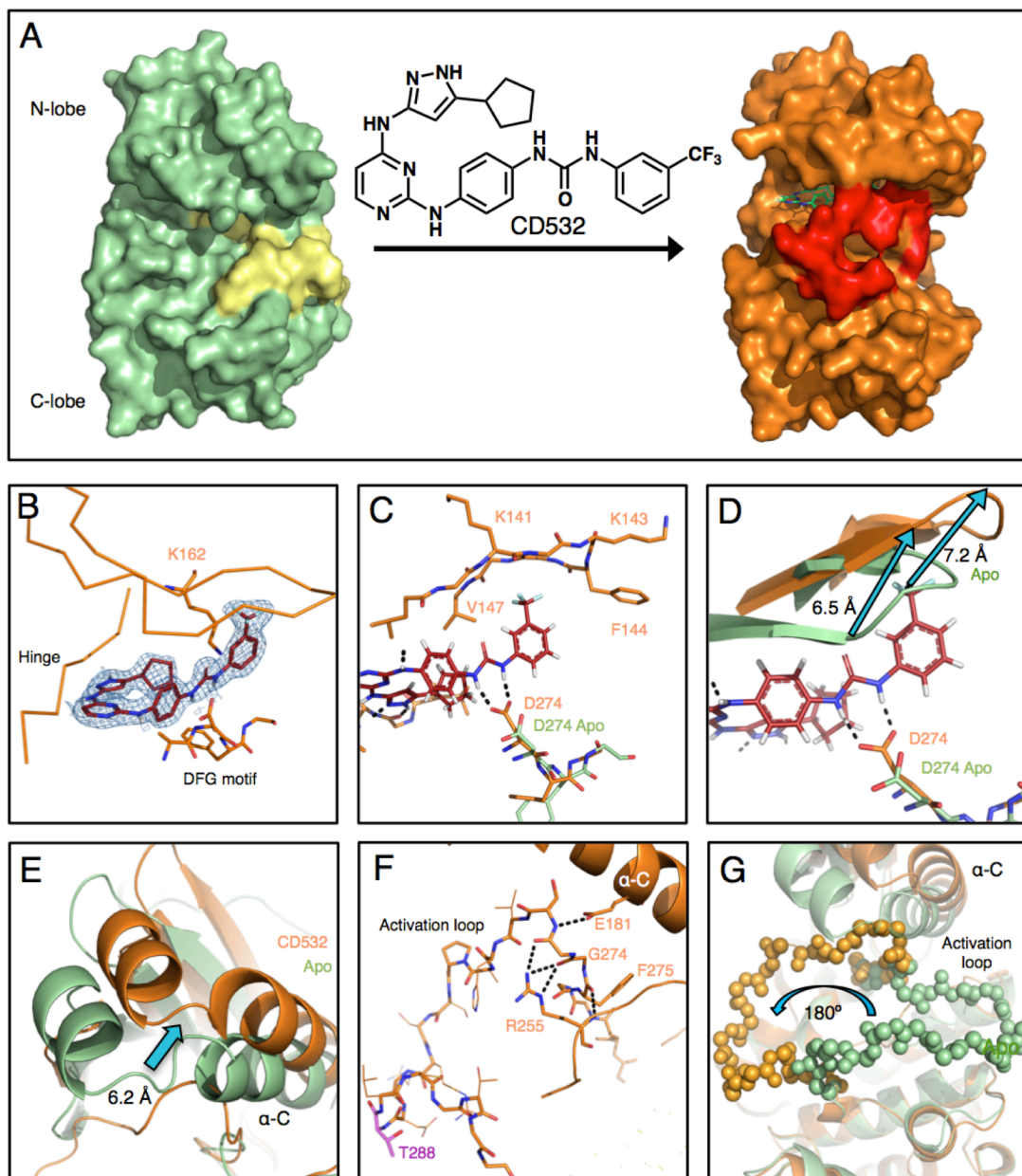
Figure 2.6: CD532 stabilizes an inactive, DFG-in conformation of Aurora A. (A) Chemical structure of CD532 and surface representations of Aurora A Apo (green, activation loop in yellow) and of Aurora A bound to CD532 (orange, activation loop in red). (B) CD532 (red sticks) in ATP binding pocket, overlaid with electron density before ligand fitting (blue mesh). (C) Interactions between CD532 (red), the DFG motif (D274) and β1/β2 (K141-V147) (D) Displacement of glycine rich loop in drug-bound structure (orange) as compared to Apo (green) due to drug binding. (E and F) Displaced α-C helix allows network of polar contacts between E181, R255, and DFG motif and (G) stabilization of inactive orientation of the activation loop (activation loop in balls). Structural comparisons are all C-terminal alignments.

	Aurora Kinase A with CD532	Aurora Kinase A Apo
Resolution range (Å)	29.07 - 1.853 (1.92 - 1.853)	44.95 - 3.135 (3.247 - 3.135)
Space group	C 2 2 21	P 31
Unit cell	83.175 92.943 74.542 90 90 90	83.783 83.783 171.777 90 90 120
Total reflections		
Unique reflections	24601 (2358)	23663 (2375)
Multiplicity		
Completeness (%)	98.82 (96.05)	99.95 (100.00)
Mean I/sigma(I)	8.53 (2.50)	18.99 (5.50)
Wilson B-factor	28.16	95.57
R-sym		
R-factor	0.1841 (0.2469)	0.1845 (0.2838)
R-free	0.2188 (0.2716)	0.2344 (0.3634)
Number of atoms	4657	17546
macromolecules	2190	8731
ligands	56	
water	172	8
Protein residues	266	1063
RMS(bonds)	0.009	0.004
RMS(angles)	1.19	0.89
Ramachandran favored (%)	97	94
Ramachandran outliers (%)	0	0.95
Clashscore	9.21	13.49
Average B-factor	38	105
macromolecules	37.8	105.1
solvent	40.6	56.4

Table 2.1: Summary of data and refinement statistics for crystal structure solutions of Aurora A Apo (4J8N) and Aurora A bound to CD532 (4J8M) generated in PHENIX.

presence of CD532, R255 and T288 are displaced by a considerable distance (Figure 2.6F). In fact, CD532-bound Aurora sequesters R255 in a manner that displaces the catalytic HRD aspartic acid from its catalytically functional orientation, disengaging HRD regulation and stabilizing the kinase in a catalytically inactive conformation.

Indeed, the displaced α-C helix and R255 together trap the most N-terminal portion of the activation loop in a network of hydrogen bonds (Figure 2.6F). This surprising interaction positions the activation loop backbone in a manner that stabilizes the entire activation loop in its inactive orientation, flipped 180° relative to its active state (Figure 2.6G). Thus, CD532 stabilizes Aurora Kinase A in a novel conformation, associated with a 6.2 Å shift in the position of the N-terminal domain relative to the C-terminal domain, a disengaged state of the regulatory HRD motif, and a 180° flip in the activation loop.

2.3.5 Degradation of MYCN requires conformation-specific inhibition of Aurora A

Although both VX-680 and CD532 bind to the ATP-binding kinase 'hinge' in an identical manner through their aminopyrazole-pyrimidine core, each contains distinct chemical components that produce highly divergent effects on MYCN in cells (Figures 2.3 and 2.7A). Our crystallographic data suggest that several chemical moieties of CD532 were critical for its ability to destabilize MYCN. As expected, altering the urea moiety of CD532 decreased biochemical potency against Aurora A, as well as efficacy against MYCN in neuroblastoma cell lines (Figure 2.7B). Our structural data also show that the 6-position of the pyrimidine backbone is oriented towards solvent, and addition of a methyl group to this position (CD15) maintained both cell-free potency and efficacy against MYCN (Figure 2.7B and E). These data are consistent with degradation of MYCN occurring as a consequence of on-target Aurora A Kinase conformation-disrupting activity of CD532.

The cyclopentyl moiety of CD532 packs neatly in a hydrophobic pocket made by V147, L194, and the leucine gatekeeper (L210) (Figure 2.7C). Thus our crystallographic data suggests
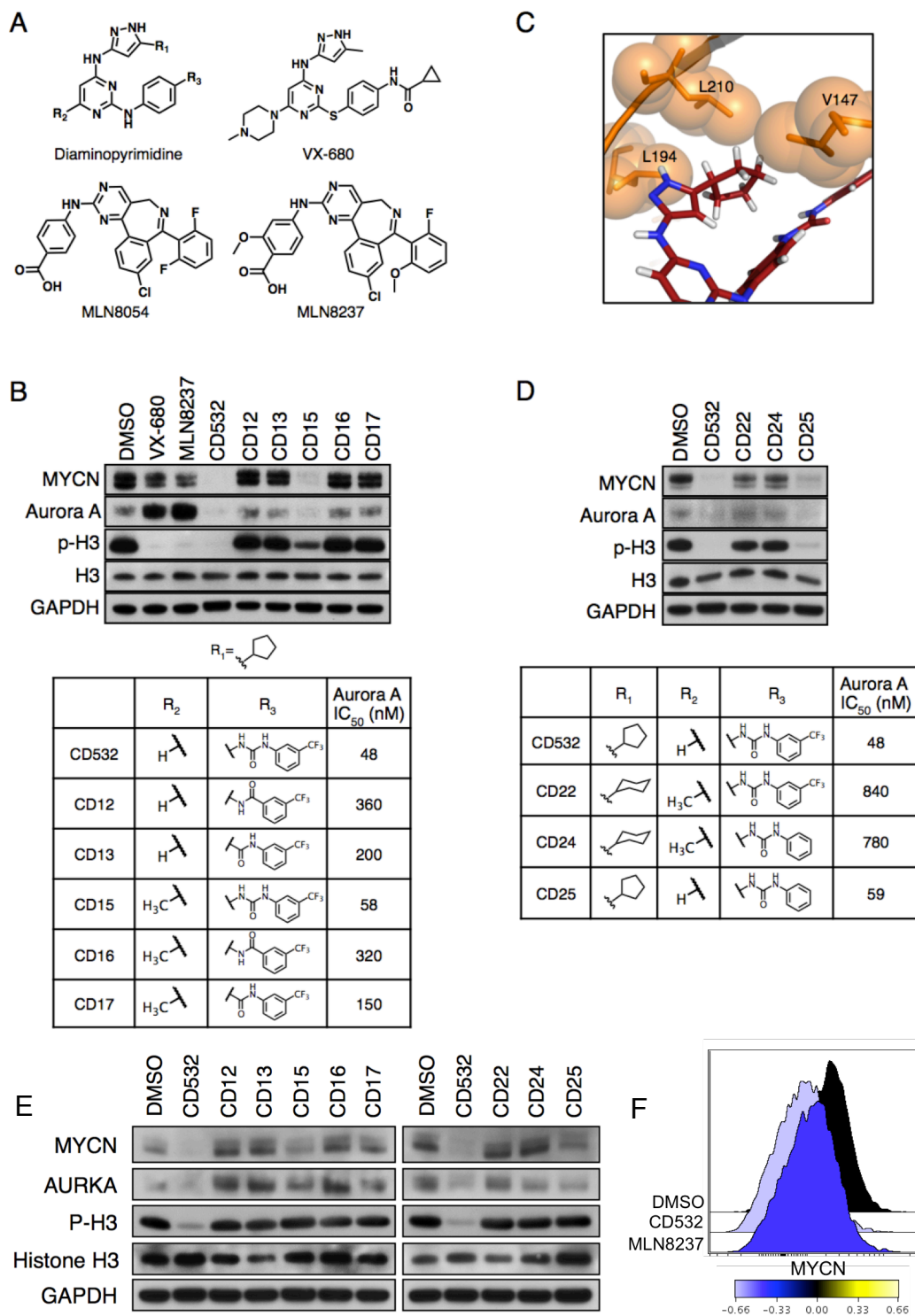
Figure 2.7: Structure-activity relationships of Aurora A inhibition and loss of MYCN.
(A) Chemical structures of CD compounds, VX-680, MLN8054, and MLN8237. (B immunoblot and table) Effect of replacement of critical urea moiety with amides and substitution at the 6-position of pyrimidine. (C) Hydrophobic packing of cyclopentyl of CD532 between V147, L194, and gatekeeper L210. (D immunoblot and table) Effect of substitution of hydrophobic ring or des-trifluoromethyl. All treatments were of SK-N-BE(2) cells for 24hrs at 1μM of compound. (E) Demonstration of structure-activity relationships in Kelly MYCN-amplified cells. (F) MYCN protein levels in SK-N-BE(2) cells as detected by flow cytometry.

37

that an additional methylene and adoption of the resulting six-membered ring into a chair conformation would preclude binding to Aurora A without abrogating binding to other kinases with a less bulky gatekeeper. Indeed, compounds CD22 and CD24 lost both potency against Aurora A and efficacy against MYCN (Figure 2.7D and E).

The sterically bulky trifluoromethyl interacts with and displaces the β1 and β2 strands, which stabilizes a global conformational change in Aurora A that is unable to protect MYCN from degradation (Figure 2.6D). We hypothesized that replacement of this group with a hydrogen would decrease the magnitude of the N-terminal displacement of Aurora A without altering binding affinity. Indeed, CD25 retained potency against Aurora Kinase A activity, demonstrated both biochemically and by loss of Histone H3 phosphorylation. However, CD25 was less effective than CD532 in driving MYCN loss, suggesting that the magnitude of the N-terminal shift of Aurora A contributes to MYCN destabilization (Figure 2.7D-F).

2.3.6 CD532 blocks S-phase entry and reduces MYCN in a mouse model of *MYCN*-amplified neuroblastoma

Both Aurora A and MYCN are critical to different phases of the cell cycle, and the functional consequences of Aurora A kinase inhibition and MYCN loss are distinct. Inhibition of Aurora A blocks mitosis, causing a G2/M arrest.[23] In contrast, MYC family proteins drive S-phase entry. Knockdown of MYCN protein blocks entry into S-phase causing a subsequent G0/G1 arrest.[26] To compare functional differences between conventional Aurora A kinase inhibition (MLN8237 or VX-680) with conformation disrupting Aurora A kinase inhibition, we treated *MYCN* amplified neuroblastoma cells and measured cell cycle by flow cytometry (Figures 2.8, 2.9, 2.10, and 2.11). As expected, treatment with MLN8237 or VX-680 resulted in G2/M arrest (Figures 2.8A and 2.9), consistent with inhibition of Aurora A kinase without a significant inhibition of MYCN. By contrast, CD532 resulted in potent loss of S-phase entry even after only 4 or 6 hrs of treatment, a result expected in response to inhibition of MYCN (Figures 2.8A, 2.9, 2.10, and 2.11C-D). This loss of S-phase was concomitant with loss of p-Histone H3 (Figures

38

2.5A and 2.8C), loss of p-pan-Aurora Kinase (Figure 2.8C), and with loss of MYCN protein (Figures 2.5B and 2.8D). As Aurora kinase inhibitors, MLN8237, VX-680 and CD532 all caused loss of phospho-pan-Aurora, detectable in a small fraction of cells by flow cytometry (Figure 2.8C). However, only CD532 also caused a loss of S-phase and MYCN (Figures 2.8A and D).
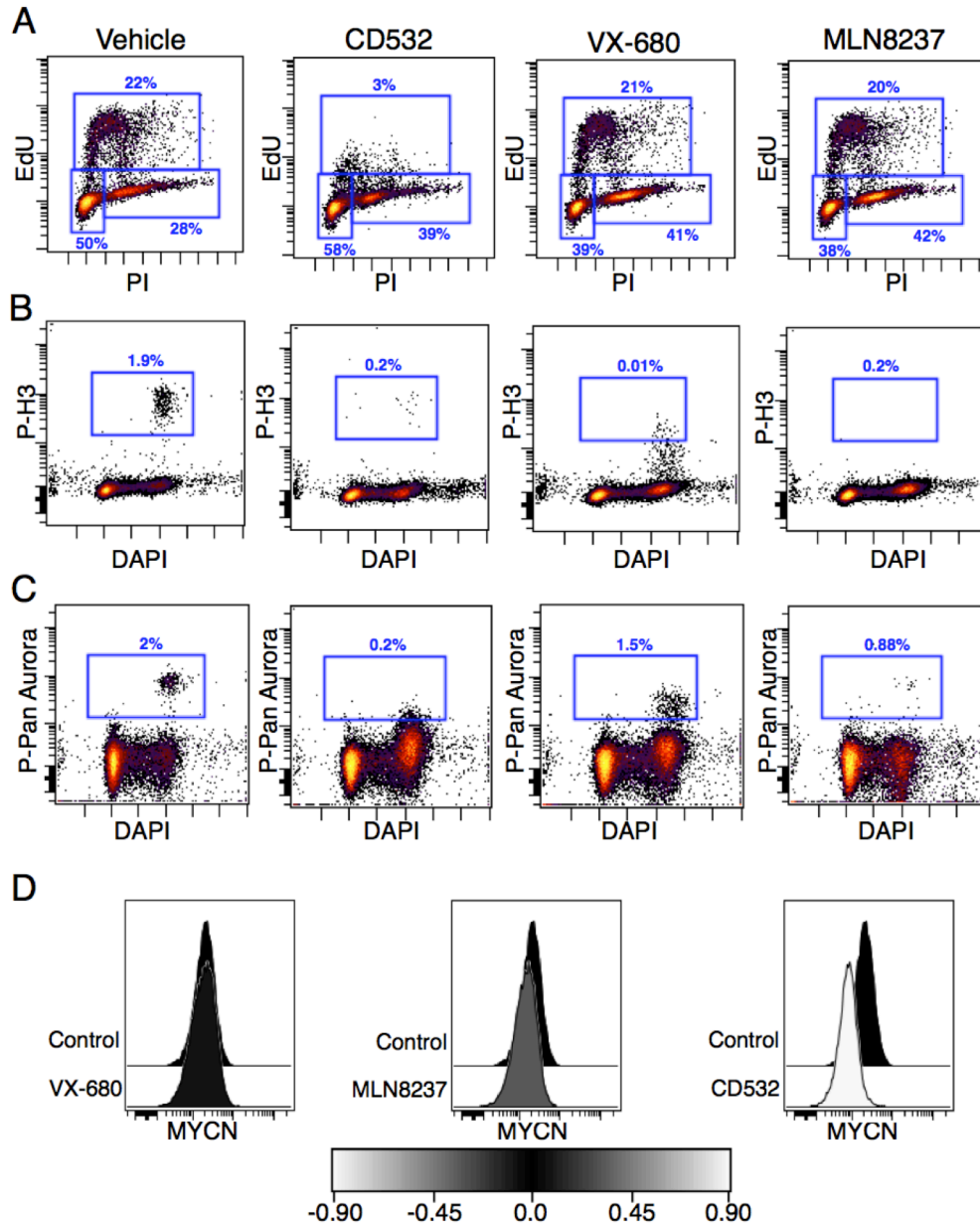
Figure 2.8: CD532 inhibits Aurora A kinase activity, downregulates MYCN, and blocks S- phase entry by flow cytometry. Cells were treated for 6hrs with the indicated drugs at 1μM and EdU was added 1hr prior to harvest to measure s-phase (A) cell cycle by EdU incorporation and propidium iodide staining (B) phospho-histone H3 (C) pan-Aurora phosphorylation (A, B, and C isoforms) and (D) MYCN protein.

39
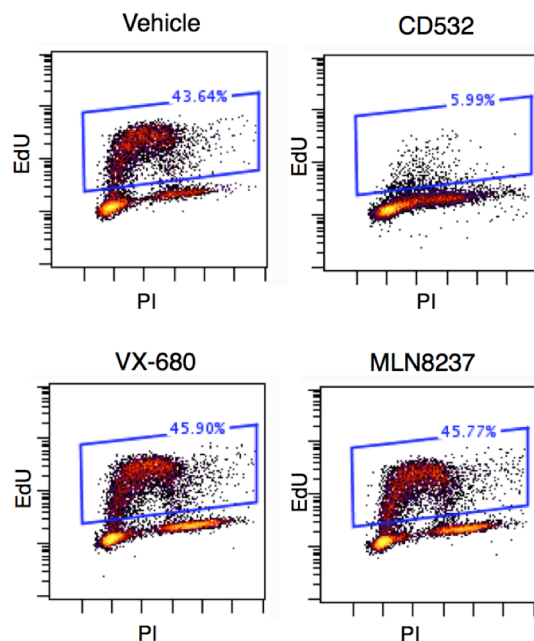
Figure 2.9: MYCN disruption causes loss of S-phase. Cell cycle analysis of MYCN-amplified Kelly neuroblastoma cells treated with 1uM of the indicated compound for 6hrs.

CD532 has the dual effect of blocking Aurora A kinase activity and driving degradation of MYCN. To further characterize the effects of CD532 on the cell cycle, we compared it with the bromodomain inhibitor JQ1, which has been shown to block MYCN downstream transcriptional activity, as well as *MYCN* gene transcription in neuroblastoma.[27] *MYCN* amplified neuroblastoma cells were treated for 24hrs with JQ1 to allow time for transcriptional events to occur. Treatment and resultant downregulation of MYCN in response to JQ1 resulted in blockade of S-phase entry and accumulation of cells in G_0/G_1 (Figure 2.10). Treatment with CD532 for 4hrs resulted in a rapid and potent loss of S-phase (consistent with the rapid and potent loss of MYCN protein) and accumulation in both G_0/G_1 and G_2, consistent with a mixed Aurora A/MYCN effect. Treatment with MLN8237 for 4hrs resulted in a modest downregulation of MYCN and accumulation of cells in G_2 and M phase, which has been described previously.[23] When JQ1 for 24hr (blocking MYCN) and MLN8237 for 4hr (blocking Aurora A kinase activity) were combined, an additive loss of S-phase and accumulation in G_2/M was observed, similar to CD532.
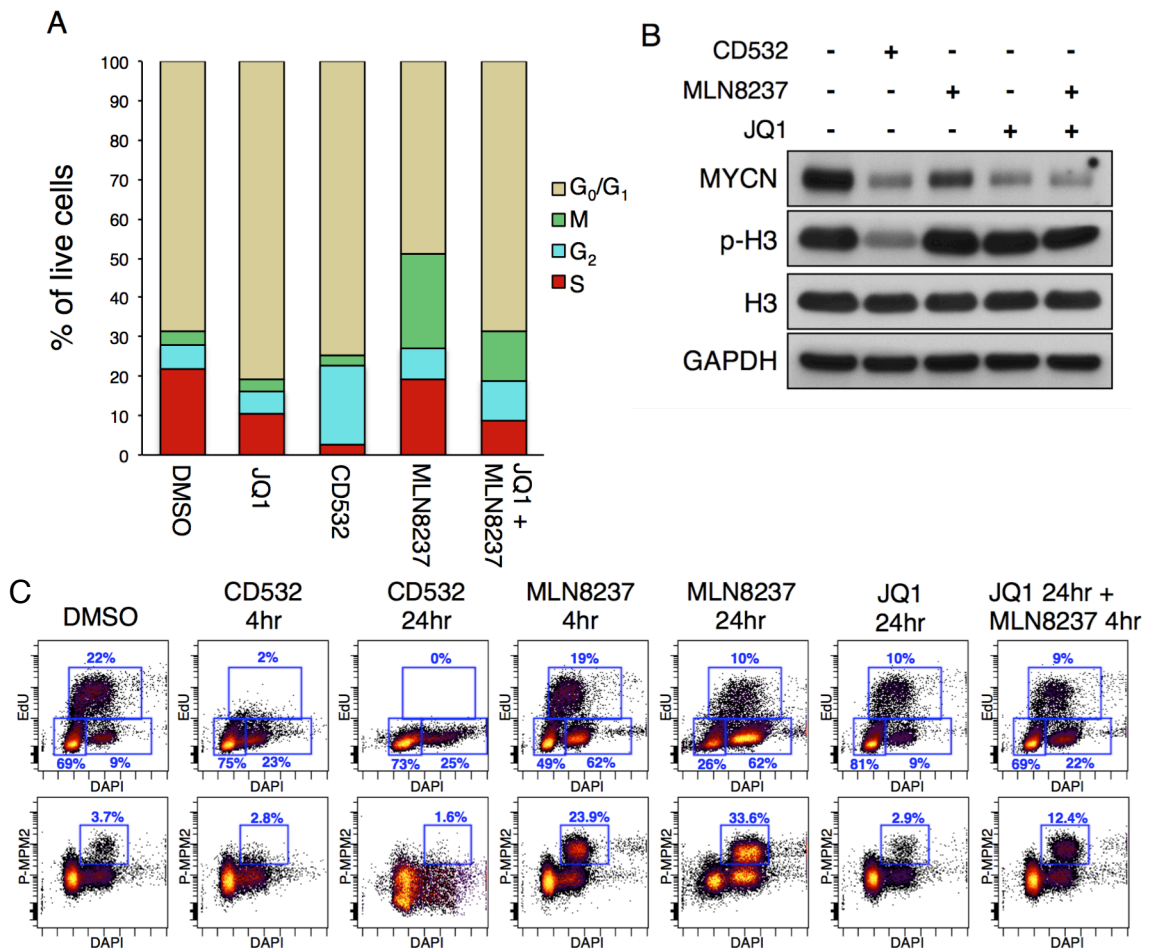
Figure 2.10: CD532 acts as a MYCN inhibitor. (A) Quantification of cell cycle of SK-N-BE(2) cells treated with CD532 (1μM, 4hr), MLN8237 (0.1μM , 4hr), JQ1 (2μM , 24hr), or MLN8237 (0.1μM, 4hr) in combinationwith JQ1 (2μM, 24hr). (B) Corresponding immunoblot demonstrating loss of MYCN in response to treatment with JQ1 and CD532 in SK-N-BE(2) cells. (C) Corresponding scatter plots to (A).

That the cell cycle and viability activity of CD532 but not MLN8237 is related to degradation of MYCN suggests that expression of MYCN might confer sensitivity to CD532. We therefore determined the cellular EC_{50} for these compounds against both GFP- and MYCN-transduced SH-EP neuroblastoma cells, which express little to no MYCN. Transduction of MYCN conferred sensitivity to CD532 but not to MLN8237 (Figure 2.11A-B). In addition, CD532-driven loss of S-phase in these cells could be rescued by the stabilizing $MYCN^{T58A/S26A}$ mutant (Figures 2.11D and E). These data suggest that the efficacy of CD532 is due primarily to loss of MYCN, whereas that of MLN8237 is due primarily to inhibition of Aurora Kinase A.
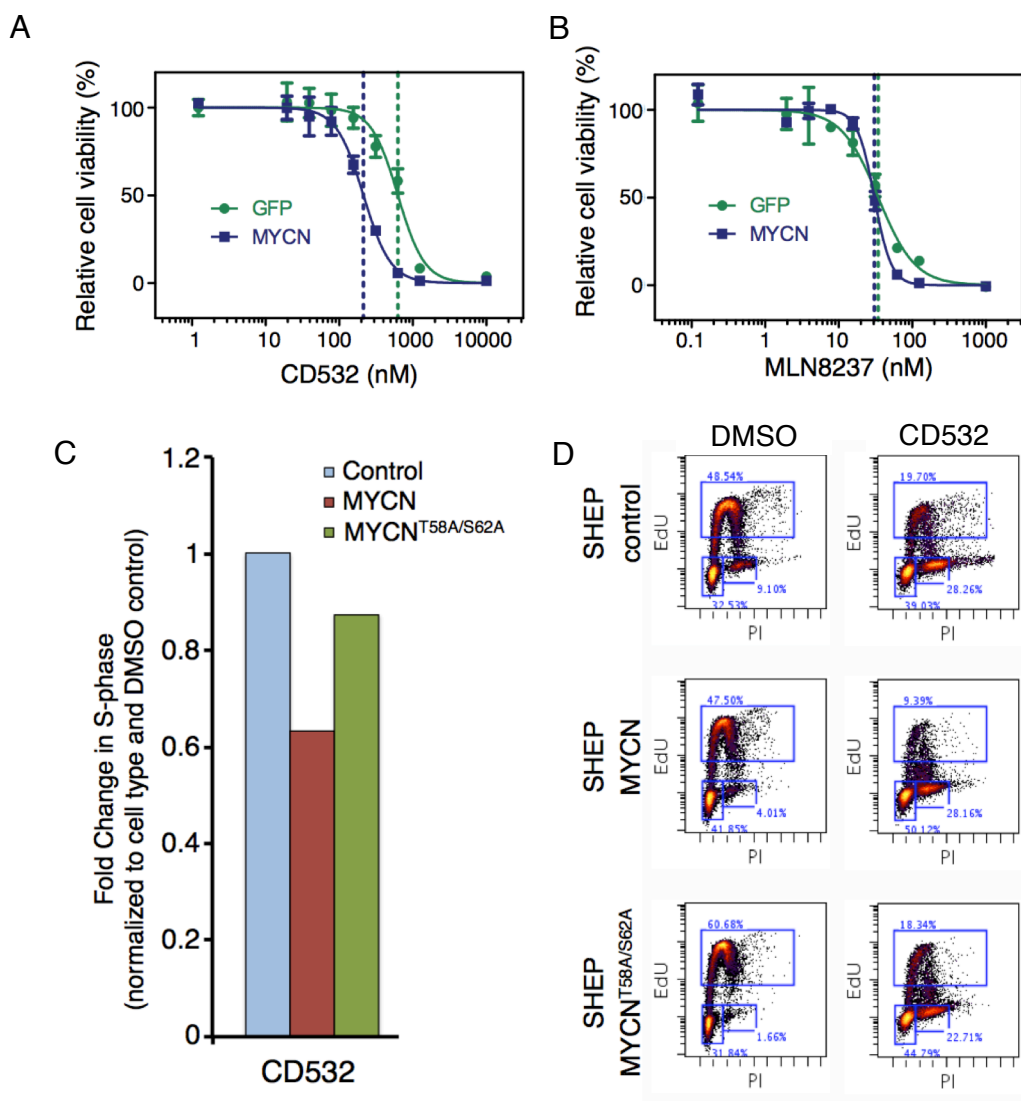
Figure 2.11: CD532 is a MYCN-directed therapy. Viability of SHEP cells transduced with MYCN or GFP after 72 hrs of treatment with (A) CD532 or (B) MLN8237. (C) Quantitation of S-phase fraction and (D) dot plot of SHEP non-MYCN-expressing neuroblastoma transduced with MYCN or mutationally-stabilized *MYCN^T58A/S62A* and treated with MLN8237 or CD532 for 6 hrs.

To determine whether MYCN might serve as a biomarker of sensitivity to CD532, we screened a panel 169 distinct tumor-derived and genetically characterized cell lines, including 93 lines for which MYCN copy number was available, and 87 lines for which mRNA expression data were available.[28] CD532 showed activity in most cell lines, with EC$_{50}$s in the nanomolar range, consistent with our results in neuroblastoma. Sensitivity to CD532 correlated with
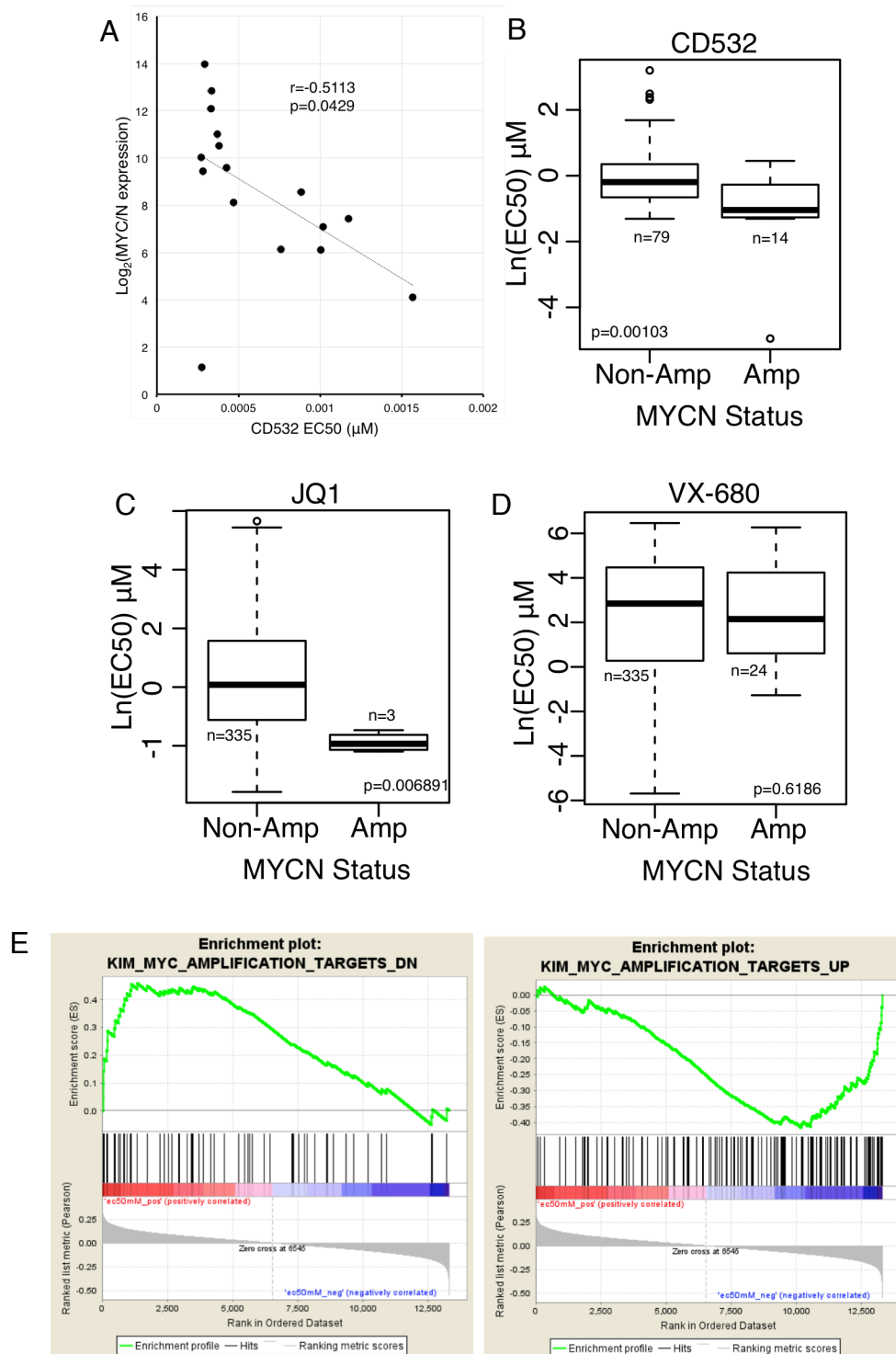
Figure 2.12: Cancer cell lines are sensitized to CD532 by MYC/N expression. (A) Plot of EC50 vs MYC+MYCN mRNA expression. Comparison of EC50s between MYCN amplified vs non-amplified cancer cell lines for (B) CD532 (C) JQ1 and (D) VX-680. Data for MLN8237 or MLN8054 were not available for this analysis. (E) Gene set enrichment analysis of 87 cancer cell lines against CD532 dose response showing enrichment of MYC-like gene expression profiles in susceptible lines, negative correlation between MYC genes up and EC_{50} and positive correlation between MYC genes down and EC_{50}.

43

expression of MYCN/MYC mRNA in neuroblastoma cells (Figure 2.12A). *MYCN* amplified cell lines were significantly more susceptible to CD532 than non-amplified lines (p=0.0010). In validation of this analysis, MYCN amplified lines were significantly more susceptible to JQ1 than non-amplified lines (p=0.0069), whereas MYCN amplified and non-amplified lines showed similar sensitivity to VX-680 (p=0.618; Figure 2.12B-D). Gene-set enrichment analysis revealed that susceptibility to CD532 correlated with a MYC signature, i.e. lowest EC_{50} in cells with highest expression of MYC targets and highest EC_{50} in cells with downregulated MYC targets (Figure 2.12E). These data support a broad potential for CD inhibitors of Aurora A against tumors in addition to neuroblastoma, and suggest a role for CD Aurora A inhibitors in both MYC and MYCN driven diseases.
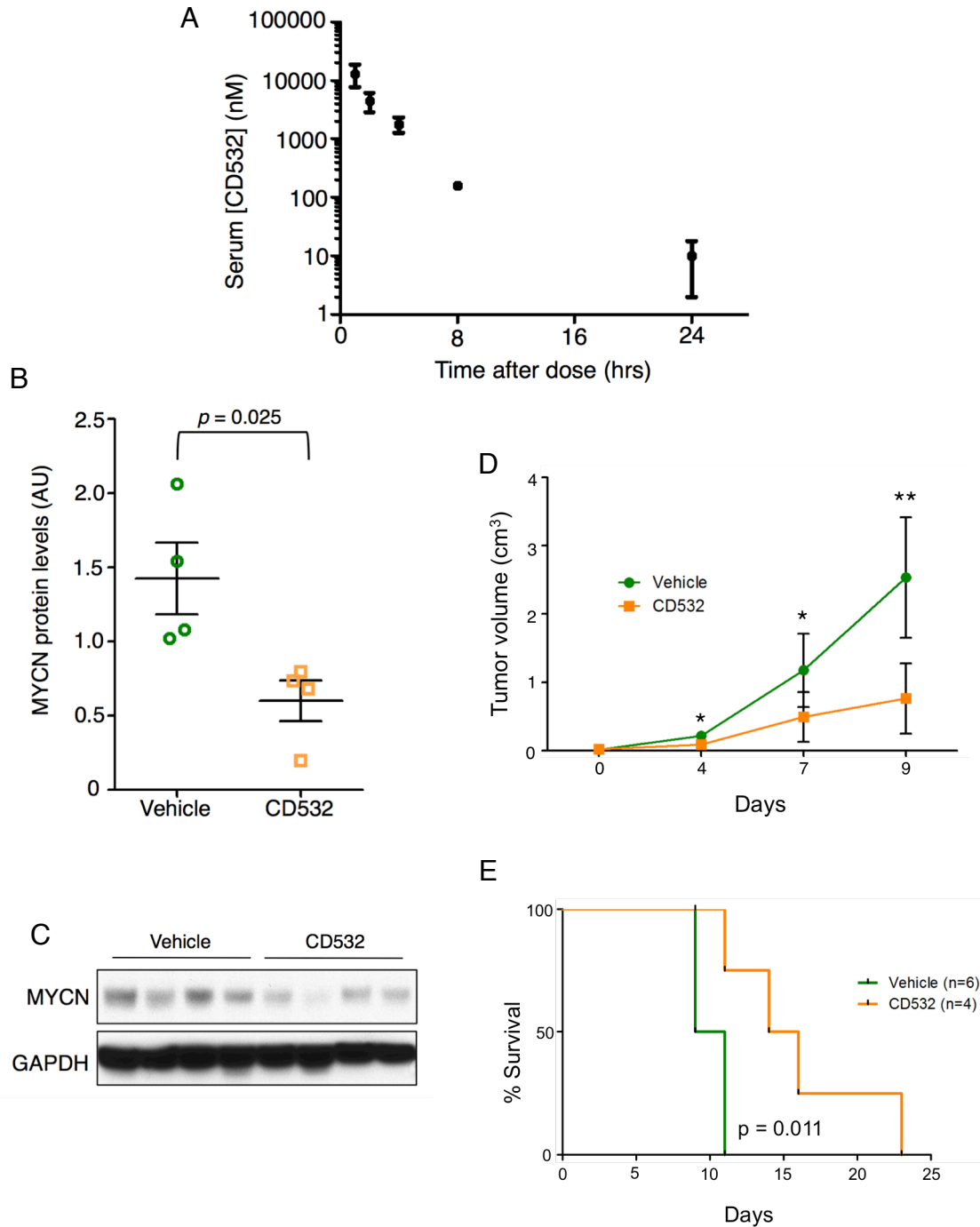
Figure 2.13: Conformation disruption of Aurora A downregulates MYCN *in vivo* and is effective in medulloblastoma. (A) Serum levels of CD532 after single intraperitoneal injection at 20 mg/kg. (B) Quantification and (C) immunoblot of MYCN protein from MYCN-amplified KCN neuroblastoma xenografts in mice treated daily for 2 days with 60 mg/kg CD532. (D) Tumor burden and (E) survival of mice with an allograft model of SHH-subtype medulloblastoma given 25 mg/kg CD532 twice weekly.

While CD532 represents a first-in-class tool compound, not yet optimized for *in vivo* pharmacokinetics, we nevertheless assessed in-vivo pharmacokinetic properties. Studies in mice revealed a serum half-life of ~1.5 hrs, providing for an AUC_{0-24} of 27 μM*h when delivered at 20 mg/kg (Figure 2.13A). This is in contrast to clinically developed compounds, such as MLN8237, which has an AUC_{0-24} of 78.4 μM*h when delivered at the same dose.[29] Nonetheless, treatment of *MYCN*-amplified neuroblastoma xenografts with CD532 led to decreased levels of MYCN protein (Figures 2.13B and C), demonstrating that CD532 can block MYCN protein *in vivo*.

To extend these in-vivo data to additional MYCN-driven tumors, we tested medulloblastoma, in which MYCN activation is prominent (Swartling et al., 2010). The sonic hedgehog (SHH) subtype of MB commonly shows misexpression of MYCN, as SHH signaling promotes both expression and post-transcriptional stabilization of MYCN (Kenney et al., 2003; Thomas et al., 2009). We treated a MYCN-expressing SHH-subtype MB allograft derived from $Ptch^{+/-};p53^{-/-}$ mice to assess for tumor burden and survival (Kim et al., 2013; Romer et al., 2004). CD532 at 25 mg/kg twice per week was sufficient to substantially reduce tumor burden as well as extend survival in these mice (Figure 2.13D-E). Notably, the only apparent toxicity was a reversible (~24 hours) functional ileus, likely due to the intraperitoneal delivery of CD532.

2.3.7 Disruption of the MYCN-Aurora A complex depends on the magnitude of conformational change in Aurora A

Despite its potency against Aurora A kinase activity and modest effect on the conformation of Aurora A,[19] MLN8237 subtly decreased MYCN protein levels compared to CD532 (Figures 2.3, 2.5A, 2.7B). To test how the degree of conformational shift in Aurora Kinase A affects binding of MYCN and Aurora A, we measured the MYCN-Aurora A interaction in *MYCN*-amplified neuroblastoma cells treated with increasing concentrations of CD532 or MLN8237. CD532 inhibited histone H3 phosphorylation at concentrations 10-fold higher than MLN8237, consistent with their respective biochemical IC_{50}s and cellular EC_{50} (Figure 2.14A-B). However, CD532 caused a dose-dependent and complete dissociation of the MYCN-Aurora A

complex at 2h, whereas MLN8237 only modestly disrupted this interaction (Figure 2.14). This dissociation did not occur with VX-680 treatment, and was specific to the MYCN-Aurora A interaction, as CD532 did not affect MYCN-MAX binding (Figure 2.15). Notably, disruption of the MYCN-Aurora A complex by CD532 occurred at doses comparable to those required to block p-H3, consistent with conformation-disruption as a consequence of CD532 binding (Figure 2.14A). This is in contrast with MLN8237, which showed only partial disruption of the complex upon maximal Aurora A inhibition. Thus MLN8237, a more potent Aurora binder, only modestly decreased the affinity of Aurora A for the MYCN complex. By comparison, CD532 binds Aurora A with lower affinity, but has a dramatic effect on Aurora A binding to the MYCN complex (Figure 2.14C).
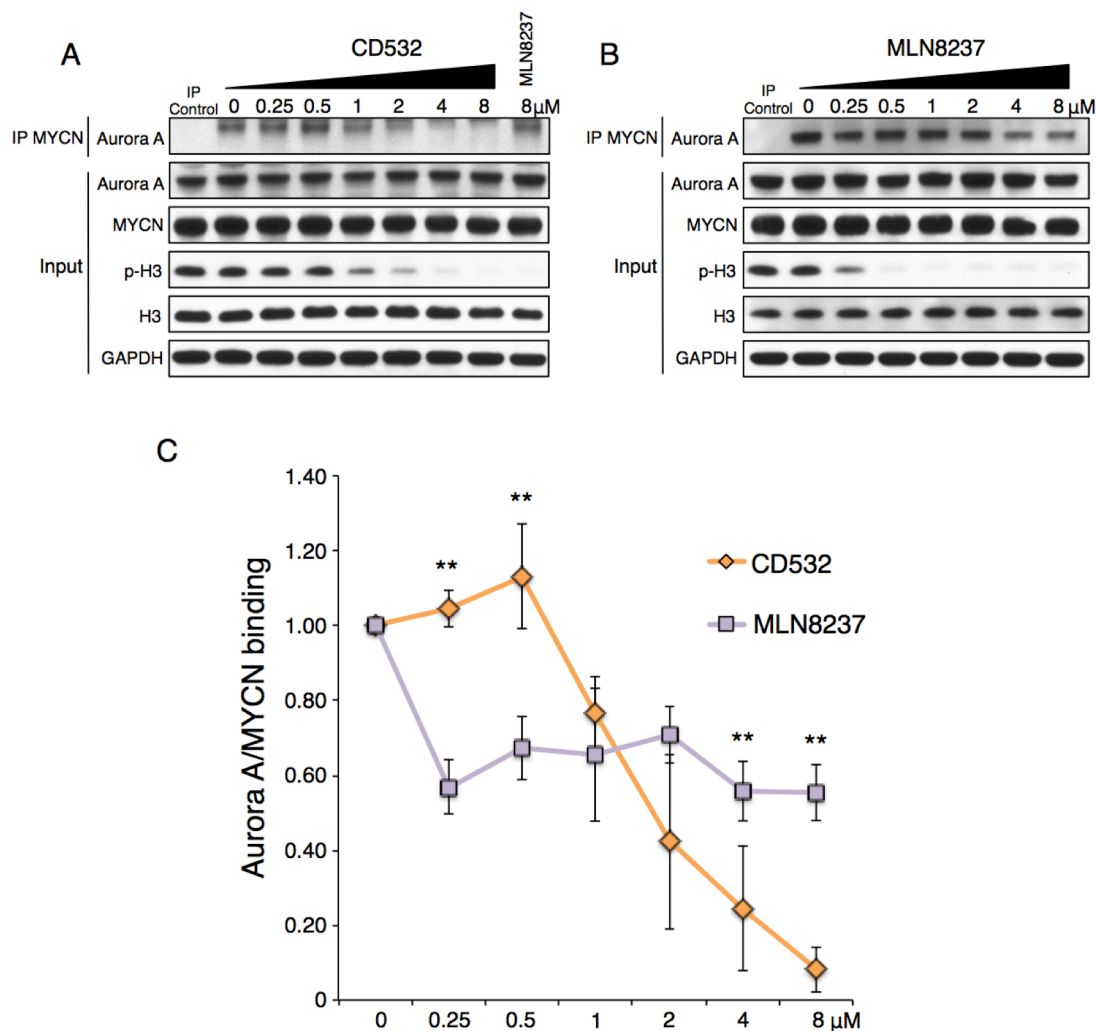
Figure 2.14: CD532 and MLN8237 have distinct kinetic effects on MYCN loss and Aurora A kinase inhibition. Representative immunoprecipitation of MYCN and immunoblots from MYCN-amplified IMR32 cells treated for 4 hrs with MG-132 and 2 hrs with increasing concentrations of (A) CD532 or (B) MLN8237. (C) Quantification of Aurora A/MYCN binding from triplicate experiments. CD532 causes complete and dose-dependent loss of Aurora A/MYCN interaction, whereas MLN8237 causes partial loss of interaction, consistent with CD532 conferring a larger magnitude scaffold disruption of Aurora A with a higher biochemical IC50 for kinase inhibition compared to MLN8237.

Data in Figure 2.3 demonstrate that VX680, MLN8237 and CD532 show increasing activity in driving destabilization of MYCN protein in *MYCN* amplified cell lines. Comparing the published structures of Aurora A bound to VX-680 and MLN8054 with our structure of Aurora A bound to CD532 demonstrates a progressive disruption of the conformation of Aurora A (Figure 2.16A). As intended through use of the diaminopyrimidine scaffold for screening, CD532 binds

to Aurora A at the hinge region via a pyrazole moiety in a manner similar to VX-680 (Figure 2.16A), yet interacts with other parts of the Aurora A binding pocket to confer distinct biological effects (loss of MYCN, decreased viability, and loss of S-phase), biophysical effects (shift in tertiary structure), and biochemical effects (disruption of the Aurora A/MYCN complex). Thus the ability of VX-680, MLN8237 and CD532 to progressively displace the a-C helix in Aurora (a structural measure which tracks directly with MYCN proteolysis, Figure 2.16B and C) illustrates how a starting scaffold can be modified to effect divergent biochemical and biological activities.
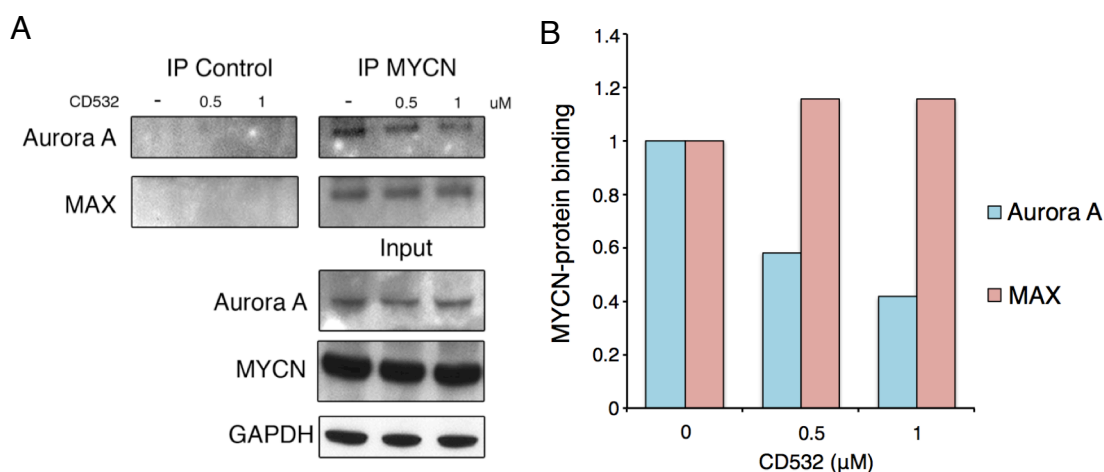
Figure 2.15: Allosteric disruption is specific to the MYCN-Aurora A complex. (A) SK-N-BE(2) cells were treated with CD532 for 2 hrs before immunoprecipitation of MYCN and immunoblot for Aurora A or MAX. (B) Quantitation of MYCN-Aurora A and MYCN-MAX interactions in response to increasing concentration of CD532.

2.4 Discussion

Earlier studies of Aurora kinases clarified a central role for Aurora Kinase A in mitosis and transformation. Inhibitors of Aurora A have therefore been developed as therapeutics, and are currently being tested across a range of cancers. Aurora A shares significant structural and sequence similarity with Aurora B, although these proteins have both distinct mitotic functions and distinct subcellular localizations. These differences in both function and localization are

attributed in part to the specific association of each kinase with a unique group of cofactor proteins (reviewed in [30]).
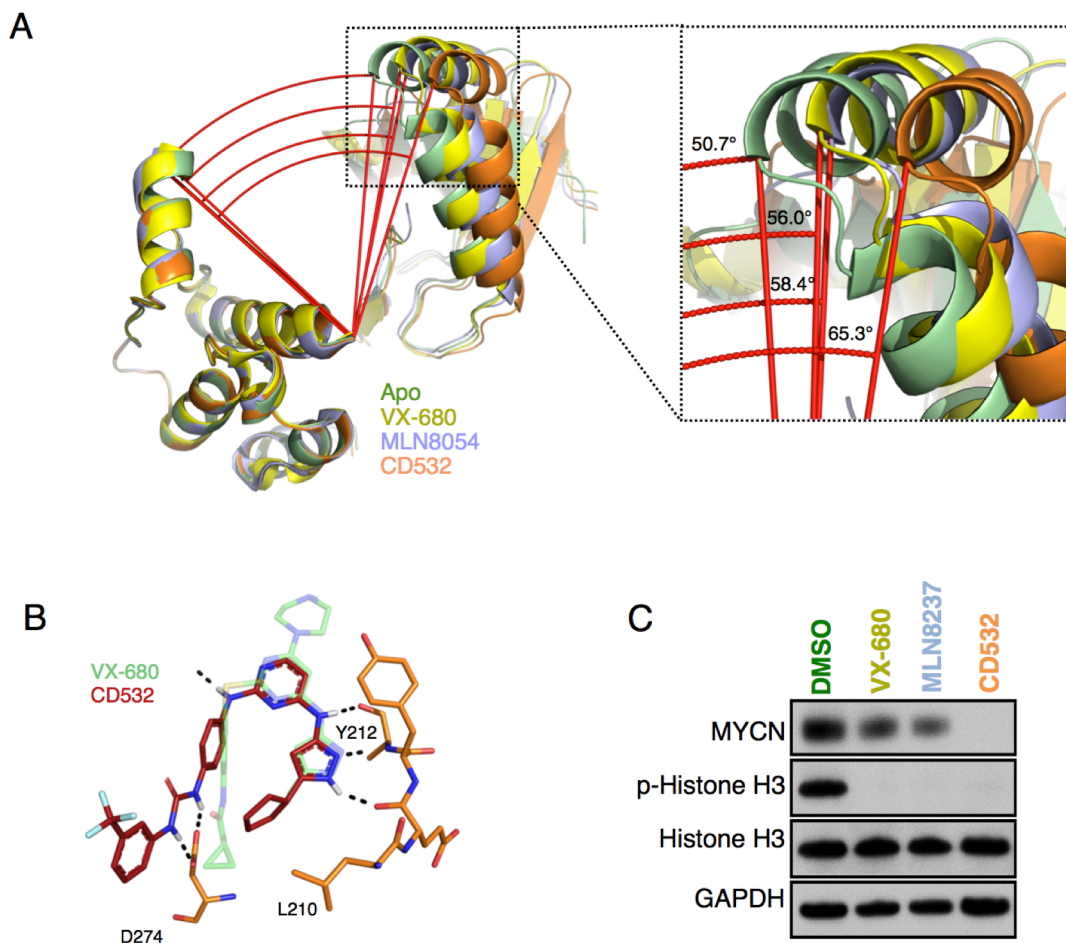
Figure 2.16: Loss of MYCN tracks with the degree of conformational change in Aurora Kinase A. (A) Angle between α-carbons of T333, E308, and A172 of Aurora A Apo (4J8N, green), Aurora A with VX-680 (3E5A, yellow), Aurora A with MLN8054 (2WTV, purple), and Aurora A with CD532 (4J8M, orange). (B) Comparison of binding modes of VX-680 and CD532 showing identical hinge binding. (C) Immunoblot of MYCN protein after 24hr treatment of SK-N-BE(2) cells with VX-680, MLN8237, and CD532.

Here we describe a class of compounds that were initially designed to bind Aurora A in a type II fashion, defined by the DFG-out orientation of D274, as a strategy for disrupting the conformation of this kinase. Thus it was surprising to observe that CD532 binds Aurora A as DFG-in, yet still induces a larger conformational disruption than the only known true type II Aurora inhibitors.[31] Comparison of CD532-bound Aurora to the Apo structure shows the

50

activation loop in the inactive orientation, accompanied by a shift in the entire N-terminal domain. Although the activation loop flip is consistent with an inactive conformation of Aurora Kinase A, polar contacts with the urea moiety of CD532 interact with the DFG motif, locking it in the active "DFG-in" orientation. This unusual conformation is achieved through a steric clash of the trifluoromethylphenyl moiety of CD532 with Aurora's N-terminal β1 and β2 strands, displacing the N-terminal lobe of Aurora A and allowing a unique network of hydrogen bonds to stabilize the activation loop in an inactive orientation.

Our structural data also suggest a novel mechanism through which an inhibitor can stabilize the inactive conformation of a kinase. Previously described inhibitors that stabilize kinases in their inactive conformation displaced the aspartic acid of the catalytic DFG motif, with a concomitant crankshaft-like 180° rotation of the DFG backbone. In contrast, CD532 induces this inactive conformation through interaction with the β1/2 strands of the N-terminal domain, without reorienting the DFG motif. Our structure thus reveals a unique "uncoupling" of the DFG-flip from the inactive state of a kinase. Whether such uncoupling plays a role in the physiological state of the kinase, perhaps as part of its regulation, or only occurs in the presence of specific pharmacological entities, remains to be determined.

Can these specific associations be exploited to identify inhibitors of Aurora Kinases that also disrupt interactions with cofactor proteins? The resulting conformation of CD532-bound Aurora A blocks both kinase-dependent and MYCN-stabilizing, kinase-independent functions of Aurora A. CD532 inhibits Aurora Kinase A at low nanomolar concentrations, and in parallel, effects proteolytic degradation of MYCN. Importantly, we were unable to uncouple kinase inhibition and MYCN proteolysis through structural modification of CD532, consistent with disruption of Aurora Kinase A's scaffold as a result of bulky pharmacophores that extend from an ATP-competitive core.

The difference in the kinetics of complex dissociation between CD532 and MLN8237 (Figure 2.14), coupled with their respective IC_{50}s and crystallographic information (Figures 2.2

and 2.6), sheds insight into the biophysical basis for disruption of the Aurora A-MYCN interaction. While MLN8237 is a potent inhibitor of Aurora A (4 nM), it only modestly disrupts the conformation of Aurora A (Figure 2.16C). Thus, while MLN8237 inhibits Aurora A kinase activity at low concentrations, even saturating doses only partially disrupt the complex between Aurora and MYCN (Figure 2.14C). In contrast, CD532 is a weaker inhibitor of Aurora Kinase A, however saturating doses lead to complete dissociation of the complex. Taken together with structural data, these observations suggest that the equilibrium of dissociation of the MYCN-Aurora A complex is dependent upon the degree of conformational disruption of Aurora A.

Several other inhibitors of Aurora kinase are in clinical development, all of which are act as mitotic poisons much like current cytotoxic chemotherapy agents. Our functional data show that CD532 acts more as a potent MYCN inhibitor, rather than a conventional Aurora A inhibitor in neuroblastoma, and has potential to act as a c-MYC inhibitor in other cell types, as measured by cell line susceptibility profiling. While the pharmacokinetic properties of CD532 have not been optimized, CD532 could effect loss of MYCN protein in neuroblastoma xenografts (Figure 2.13), providing motivation for additional medicinal chemistry and optimization of this family of compounds for use *in vivo*.

Neuroblastoma is the most common extracranial solid tumor of childhood and *MYCN* amplification is the best-described genetic lesion marking high-risk, chemotherapy resistant disease. Targeted expression of MYCN drives neuroblastoma in systems from mice to zebrafish.[32,33] We have previously finessed destabilization of MYCN through blockade of upstream PI3K/mTOR inhibition[34,35] and through an alternative approach to block MYCN and its transcriptional targets is through use of BRD4-based bromodomain inhibitors.[27] Here we propose a third strategy to block MYCN in cancer. These three interventions, at distinct nodes in the same oncogenic pathway, present a unique opportunity for combinatorial, targeted therapeutics to block emergent resistance, while maximizing the blockade of MYCN in neuroblastoma and potentially in other *MYCN*- and *MYC*-driven cancers.

Allostery is most generally defined as a phenomenon whereby a perturbation by an effector at one site of the molecule leads to a functional change at another through alteration of shape and/or dynamics.[36] There are several recent examples of allosteric inhibitors for the treatment of cancer including arsenic trioxide, an anti-leukemic which binds to zinc fingers within the PML-RARAα fusion protein of acute promyelocytic leukemia to induce a conformational change favoring oligomerization and eventual degradation[37] and biculutamide which binds to the androgen receptor to block transcription in prostate cancer.[38] Enzymes, including but not exclusive to kinases like Aurora A, may have important non-enzymatic activities including scaffolding, regulation, and localization of other proteins. As such, many molecular interactions necessary for cellular function and carcinogenesis are not targetable directly with small molecules, either because they have no amenable binding pocket (as with MYC proteins) or because their affinity for natural substrate is too high (as with many GTPases such as RAS). By contrast, orthosteric targeting of small molecules to enzymes like kinases has become relatively trivial. Here we refer to an ATP-mimetic ligand that binds the active site of Aurora A to alter its kinase-independent stabilization of MYCN, but also, obligately, its kinase activity. We propose that such an inhibitor be referred to as "amphosteric", denoting an inhibitor that is simultaneously both orthosteric (inhibiting kinase activity) and allosteric (disrupting protein-protein interactions). Thus, CD532 represents the prototype of a new class of amphosteric inhibitors that induce an allosteric change to disrupt non-enzymatic functions of enzymes. As these amphosteric effects are neglected in most current inhibitor screening, development of small molecule screens for other amphosteric inhibitors has the potential to target other undruggable oncoprotein targets.

2.5 Materials and Methods

Cell culture, inhibitors, and western blotting

Neuroblastoma tumor cell lines were obtained from the University of California San Francisco Cell Culture Facility (Kelly, SK-N-BE2, and SH-EP). SMS-KCN, SHEP MYCN^{wt} and MYCN$^{T58A/S62A}$ cells were obtained from Martin Eilers lab. All cells were grown in RPMI with 10% FBS. Neuroblastoma cells were harvested and lysed with Cell Signaling Lysis buffer + 1% SDS, sonicated and supernatants boiled in LDS sample buffer (Invitrogen). Western blots were performed as described previously,[34] with primary antibodies to MYCN (ab24193, Abcam), Histone H3, P-Histone H3 (S10), Aurora A (Cell signaling), and GAPDH (Millipore). Western blot quantitation performed with ImageJ software. VX-680 (S1048) and MLN8237 (S1133) were obtained from Selleck chemicals.

Flow cytometry and viability

Neuroblastoma cells were treated for the indicated time, trypsinized, washed, stained with Dylight 800 at 0.3 µg/mL (Pierce, 46421), fixed with 1.5% PFA, and permeabilized with 100% methanol. Cells were then stained with antibodies against p-MPM2 (Millipore, 16-155), p-pan-Aurora (Cell Signaling, 2914), MYCN (Thermo, PA5-17403), rabbit IgG (Invitrogen, A10542), or mouse IgG (BioLegend, 405307). Cells were stained with DAPI at 0.3 µg/mL (Invitrogen, D21490) and analyzed on the BD LSR II flow cytometer. For cell cycle analysis, cells were stimulated with EdU for 2 hours prior to harvest, then probed using the Click-iT EdU Flow Cytometry Assay Kit (Invitrogen, C10424). Cells were stained with propidium iodide (BD, 556547) and analyzed on the BD FACSCalibur flow cytometer. Data was gated using Cytobank. For viability studies, neuroblastoma cells were plated in 96-well plates at a density of 1,000 cells/well for SHEP or 4,000 cells/well for Kelly or SK-N-BE2 cells, then incubated with indicated concentrations of drug for 72 hours at 37°C. Plates were frozen at -80°C to induce cell lysis. CyQUANT reagent mixture (Invitrogen, C7026) was added to thawed plates, then

fluorescence was measured. Alternatively, resazurin (Sigma-Aldrich, R7017) was added directly to wells following drug treatment then incubated for 4 hours at 37°C prior to measuring fluorescence. Data was analyzed using GraphPad Prism software.

Pulldowns

Cells were pretreated with MG-132 (Calbiochem, 474790) at 5 ug/ml for 4 hours and with drug (CD532, MLN8237, or VX-680) for 2 hours before lysis with TNN lysis buffer in the presence of protease inhibitor (Sigma-Aldrich, P8849). Pulldowns were performed with anti-N-Myc antibody (Santa Cruz, SC-53993) and Protein G sepharose beads (Sigma-Aldrich, P3296). Immunoblots were performed as described above.

Chemical synthesis

Starting materials were purchased from Sigma-Aldrich or Alfa Aesar. Unless otherwise noted, reactions were performed in dry, argon-charged, glass roundbottom flasks and monitored by thin layer chromatography (TLC) or liquid chromatography-mass spectrometry (LCMS). Compounds were characterized by LCMS and nuclear magnetic resonance (NMR) spectroscopy. LCMS retention times (RT) are reported in minutes based on a gradient of 5-95% ACN/H_2O from t=0.1-1.9 min. NMR shifts (δ) are reported in ppm as singlets (s), doublets (d), quartets (q), quintets (quin), or multiplets (m). High-performance liquid chromatography (HPLC) was conducted using a Waters 2545 binary gradient module, Waters 2767 sample manager, and Waters 2998 photodiode array detector running MassLynx v4.1. Flash/silica gel chromatography was performed on an AnaLogix Intelliflash using SuperFlash Si50 columns (Agilent). Synthetic procedures can be found in Section 2.6 below.

Expression and purification of Aurora A Kinase

Purification and expression of Aurora A was performed as described previously,[31] with the following modifications. Aurora A (residues 123-390, T287D) was cloned into a pET28a plasmid providing fusion with a PreScission Protease-cleavable hexahistidine tag. The protein was overexpressed in BL-21(DE3) cells at 18º C. Digestion with PreScission protease was

performed overnight at 4º C in a 10 kD MWCO dialysis cartridge (Thermo Scientific, Inc) with dialysis buffer containing 50 mM MES (pH 6.5), 300 mM NaCl, and 1 mM DTT, followed by 4 hours of dialysis with buffer containing 50 mM MES (pH 6.5) and 1 mM DTT before loading onto ion exchange column. Pooled fractions were concentrated to 5 mg/mL (Amicon Ultra 10 kD MWCO, Millipore) and loaded onto a HiLoad Prep Grade Superdex 200 column (GE Healthcare) equilibrated with 50 mM HEPES (pH 7.4) and 1 mM DTT to yield monomeric enzyme for use in both kinase assays and crystallization.

Gene Set Enrichment Analysis (GSEA)

Normalized gene expression (Affymetrix HT-HGU133A) was downloaded from the Genomics of Drug Sensitivity in Cancer website (http://www.cancerrxgene.org/downloads/) and log-transformed. 87 cell lines had both unambiguous EC_{50} (calculated using four-parameter non-linear regression within GraphPad Prism) and gene expression data.

GSEA software [39] was used to identify groups of functionally related genes correlated with sensitivity to CD-532. GSEA was run on these 87 cell lines using the collections of 4,722 curated gene sets (C2) and 615 transcription factor targets (C3) from MSigDB (v4.0). Using the individual EC_{50} of each cell line as a continuous phenotype, genes were ranked using Pearson's correlation, and P values were calculated using 1,000 gene set permutations. Gene sets with less than 15 genes or more than 500 genes were excluded from the analysis. Gene sets with an FDR $\leq$ 0.05 and a nominal P $\leq$ 0.05 were considered significant.

Cell-line status for MYCN amplification and drug sensitivity data for VX-680 were downloaded from the Genomics of Drug Sensitivity in Cancer website. Cell-line sensitivity to JQ1 has been previously published.[27] Amplified cells possessed MYCN copy number $\geq$ 8. The significance of sensitivity of CD-532 (EC_{50} calculated using the four-parameter log-logistic function in R using the "drc" package), JQ1, and VX-680 in relation to MYCN amplification status was assessed using the Wilcoxon Rank Sum test in R.

In vivo studies

For pharmacokinetic studies, CD532 was formulated at 20 mg/ml in 7.5% DMSO and 92.5% PEG300. LC-MS/MS detection of CD532 was performed using a Waters 2545 binary gradient module, Waters 2767 sample manager, and Waters 2998 photodiode array detector running MassLynx v4.1. For neuroblastoma studies, NOD scid gamma mice (Jackson Laboratory) with renal capsule SMS-KCN xenografts were treated for two days with 60 mg/kg CD532 before tumors were flash frozen for analysis. For medulloblastoma studies, homozygous nu/nu mice (Simonsen labs) with flank subcutaneous allografts of SHH-subtype MYCN-expressing medulloblastoma were started on treatment once tumors reached 25 mm^3 in volume. Mice were treated with vehicle (5% DMSO in PEG300) or CD532 (25 mg/kg, formulated at 7.5 mg/ml) twice per week. Mice were euthanized once maximum tumor length reached 2.0 cm, per IACUC protocol. Difference in tumor burden was evaluated by two-tailed student's T-test, and difference in survival by log-rank test. Mice were injected intraperitoneally.

In vitro kinase assays

Kinase assays for Aurora A were performed in 10 mM HEPES pH 7.5, 10 mM MgCl$_2$, 0.01% Triton, 4% v/v DMSO, 5 nM kinase, and either 4 μM histone H3 or 30 μM synthetic peptide AKRRRLSSLRA (Elim Biopharmaceuticals, Inc). Drug concentration ranged from 2000-5 nM. Reactions were preincubated with inhibitor for ten minutes before initiation by addition of 100 μM nonradioactive ATP supplemented with ^{32}P ATP (1 mCi in 200 μL, Perkin-Elmer, 0.8 μCi per reaction). Reactions were quenched at 10 min by spotting 3 μL quantity onto P81 phosphocellulose (Whatman), which were washed 5x5' in 0.1% phophoric acid and dried. Radioactivity was measured by phophorimaging and recorded on a Typhoon fluorescence imager (Molecular Dynamics). Data were quantified using Spot[40] and fit to a sigmoidal dose-response curve using Prism software (GraphPad Software, Inc) to obtain IC$_{50}$ values.

Crystallization and data collection

After gel separation, purified fractions of Aurora A were pooled and concentrated in the presence of drug to a final concentration of 20 mg/ml Aurora A and 1 mM drug. All crystallization reagents were obtained from Hampton Research (Aliso Viejo, CA). Crystals were generated by hanging drop vapor diffusion at room temperature using a 1:1 mixture of protein solution and well solution. For Aurora A apo, well solution consisted of 10% Tacsimate (pH 7.0) and 20% PEG 3350. For Aurora A with CD532, well solution consisted of 0.2 M magnesium acetate tetrahydrate, 0.1 M sodium cacodylate trihydrate and 20% w/v PEG8,000 at pH 6.0. Crystals did not grow in the Apo conditions in the presence of drug, or in the drug conditions in the absence of compound. CD532-bound and apo crystals were cryoprotected with well solution supplemented with 10% and 25% ethylene glycol, respectively, and stored in liquid nitrogen. Diffraction data were recorded on Beamline 8.2.2 at the Lawrence-Berkeley Advanced Light Source at a temperature of 100 K and wavelength of 1.0088 nm. Data were indexed using HKL2000 (HKL Research, Inc). The drug-bound crystals belong to the $C222_1$ space group with one monomer in the asymmetric unit, and apo crystals belong to the $P3_1$ space group with four monomers in the asymmetric unit. Molecular replacement and refinement were performed using Phaser-MR and phenix.refine in PHENIX,[41] model building was performed using Coot,[42] and figures were drawn using MacPYMOL 1.5.0 (Schrodinger, LLC). Data and refinement statistics are shown in Supplementary Table S1. Atomic coordinates and structure factors for CD532-bound and Apo Aurora A have been deposited in the PDB as 4J8M and 4J8N, respectively.

2.6 Synthetic procedures

CD532, CD25:

3-cyclopentyl-3-oxopropanenitrile (JM2)

To a dried, argon-charged roundbottom flask with large stir bar was added anhydrous tetrahydrofuran (160 ml), which was then cooled to -78o C before addition of 2.5 M n-Butyllithium in hexanes (64 mL, 160 mmol). Reaction was stirred for 5 minutes before addition of anhydrous acetonitrile (8.48 mL, 160 mmol) dropwise over 5 minutes. Reaction was stirred for 90 minutes at -78o C, followed by dropwise addition methylcyclopentane carboxylate (10.28 ml, 80.4 mmol) over 10 minutes. Reaction was allowed to stir for another 2 hours at -78o C, allowed to warm to room temperature, and stirred for an additional 30 minutes. Reaction was quenched with 240 ml H_2O and stirred until all solids dissolved. Aqueous layer was washed with ether (3x120 ml), and aqueous layer was slowly brought to pH 3.0 with dropwise addition of HCl, forming visible precipitate of product, which was extracted from aqueous with ether (3x120 ml), dried with $MgSO_4$, filtered, and evaporated under reduced pressure to afford 10.4g (75.9 mmol, 94.4% yield) of a viscous yellow oil. Purity of product was sufficient to carry on to next step. LCMS (RT=1.35): 137.2 (100%); 138.2 (10%); 139.2 (3%).

5-cyclopentyl-1H-pyrazol-3-amine (JM3)

3-cyclopentyl-3-oxopropanenitrile (10.4 g, 75.9 mmol) and hydrazine monohydrate 65% (7.8 ml, 152 mmol) were dissolved in 95% EtOH (85 ml). Reaction was heated to reflux for 2.5 hours and followed to completion by thin layer chromatography. Excess hydrazine and ethanol were evaporated under reduced pressure, crude product dissolved in CHCl3, and purified by flash chromatography with 0-10% MeOH in CHCl3. Recovered 8.93 g (59 mmol, 77.7% yield). LCMS (RT=0.64): 151.3 (100%); 152.4 (14%); 153.4 (4%). NMR, 1H, DMSO (400 MHz): 11.07 (s, 1H), 5.18 (s, 1H), 4.42 (s, 2H), 2.86 (quin, 1H), 1.91-1.48 (m, 8H).

2-chloro-N-(5-cyclopentyl-1H-pyrazol-3-yl)pyrimidin-4-amine (JM5)

5-cyclopentyl-1H-pyrazol-3-amine (1.51 g, 10.0 mmol) and 2,4-dichloropyrimidine (1.49 g, 10 mmol) were dissolved in a 1:1 mixture of THF:H2O (70 ml), and KOAc (98.15 g, 300 mmol) was added to the mixture. Reaction was stirred vigorously at 55° C for 48 hours. Organic layer was separated and evaporated under reduced pressure, dissolved in CH2Cl2 (45 ml), and kept at -20° C for 3 hours. Precipitated solid was filtered, washed with cold CH2Cl2 (15 ml), and dried to yield 0.46 g of N2-(4-aminophenyl)-N4-(5-cyclopentyl-1H-pyrazol-3-yl)pyrimidine-2,4-diamine (1.74 mmol, 17.4% yield). LCMS (RT=1.31): 262.9 (100%); 264.9 (60%); 263.9 (25%); 265.8 (10%). NMR, 1H, DMSO (400 MHz): 12.15 (s, 1H), 10.26 (s, 1H), 8.12 (s, 1H), 2.99 (quin, 1H), 1.98-1.50 (m, 8H).

N2-(4-aminophenyl)-N4-(5-cyclopentyl-1H-pyrazol-3-yl)pyrimidine-2,4-diamine (JM8)

JM5 (78 mg, 0.3 mmol) and p-phenylenediamine (35.6 mg, 0.33 mmol) were dissolved in n-butanol and stirred at 90° C for 3 hrs. Solvent was evaporated under reduced pressure and crude product was purified by HPLC (10-75% ACN/H2O) and lyophilized to give 32 mg of JM8 (0.096 mmol, 32% yield). LCMS (RT=0.84): 335.3 (100%); 336.3 (25%); 337.4 (4%). NMR, 1H, DMSO (400 MHz): 9.62 (s, 1H), 8.75 (s, 1H), 8.11 (s, 1H), 7.83 (d, 1H), 7.23 (d, 2H), 6.50 (m, 2H), 6.26 (s, 1H), 6.17 (s, 1H), 2.94 (quin, 1H), 1.94-1.53 (m, 8H).

1-(4-((4-((5-cyclopentyl-1H-pyrazol-3-yl)amino)pyrimidin-2-yl)amino)phenyl)-3-(3-(trifluoromethyl)phenyl)urea (CD532)

JM8 (13.5 mg, 40.3 μmol) was dissolved in DMF (2 ml) in a dry, argon-charged roundbottom flask. 3-(trifluoromethyl)phenyl isocyanate (6.23 μl, 44.3 μmol) was added and reaction was stirred overnight under argon gas. Crude product was purified by HPLC (10-75% ACN/H2O) and 3.6 mg of NHC53-2 (6.89 μmol, 17% yield) was recovered as a white powder. LCMS (RT=1.32): 522.2 (100%); 523.3 (30%); 524.4 (5%). NMR, 1H, DMSO (400 MHz): 9.69 (s, 1H), 9.51 (s, 1H), 9.29 (s, 1H), 8.94 (s, 1H), 8.25 (s, 1H), 8.04 (s, 1H), 7.91 (d, 1H), 7.65-7.51 (m, 3H), 7.45 (quin, 1H), 7.40-7.32 (m, 2H), 7.23 (d, 1H), 6.32 (s, 1H), 6.19 (s, 1H), 2.93 (quin, 1H), 2.06-1.39 (m, 8H).

3-[4-({4-[(5-cyclopentyl-1H-pyrazol-3-yl)amino]pyrimidin-2-yl}amino)phenyl]-1-phenylurea (CD25)

JM8 (3.0 mg, 8.95 μmol) was dissolved in dry DMF (3 ml) in a dry, argon-charged flask, and isocyanatobenzene (1.07 μl, 9.84 μmol) was added. Reaction was stirred at ambient temperature for 1 hour under positive pressure. Solvent was evaporated under reduced pressure, and product was purified by HPLC (30-70% ACN/H2O) to recover 0.7 mg (17% yield) of a white powder. LCMS (RT=1.22): 454.3 (100%), 455.4 (30%), 456.4 (4%). NMR, 1H, DMSO (400 MHz): 9.51 (s, 1H), 8.94 (s, 1H), 8.68 (s, 1H), 8.58 (s, 1H), 8.14 (s, 1H), 7.92 (s, 1H), 7.57 (d, 2H), 7.42 (m, 2H), 7.32 (d, 2H), 7.24 (d, 2H), 6.91 (s, 1H), 6.33 (s, 1H), 6.18 (s, 1H), 3.70 (s, 1H), 2.96 (s, 1H), 1.98-1.43 (m, 8H).

CD15:

2-chloro-N-(5-cyclopentyl-1H-pyrazol-3-yl)-6-methylpyrimidin-4-amine (JM4)

5-cyclopentyl-1H-pyrazol-3-amine (1.51 g, 10 mmol) and 2,4-dichloro-6-methylpyrimidine (1.63 g, 10 mmol) were dissolved in a 1:1 mixture of THF:H2O (70 ml) and treated with KOAc (29.45 g, 300 mmol). Reaction was stirred vigorously at 55° C for 48 hrs. Layers were separated, organic layer was evaporated under reduced pressure, and resulting solid was purified by flash chromatography (2-10% MeOH/CHCl3) to afford 1.69 g (61% yield) of a white powder. LCMS (RT=1.26): 277.2 (100%); 279.2 (60%); 278.3 (25%); 280.2 (8%). NMR, 1H, DMSO (400 MHz): 8.28 (s, 1H), 7.35 (s, 1H), 6.64 (s, 1H), 5.25 (s, 1H), 2.05 (s, 3H), 1.72-1.51 (m, 8H).

N2-(4-aminophenyl)-N4-(5-cyclopentyl-1H-pyrazol-3-yl)-6-methylpyrimidine-2,4-diamine (JM14)

2-chloro-N-(5-cyclopentyl-1H-pyrazol-3-yl)-6-methylpyrimidin-4-amine (73 mg, 0.26 mmol) and p-phenylenediamine (56.2 mg, 0.52 mmol) were dissolved in n-BuOH (3 mL) and stirred at 90° C for 5 hours. Reaction was allowed to cool to ambient temperature, solvent was evaporated under reduced pressure, and product was purified by HPLC (10-75% ACN/H2O) to afford 33 mg (36% yield) of JM14. LCMS (RT=0.84): 349.3 (100%); 350.3 (22%); 351.3 (4%). NMR, 1H, CDCl3:

8.54 (s, 1H), 7.20 (d, 2H), 6.62 (d, 2H), 2.90 (quin, 1H), 2.22 (s, 3H), 1.98-1.93 (m, 2H), 1.75-1.43 (m, 6H).

1-(4-((4-((5-cyclopentyl-1H-pyrazol-3-yl)amino)-6-methylpyrimidin-2-yl)amino)phenyl)-3-(3-(trifluoromethyl)phenyl)urea (CD15)

To a dry, argon-charged roundbottom flask with stir bar was added JM14 (17 mg, 0.049 mmol) and dry DMF. 3-(trifluoromethyl)phenyl isocyanate (13.3 μL, 1.1 eq) was added by syringe and reaction was stirred under argon until depletion of JM14 by LCMS (2 hours). Solvent was evaporated under reduced pressure and solid was dissolved in minimal DMSO for purification by HPLC (10-90% ACN/H2O) to afford 4.2 mg (16% yield) of a white powder. LCMS (RT=1.33): 536.3 (100%); 537.3 (40%); 538.3 (8%). NMR, 1H, DMSO (400 MHz): 9.39 (s, 1H), 9.28 (s, 1H), 8.93 (s, 1H), 8.89 (s, 1H), 8.17 (s, 1H), 8.03 (s, 1H), 7.61 (d, 2H), 7.54 (d, 1H), 7.44 (t, 1H), 7.32 (d, 2H), 7.24 (d, 1H), 6.28-6.09 (b, 2H), 2.94 (quin, 1H), 2.14 (s, 3H), 2.02-1.88 (m, 2H), 1.77-1.45 (m, 6H).

CD22, CD24:

3-cyclohexyl-3-oxopropanenitrile (JM18)

To a dried, argon-charged roundbottom flask with large stir bar was added anhydrous tetrahydrofuran (80 ml), which was cooled to -78o C before addition of 2.5 M n-Butyllithium in hexanes (32 mL, 80 mmol). Reaction was stirred for 5 minutes before addition of anhydrous acetonitrile (4.23 mL, 80 mmol) dropwise over 5 minutes. Reaction was stirred for 90 minutes at -78o C, followed by dropwise addition of methylcyclohexane carboxylate (5.72 ml, 40 mmol) over 15 minutes. Reaction was allowed to stir for another 2 hours at -78o C, allowed to warm to room temperature, and stirred for an additional 30 minutes. Reaction was quenched with 100 ml H2O and stirred until all solids dissolved. Aqueous layer was washed with ether (2x100 ml), and aqueous layer was slowly brought to pH 3.0 with dropwise addition of HCl, forming visible precipitate of product, which was extracted from aqueous with ether (3x100 ml), dried with MgSO4, filtered, and evaporated under reduced pressure to yield 5.3 g (87.6% yield) of a viscous

yellow oil. Purity of product was sufficient to carry on to next step. LCMS (RT=1.36): 151.2 (100%), 152.2 (12%), 153.2 (3%).

5-cyclohexyl-1H-pyrazol-3-amine (JM19)

3-cyclohexyl-3-oxopropanenitrile (5.3 g, 35 mmol) was dissolved in 95% EtOH (45 ml), to which was added hydrazine monohydrate (3.5 ml, 70 mmol). Reaction was stirred under reflux for 2.5 hrs, solvent was evaporated under reduced pressure, and product was purified by flash chromatography (0-10% MeOH/CHCl3) to give 3.52 g (61% yield) of a viscous reddish oil. LCMS (RT=0.89): 165.3 (100%), 166.3 (20%), 167.3 (8%). NMR, 1H, DMSO (400 MHz): 10.97 (s, 1H), 5.13 (s, 1H), 4.34 (s, 2H), 2.39 (m, 1H), 1.80-1.15 (m, 10H).

2-chloro-N-(5-cyclohexyl-1H-pyrazol-3-yl)-6-methylpyrimidin-4-amine (JM20)

5-cyclohexyl-1H-pyrazol-3-amine (1.65 g, 10 mmol) and 2,4-dichloro-6-methylpyrimidine (1.63 g, 10 mmol) were dissolved in a 1:1 mixture of THF/H2O (70 ml) in a roundbottom flask with stir bar. Reaction was treated with KOAc (30 eq, 29.45 g) and stirred vigorously for 48 hours at 55º C. Organic layer was separated and evaporated under reduced pressure, and crude product was dissolved in CHCl3 (10 ml) and purified by flash column chromatography (0-10% MeOH/CHCl3) to recover 1.14 g (39% yield) of a white powder. LCMS (RT=1.51): 291.3 (100%), 293.2 (60%), 292.3 (28%), 294.2 (10%). NMR, 1H, DMSO (400 MHz): 9.87 (s, 1H), 9.09 (s, 1H), 6.85 (s, 1H), 6.01 (s, 1H), 2.61 (quin, 1H), 2.27 (s, 3H), 1.79-1.21 (m, 10H).

2-N-(4-aminophenyl)-4-N-(5-cyclohexyl-1H-pyrazol-3-yl)-6-methylpyrimidine-2,4-diamine (JM21)

JM20 (231 mg, 0.79 mmol) and p-phenylenediamine (94.0 mg, 0.87 mmol) were dissolved in n-butanol (6 ml) and stirred at 85 C for 2.5 hrs under argon gas. Solvent was evaporated under reduced pressure, crude solid was dissolved with DMSO (1 ml) and 1:1 ACN/H2O (8 ml) and purified by HPLC (5-25% ACN/H2O) to yield 74 mg (20% yield) of a grey powder. LCMS (RT=0.99): 364.3 (100%), 365.3 (20%), 366.3 (4%). NMR, 1H, CDCl3: 8.41 (s, 1H), 7.18 (d,

2H), 6.60 (d, 2H), 6.04 (s, 1H), 5.97 (s, 1H), 3.95 (s, 2H), 3.76 (m, 3H), 2.22 (s, 3H), 1.94-1.09 (m, 10H).

3-[4-({4-[(5-cyclohexyl-1H-pyrazol-3-yl)amino]-6-methylpyrimidin-2-yl}amino)phenyl]-1-[3-(trifluoromethyl)phenyl]urea (CD22)

JM21 (3.9 mg, 10.7 μmol) was dissolved in DMF (3 ml) in a dry, argon-charged roundbottom flask. 3-(trifluoromethyl)phenyl isocyanate (1.65 μl, 11.8 μmol) was added and reaction was stirred for 4 hours under argon gas. Product was purified by HPLC (20-75% ACN/H2O) and 3.05 mg of a white powder (5.54 μmol, 52% yield) was recovered. LCMS (RT=1.40): 550.3 (100%), 551.4 (30%), 552.4 (4%). NMR, 1H, DMSO (400 MHz): 9.40 (s, 1H), 9.14 (s, 1H), 8.95 (s, 1H), 8.75 (s, 1H), 8.14 (s, 1H), 8.04 (s, 1H), 7.61 (d, 2H), 7.52-7.42 (m, 2H), 7.33 (d, 2H), 7.25 (d, 1H), 6.17 (b, 2H), 2.53 (quin, 1H), 2.14 (s, 3H), 1.94-1.81 (m, 2H), 1.79-1.65 (m, 2H), 1.59-1.55 (m, 1H), 1.37-1.18 (m, 5H).

3-[4-({4-[(5-cyclohexyl-1H-pyrazol-3-yl)amino]-6-methylpyrimidin-2-yl}amino)phenyl]-1-phenylurea (CD24)

JM21 (3.9 mg, 10.7 μmol) was dissolved in DMF (3 ml) in a dry, argon-charged roundbottom flask. Phenyl isocyanate (1.28 μl, 11.8 μmol) was added and reaction was stirred for 4 hours under argon gas. Product was purified by HPLC (30-75% ACN/H2O) and 2.15 mg of a white powder (4.46 μmol, 42% yield) was recovered. LCMS (RT=1.27): 482.3 (100%), 483.3 (28%), 484.3 (7%). NMR, 1H, DMSO (400 MHz): 9.40 (s, 1H), 8.92 (s, 1H), 8.86 (s, 1H), 8.74 (s, 1H), 8.19 (s, 1H), 7.59 (d, 2H), 7.42 (d, 2H), 7.31 (d, 2H), 7.23 (t, 2H), 6.90 (t, 1H), 6.22 (s, 1H), 6.14 (s, 1H), 2.53 (m, 1H), 2.14 (s, 3H), 1.86 (m, 2H), 1.72 (m, 2H), 1.59 (m, 1H), 1.35-1.18 (m, 5H).

CD12, CD13, CD16, CD17:

4-nitro-N-[3-(trifluoromethyl)phenyl]benzamide (JM6)

3-(trifluoromethyl)aniline (7.55 ml, 60 mmol) was dissolved in pyridine (200 ml) at ambient temperature under argon gas. 4-nitrobenzoyl chloride (12.25 g, 66 mmol) was added and mixture was refluxed for 4 hrs at 115° C. Reaction was cooled to ambient temperature, poured into

ice/water (500 ml), and resulting precipitate was collected by filtration. Precipitate was resuspended in CH2Cl2, left at -20° C for 2 hrs, and collected by filtration to yield 18 g (96.7%) of a white powder. LCMS (RT=1.69): 310.1 (100%), 311.2 (15%), 312.1 (3%).

4-amino-N-[3-(trifluoromethyl)phenyl]benzamide (JM7)

4-nitro-N-[3-(trifluoromethyl)phenyl]benzamide (1.55 g, 5 mmol) was dissolved in THF (50 ml) containing powdered Zn (30 eq). Glacial acetic acid (20 eq) was added and reaction was stirred vigorously overnight under argon gas. Reaction was filtered with celite and solvent was evaporated under reduced pressure. Resulting solid was recrystallized from CH2Cl2 to give 0.78 g (55%) of an orange crystalline solid. LCMS (RT=1.44): 280.1 (100%), 281.1 (10%), 282.1 (3%). NMR, 1H, DMSO (400 MHz): 10.05 (s, 1H), 8.24 (s, 1H), 8.02 (d, 1H), 7.73 (d, 2H), 7.54 (t, 1H), 7.37 (d, 1H), 6.61 (d, 2H), 5.82 (s, 2H).

N-(4-nitrophenyl)-3-(trifluoromethyl)benzamide (JM9)

4-nitroaniline (2.07 g, 15 mmol) and 3-(trifluoromethyl)benzoyl chloride (3.44 g, 16.5 mmol) were used to generate the title compound in a manner similar to JM6 to afford 3.95 g (84.7%) of a yellow crystalline solid. LCMS (RT=2.04): 310.1 (100%), 311.2 (10%), 312.2 (3%).

N-(4-aminophenyl)-3-(trifluoromethyl)benzamide (JM10) was generated in a manner similar to JM7 to afford 0.58 g (41%) of a beige crystalline powder. LCMS (RT=1.03): 280.2 (100%), 281.3 (25%), 282.3 (3%). NMR, 1H, DMSO (400 MHz): 10.10 (s, 1H), 8.25 (s, 1H), 8.23 (d, 1H), 7.92 (d, 1H), 7.75 (t, 1H), 7.37 (d, 2H), 6.55 (d, 2H), 4.97 (s, 2H).

4-({4-[(5-cyclopentyl-1H-pyrazol-3-yl)amino]pyrimidin-2-yl}amino)-N-[3-(trifluoromethyl)phenyl]benzamide (CD12)

JM5 (52.7 mg, 0.2 mmol) and 4-amino-N-[3-(trifluoromethyl)phenyl]benzamide (56.0 mg, 0.2 mmol) were dissolved in n-butanol and heated to 90° C. HCl (30 μl) was added and reaction was stirred under argon gas overnight. Reaction was cooled to ambient temperature, stirbar was removed, and reaction was left at -20° C for 2h. Resulting precipitate was filtered and washed with n-butanol (5 ml) and cold ether (5 ml) to afford a white crystalline powder, which was

further purified by HPLC (10-65% ACN/H2O) to afford 26.9 mg (24%) of product. LCMS (RT=1.33): 507.3 (100%), 508.4 (25%), 509.4 (5%). NMR, 1H, DMSO (400 MHz): 9.65 (s, 1H), 9.57 (s, 1H), 8.23 (s, 1H), 8.15 (s, 1H), 8.04-7.98 (m, 2H), 7.91-7.75 (m, 5H), 7.56 (t, 1H), 7.40 (d, 1H), 6.48 (s, 1H), 6.23 (s, 1H), 2.98 (quin, 1H), 2.02-1.93 (m, 2H), 1.73-1.51 (m, 6H).

N-[4-({4-[(5-cyclopentyl-1H-pyrazol-3-yl)amino]pyrimidin-2-yl}amino)phenyl]-3-(trifluoromethyl)benzamide (CD13)

N-(4-aminophenyl)-3-(trifluoromethyl)benzamide (56 mg, 0.20 mmol) and 2-chloro-N-(5-cyclopentyl-1H-pyrazol-3-yl)pyrimidin-4-amine (52.7 mg, 0.20 mmol) were dissolved in n-butanol (3 ml) and heated to 100° C. HCl (33 μl) was added and precipitate observed to form. Reaction was allowed to proceed overnight, cooled to ambient temperature, and precipitate was filtered and washed with cold butanol (5 ml). Product was purified by HPLC (10-75% ACN/H2O) to yield 19.2 mg of a white powder. LCMS (RT=1.42): 507.3 (100%), 508.2 (35%), 509.2 (4%). NMR, 1H, DMSO (400 MHz): 10.37 (s, 1H), 9.58 (s, 1H), 9.12 (s, 1H), 8.29 (s, 1H), 8.26 (d, 1H), 8.14 (s, 1H), 7.98-7.95 (m, 2H), 7.78 (t, 1H), 7.73-7.65 (m, 4H), 6.42 (s, 1H), 6.22 (s, 1H), 2.98 (quin, 1H), 2.05-1.93 (m, 2H), 1.77-1.51 (m, 6H).

4-({4-[(5-cyclopentyl-1H-pyrazol-3-yl)amino]-6-methylpyrimidin-2-yl}amino)-N-[3-(trifluoromethyl)phenyl]benzamide (CD16)

2-chloro-N-(5-cyclopentyl-1H-pyrazol-3-yl)-6-methylpyrimidin-4-amine (83.3 mg, 0.30 mmol) and 4-amino-N-[3-(trifluoromethyl)phenyl]benzamide (84.1 mg, 0.30 mmol) were dissolved in n-butanol (6 ml) and heated to 100° C. HCl was added (50 μl) and reaction allowed to proceed overnight. Mixture was cooled to -20° C for 2h and precipitate was filtered and washed with cold butanol (3 ml) and cold ether (5 ml). Product was purified by HPLC (10-65% ACN/H2O) and 18.1 mg (11%) of a white powder was recovered. LCMS (RT=1.33): 521.3 (100%), 522.4 (28%), 523.3 (4%). NMR, 1H, DMSO (400 MHz): 10.30 (s, 1H), 9.53 (s, 1H), 9.47 (s, 1H), 8.23 (s, 1H), 8.17 (s, 1H), 8.01 (d, 1H), 7.93-7.87 (m, 4H), 7.55 (t, 1H), 7.39 (d, 1H), 6.38 (s, 1H), 6.17 (s, 1H), 2.97 (quin, 1H), 2.20 (s, 3H), 2.01-1.92 (m, 2H), 1.69-1.51 (m, 6H).

N-[4-({4-[(5-cyclopentyl-1H-pyrazol-3-yl)amino]-6-methylpyrimidin-2-yl}amino)phenyl]-3-(trifluoromethyl)benzamide (CD17)

2-chloro-N-(5-cyclopentyl-1H-pyrazol-3-yl)-6-methylpyrimidin-4-amine (41.7 mg, 0.15 mmol) and N-(4-aminophenyl)-3-(trifluoromethyl)benzamide (43 mg, 0.15 mmol) were dissolved in butanol (2 ml), heated to 95° C, and HCl (20 μl) was added. Reaction was allowed to proceed overnight, and cooled to -20° C for 2h. Precipitated was filtered and washed with cold butanol (3 ml) and cold ether (5 ml). Crude solid was purified by HPLC (10-65% ACN/H2O) to give 31.5 mg (40%) of a white solid. LCMS (RT=1.26): 521.3 (100%), 522.4 (28%), 523.4 (4%). NMR, 1H, DMSO (400 MHz): 10.34 (s, 1H), 9.43 (s, 1H), 9.08 (s, 1H), 8.25 (s, 1H), 8.23 (d, 1H), 8.19 (s, 1H), 7.92 (d, 1H), 7.75 (t, 1H), 7.72 (s, 1H), 7.69 (s, 1H), 7.64-7.59 (m, 2H), 6.29 (s, 1H), 6.15 (s, 1H), 2.95 (quin, 1H), 2.17 (s, 3H), 2.00-1.91 (m, 2H), 1.70-1.51 (m, 6H).

CD532 (large scale)

3-(4-aminophenyl)-1-[3-(trifluoromethyl)phenyl]urea (JM149)

P-phenylenediamine (4.33 g, 40 mmol) was dissolved in 100 ml CH2Cl2 in a dried, argon-charged roundbottom flask with stirbar. Mixture was cooled to 0° C before dropwise addition of 3-(trifluoromethyl)phenyl isocyanate (5.64 ml, 40 mmol). Reaction was allowed to warm to ambient temperature over 3 hours, and precipitate was filtered and washed with cold CH2Cl2 (50 ml) to yield a white solid. LCMS (RT=1.10): 295.2 (100%), 296.2 (30%), 297.3 (5%).

1-(4-((4-((5-cyclopentyl-1H-pyrazol-3-yl)amino)pyrimidin-2-yl)amino)phenyl)-3-(3-(trifluoromethyl)phenyl)urea (CD532)

2-chloro-N-(5-cyclopentyl-1H-pyrazol-3-yl)pyrimidin-4-amine (JM5; 1.98 g, 1 mmol) and JM149 (2.21 g, 1 mmol) were dissolved in BuOH 40 ml and stirred at 85° C before dropwise addition of HCl (120 μl). Product formed immediately, and reaction was cooled to ambient temperature and filtered to yield 3.4 g (6.51 mmol, 87%) of a light purple solid. 0.51 g of crude product was purified by HPLC to yield 332 mg of a white solid (65.2% recovery). LCMS (RT=1.32): 522.2 (100%); 523.3 (28%); 524.4 (4%). NMR, 1H, DMSO (400 MHz): 9.69 (s, 1H),

9.51 (s, 1H), 9.29 (s, 1H), 8.94 (s, 1H), 8.25 (s, 1H), 8.04 (s, 1H), 7.91 (d, 1H), 7.65-7.51 (m, 3H), 7.45 (quin, 1H), 7.40-7.32 (m, 2H), 7.23 (d, 1H), 6.32 (s, 1H), 6.19 (s, 1H), 2.93 (quin, 1H), 2.06-1.39 (m, 8H).

2.7 Chapter 2 References

(1)   Nie, Z.; Hu, G.; Wei, G.; Cui, K.; Yamane, A.; Resch, W.; Wang, R.; Green, D. R.; Tessarollo, L.; Casellas, R.; et al. C-Myc Is a Universal Amplifier of Expressed Genes in Lymphocytes and Embryonic Stem Cells. **2012**, *151*, 68–79.

(2)   Lin, C. Y.; Lovén, J.; Rahl, P. B.; Paranal, R. M.; Burge, C. B.; Bradner, J. E.; Lee, T. I.; Young, R. A. Transcriptional Amplification in Tumor Cells with Elevated C-Myc. *Cell* **2012**, *151*, 56–67.

(3)   Filippakopoulos, P.; Qi, J.; Picaud, S.; Shen, Y.; Smith, W. B.; Fedorov, O.; Morse, E. M.; Keates, T.; Hickman, T. T.; Felletar, I.; et al. Selective Inhibition of BET Bromodomains. *Nature* **2010**, *468*, 1067–1073.

(4)   Mertz, J. A.; Conery, A. R.; Bryant, B. M.; Sandy, P.; Balasubramanian, S.; Mele, D. A.; Bergeron, L.; Sims, R. J. Targeting MYC Dependence in Cancer by Inhibiting BET Bromodomains. **2011**, *108*, 16669–16674.

(5)   Delmore, J. E.; Issa, G. C.; Lemieux, M. E.; Rahl, P. B.; Shi, J.; Jacobs, H. M.; Kastritis, E.; Gilpatrick, T.; Paranal, R. M.; Qi, J.; et al. BET Bromodomain Inhibition as a Therapeutic Strategy to Target C-Myc. *Cell* **2011**, *146*, 904–917.

(6)   Gustafson, W. C.; Weiss, W. A. Myc Proteins as Therapeutic Targets. *Oncogene* **2010**, *29*, 1249–1259.

(7)   Toyoshima, M.; Howie, H. L.; Imakura, M.; Walsh, R. M.; Annis, J. E.; Chang, A. N.; Frazier, J.; Chau, B. N.; Loboda, A.; Linsley, P. S.; et al. Functional Genomics Identifies Therapeutic Targets for MYC-Driven Cancer. **2012**.

(8)   Soucek, L.; Whitfield, J. R.; Sodir, N. M.; Masso-Valles, D.; Serrano, E.; Karnezis, A. N.; Swigart, L. B.; Evan, G. I. Inhibition of Myc Family Proteins Eradicates KRas-Driven Lung Cancer in Mice. *Genes Dev* **2013**, *27*, 504–513.

(9)   Prochownik, E. V.; Vogt, P. K. Therapeutic Targeting of Myc. **2010**, *1*, 650–659.

(10)   Otto, T.; Horn, S.; Brockmann, M.; Eilers, U.; Schüttrumpf, L.; Popov, N.; Kenney, A. M.; Schulte, J. H.; Beijersbergen, R.; Christiansen, H.; et al. Stabilization of N-Myc Is a Critical Function of Aurora a in Human Neuroblastoma. *Cancer Cell* **2009**, *15*, 67–78.

(11)   Zhao, B.; Smallwood, A.; Yang, J.; Koretke, K.; Nurse, K.; Calamari, A.; Kirkpatrick, R. B.; Lai, Z. Modulation of Kinase-Inhibitor Interactions by Auxiliary Protein Binding: Crystallography Studies on Aurora a Interactions with VX-680 and with TPX2. *Protein Sci* **2008**, *17*, 1791–1797.

(12)   Scrittori, L.; Hans, F.; Angelov, D.; Charra, M.; Prigent, C.; Dimitrov, S. pEg2 Aurora-a Kinase, Histone H3 Phosphorylation, and Chromosome Assembly in Xenopus Egg Extract. **2001**, *276*, 30002–30010.

(13)   Liu, Q.; Kaneko, S.; Yang, L.; Feldman, R. I.; Nicosia, S. V.; Chen, J.; Cheng, J. Q. Aurora-a Abrogation of P53 DNA Binding and Transactivation Activity by Phosphorylation of Serine 215. **2004**, *279*, 52175–52182.

(14)   Ouchi, M. BRCA1 Phosphorylation by Aurora-a in the Regulation of G2 to M Transition. **2004**, *279*, 19643–19648.

(15)   Crosio, C.; Fimia, G. M.; Loury, R.; Kimura, M.; Okano, Y.; Zhou, H.; Sen, S.; Allis, C. D.; Sassone-Corsi, P. Mitotic Phosphorylation of Histone H3: Spatio-Temporal Regulation by Mammalian Aurora Kinases. *Mol Cell Biol* **2002**, *22*, 874–885.

(16)   Shang, X.; Burlingame, S. M.; Okcu, M. F.; Ge, N.; Russell, H. V.; Egler, R. A.; David, R. D.; Vasudevan, S. A.; Yang, J.; Nuchtern, J. G. Aurora a Is a Negative Prognostic Factor and a New Therapeutic Target in Human Neuroblastoma. *Molecular cancer therapeutics* **2009**, *8*, 2461–2469.

(17)   Maris, J. M.; Morton, C. L.; Gorlick, R.; Kolb, E. A.; Lock, R.; Carol, H.; Keir, S. T.; Reynolds, C. P.; Kang, M. H.; Wu, J.; et al. Initial Testing of the Aurora Kinase a

Inhibitor MLN8237 by the Pediatric Preclinical Testing Program (PPTP). *Pediatr Blood Cancer* **2010**, *55*, 26–34.

(18)   Brockmann, M.; Poon, E.; Berry, T.; Carstensen, A.; Deubzer, H. E.; Rycak, L.; Jamin, Y.; Thway, K.; Robinson, S. P.; Roels, F.; et al. Small Molecule Inhibitors of Aurora-a Induce Proteasomal Degradation of N-Myc in Childhood Neuroblastoma. *Cancer Cell* **2013**.

(19)   Dodson, C. A.; Kosmopoulou, M.; Richards, M. W.; Atrash, B.; Bavetsias, V.; Blagg, J.; Bayliss, R. Crystal Structure of an Aurora-a Mutant That Mimics Aurora-B Bound to MLN8054: Insights Into Selectivity and Drug Design. *Biochem J* **2010**, *427*, 19–28.

(20)   Mosse, Y. P.; Lipsitz, E.; Fox, E.; Teachey, D. T.; Maris, J. M.; Weigel, B.; Adamson, P. C.; Ingle, M. A.; Ahern, C. H.; Blaney, S. M. Pediatric Phase I Trial and Pharmacokinetic Study of MLN8237, an Investigational Oral Selective Small-Molecule Inhibitor of Aurora Kinase a: a Children's Oncology Group Phase I Consortium Study. *Clinical Cancer Research* **2012**, *18*, 6058–6064.

(21)   Dietrich, J.; Hulme, C.; Hurley, L. H. The Design, Synthesis, and Evaluation of 8 Hybrid DFG-Out Allosteric Kinase Inhibitors: a Structural Analysis of the Binding Interactions of Gleevec, Nexavar, and BIRB-796. **2010**, *18*, 5738–5748.

(22)   Filomia, F.; De Rienzo, F.; Menziani, M. C. Insights Into MAPK P38alpha DFG Flip Mechanism by Accelerated Molecular Dynamics. **2010**, *18*, 6805–6812.

(23)   Manfredi, M. G.; Ecsedy, J. A.; Chakravarty, A.; Silverman, L.; Zhang, M.; Hoar, K. M.; Stroud, S. G.; Chen, W.; Shinde, V.; Huck, J. J.; et al. Characterization of Alisertib (MLN8237), an Investigational Small-Molecule Inhibitor of Aurora a Kinase Using Novel in Vivo Pharmacodynamic Assays. *Clin Cancer Res* **2011**, *17*, 7614–7624.

(24)   Görgün, G.; Calabrese, E.; Hideshima, T.; Ecsedy, J.; Perrone, G.; Mani, M.; Ikeda, H.; Bianchi, G.; Hu, Y.; Cirstea, D.; et al. A Novel Aurora-a Kinase Inhibitor MLN8237 Induces Cytotoxicity and Cell-Cycle Arrest in Multiple Myeloma. *Blood* **2010**, *115*, 5202–5213.

(25)   Wen, Q.; Goldenson, B.; Silver, S. J.; Schenone, M.; Dancik, V.; Huang, Z.; Wang, L.-Z.; Lewis, T. A.; An, W. F.; Li, X.; et al. Identification of Regulators of Polyploidization Presents Therapeutic Targets for Treatment of AMKL. *Cell* **2012**, *150*, 575–589.

(26)   Gogolin, S.; Ehemann, V.; Becker, G.; Brueckner, L. M.; Dreidax, D.; Bannert, S.; Nolte, I.; Savelyeva, L.; Bell, E.; Westermann, F. CDK4 Inhibition Restores G(1)-S Arrest in MYCN-Amplified Neuroblastoma Cells in the Context of Doxorubicin-Induced DNA Damage. *Cell Cycle* **2013**, *12*, 1091–1104.

(27)   Puissant, A.; Frumm, S. M.; Alexe, G.; Bassil, C. F.; Qi, J.; Chanthery, Y. H.; Nekritz, E. A.; Zeid, R.; Gustafson, W. C.; Greninger, P.; et al. Targeting MYCN in Neuroblastoma by BET Bromodomain Inhibition. *Cancer Discovery* **2013**, *3*, 308–323.

(28)   Garnett, M. J.; Edelman, E. J.; Heidorn, S. J.; Greenman, C. D.; Dastur, A.; Lau, K. W.; Greninger, P.; Thompson, I. R.; Luo, X.; Soares, J.; et al. Systematic Identification of Genomic Markers of Drug Sensitivity in Cancer Cells. *Nature* **2012**, *483*, 570–575.

(29)   Carol, H.; Boehm, I.; Reynolds, C. P.; Kang, M. H.; Maris, J. M.; Morton, C. L.; Gorlick, R.; Kolb, E. A.; Keir, S. T.; Wu, J.; et al. Efficacy and Pharmacokinetic/Pharmacodynamic Evaluation of the Aurora Kinase a Inhibitor MLN8237 Against Preclinical Models of Pediatric Cancer. *Cancer Chemotherapy and Pharmacology* **2011**, *68*, 1291–1304.

(30)   Carmena, M.; Ruchaud, S.; Earnshaw, W. C. Making the Auroras Glow: Regulation of Aurora a and B Kinase Function by Interacting Proteins. *Curr. Opin. Cell Biol.* **2009**, *21*, 796–805.

(31)   Martin, M. P.; Zhu, J.-Y.; Lawrence, H. R.; Pireddu, R.; Luo, Y.; Alam, R.; Ozcan, S.; Sebti, S. M.; Lawrence, N. J.; Schönbrunn, E. A Novel Mechanism by Which Small Molecule Inhibitors Induce the DFG Flip in Aurora A. *ACS Chem Biol* **2012**.

(32)   Weiss, W. A.; Weiss, W. A.; Aldape, K.; Aldape, K.; Mohapatra, G.; Mohapatra, G.; Feuerstein, B. G.; Feuerstein, B. G.; Bishop, J. M.; Bishop, J. M. Targeted Expression of MYCN Causes Neuroblastoma in Transgenic Mice. *EMBO J* **1997**, *16*, 2985–2995.

(33)   Zhu, S.; Lee, J.-S.; Guo, F.; Shin, J.; Perez-Atayde, A. R.; Kutok, J. L.; Rodig, S. J.; Neuberg, D. S.; Helman, D.; Feng, H.; et al. Activated ALK Collaborates with MYCN in Neuroblastoma Pathogenesis. *Cancer Cell* **2012**, *21*, 362–373.

(34)   Chanthery, Y. H.; Gustafson, W. C.; Itsara, M.; Persson, A.; Hackett, C. S.; Grimmer, M.; Charron, E.; Yakovenko, S.; Kim, G.; Matthay, K. K.; et al. Paracrine Signaling Through MYCN Enhances Tumor-Vascular Interactions in Neuroblastoma. *Sci Transl Med* **2012**, *4*, 115ra3.

(35)   Chesler, L.; Schlieve, C.; Goldenberg, D. D.; Kenney, A.; Kim, G.; McMillan, A.; Matthay, K. K.; Rowitch, D.; Weiss, W. A. Inhibition of Phosphatidylinositol 3-Kinase Destabilizes Mycn Protein and Blocks Malignant Progression in Neuroblastoma. *Cancer Res* **2006**, *66*, 8139–8146.

(36)   Nussinov, R.; Tsai, C.-J. Allostery in Disease and in Drug Discovery. *Cell* **2013**, *153*, 293–305.

(37)   Zhang, X. W.; Yan, X. J.; Zhou, Z. R.; Yang, F. F.; Wu, Z. Y.; Sun, H. B.; Liang, W. X.; Song, A. X.; Lallemand-Breitenbach, V.; Jeanne, M.; et al. Arsenic Trioxide Controls the Fate of the PML-RAR Oncoprotein by Directly Binding PML. *Science* **2010**, *328*, 240–243.

(38)   Osguthorpe, D. J.; Hagler, A. T. Mechanism of Androgen Receptor Antagonism by Bicalutamide in the Treatment of Prostate Cancer. *Biochemistry* **2011**, *50*, 4105–4113.

(39)   Subramanian, A.; Tamayo, P.; Mootha, V. K.; Mukherjee, S.; Ebert, B. L.; Gillette, M. A.; Paulovich, A.; Pomeroy, S. L.; Golub, T. R.; Lander, E. S.; et al. Gene Set Enrichment Analysis: a Knowledge-Based Approach for Interpreting Genome-Wide Expression Profiles. *Proceedings of the National Academy of Sciences of the United States of America* **2005**, *102*, 15545–15550.

(40)   Knight, Z. A.; Feldman, M. E.; Balla, A.; Balla, T.; Shokat, K. M. A Membrane Capture Assay for Lipid Kinase Activity. *Nat Protoc* **2007**, *2*, 2459–2466.

(41)   Adams, P. D.; Afonine, P. V.; Bunkoczi, G.; Chen, V. B.; Davis, I. W.; Echols, N.; Headd, J. J.; Hung, L.-W.; Kapral, G. J.; Grosse-Kunstleve, R. W.; et al. PHENIX: a Comprehensive Python-Based System for Macromolecular Structure Solution. *Acta Crystallogr. D Biol. Crystallogr.* **2010**, *66*, 213–221.

(42)   Emsley, P.; Lohkamp, B.; Scott, W. G.; Cowtan, K. Features and Development of Coot. *Acta Crystallogr. D Biol. Crystallogr.* **2010**, *66*, 486–501.

CHAPTER 3

Targeting the translational apparatus in MYCN-driven medulloblastoma
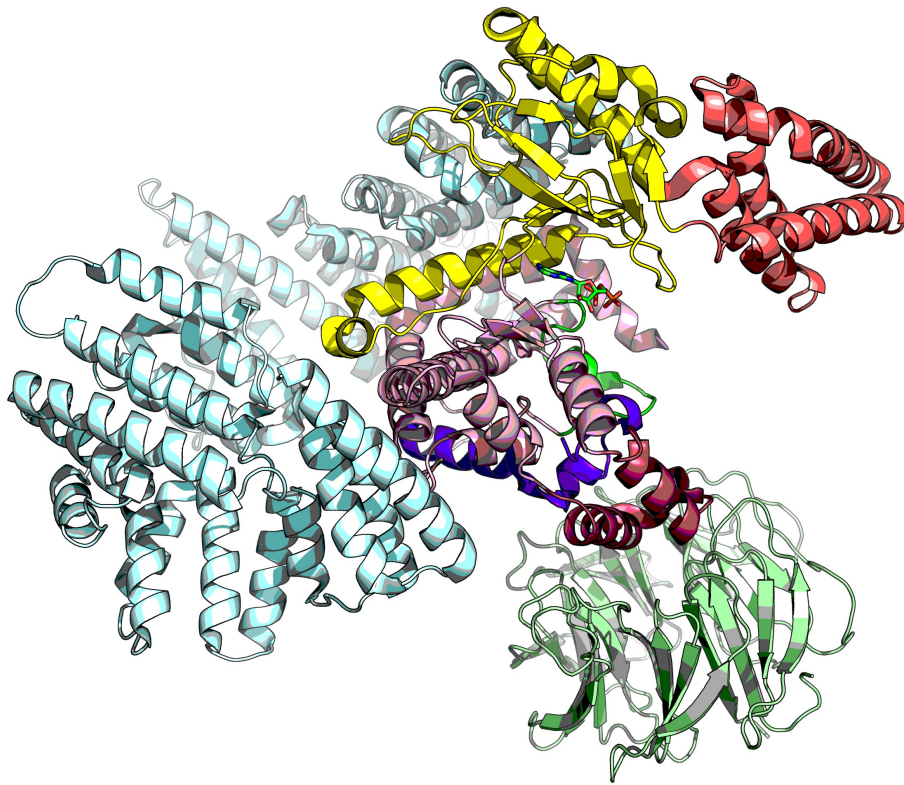
3.1 Abstract

Medulloblastoma is the most common malignant brain tumor in children. Aggressive molecular subgroups have poorly understood biology and few targeted therapies. A high risk subgroup of SHH driven-tumors also shows amplification of the *MYCN* proto-oncogene, while 4 tumors demonstrate increased levels or amplification of MYCN. In both prostate and hematopoietic tumors, MYC drives tumorigenesis through interacting with the translational apparatus downstream of the mammalian target of rapamycin (mTOR) a master regulator of

73

translation. The mTOR complex 1 (mTORC1) signals through Ribosomal Protein S6 kinase (S6K) and the translation initiation factor eIF4E. A new class of mTOR kinase inhibitors disrupts signaling through both mTORC1 effectors, whereas clinical allosteric binders (rapamycin and analogues) disrupt only S6K. These mechanistically distinct activities have enormous therapeutic implications, as in our Group 4 medulloblastoma model, mTOR kinase inhibitors, but not rapamycin, show efficacy. Importantly, we found cross-talk between MYCN and mTOR during medulloblastoma development. Our data point to a critical role for eIF4E in tumorigenesis at this nexus between MYCN and mTOR. These observations suggest that S6K is dispensable, whereas eIF4E is required for MYC/MYCN-driven medulloblastoma.

3.2 Introduction

Medulloblastoma is the most common malignant brain tumor in children, with a five-year survival rate above 60-70% overall, but with severe cognitive disability among survivors.[1-5] Several recent studies have separated medulloblastoma into four distinct molecular subgroups that differ in their epidemiology, mutational and copy number profiles, transcriptional networks, and clinical features.[6-10] Therapies targeted to the SHH subgroup show promising preliminary result, though resistance develops post-treatment, suggesting a need for up-front combination therapies. Since WNT pathway tumors have the best outcomes, planned clinical trials will reduce the dose of craniospinal irradiation in WNT patients. In parallel, both Pharma and academic labs are pursuing preclinical development and testing of WNT pathway inhibitors.[11,12]

WNT and SHH tumors respectively encompass ~10% and ~30% of patients with medulloblastoma, with most tumors less aggressive clinically than the other subgroups, known as Groups 3 and 4[10] These latter groups predict the worst outcome of any subtype.[6] A large portion of these subgroups are characterized by activation of MYC or MYCN protein—functional markers that predict the worst prognosis of any single factor, with survival as low as 13%.[13,14]

Expression of *MYCN* is essential for SHH medulloblastoma in mouse models,[15-18] with amplification also marking a subset of poor-outcome SHH-driven human tumors.[19] MYCN is also expressed in WNT and Group 4 tumors, with targeted expression of *MYCN* driving group 4 medulloblastoma in transgenic mice.[15,18,20,21] Group 3 tumors express MYC rather than MYCN.[19,21] Thus MYC genes play critical roles in all subgroups of this disease. We have transduced an activated allele of MYCN into murine neurospheres, generating both SHH-dependent (in E16 spheres) and SHH-independent (in P0 spheres) models for MYCN-driven medulloblastoma, that latter of which most closely resemble group 4 medulloblastoma.[15,21,22]

The cellular-myelocytomatosis (MYC) protein and the closely related neuroblastoma-derived MYC (MYCN) are basic helix-loop-helix leucine zipper transcription factors that localize to the nucleus and form heterodimers with the protein MAX, which binds to DNA at specific "E-box" sequences to drive transcription of targets important for proliferation.[23,24] The wide range of MYC and MYCN transcriptional targets (cell cycle control, differentiation, multidrug resistance, and biogenesis of ribosomes as well as oncogenic miRNAs) speaks to their critical role in oncogenesis.[25-28] Specifically in its role as a master regulator of protein synthesis, MYC has been shown to be a key transcription factor for many genes encoding protein synthesis components, including translation elongation factors, eIF4E and other translation initiation factors (eIFs), tRNA synthetases, nucleolar assembly components and ribosomal proteins belonging to the small and large subunits.[29-34] The effect of MYC in regulating the expression of many translational components has been observed in a variety of cells of distinct histological origins, and this effect is evolutionarily conserved.[35] Importantly, we have shown previously that MYC's ability to augment protein synthesis is necessary for its oncogenic potential.[36-38] Like MYC, mTORC1 represents a distinct oncogenic pathway that relies on its role in directing translation control for its oncogenic activity. mTORC1, an essential regulator of cell growth and survival, cooperates with MYC to promote tumorigenesis, through a still poorly understood mechanism.[1,35,39,40]

The mTOR pathway has a well-established role in translational regulation, primarily through two effectors (Figure 3.1). One is p70 ribosomal protein S6 kinase (S6K). Phosphorylation and activation of S6K results in S6K phosphorylation of targets such as eIF4B and ribosomal protein S6 (rpS6), however it is not well understood whether and how S6K and downstream targets impact translation control.[41,42] The second major output of mTOR signaling is via regulation of the eukaryotic initiation complex eIF4F, which recruits mRNA to the ribosome and consists of three proteins:

1) eIF4A, an RNA helicase.

2) eIF4E, a protein that binds to and recruits the m^7GTP cap of mRNA to the eIF4F complex.

3) eIF4G, which serves a scaffolding function by directly binding to eIF4E, eIF4A, and the ribosome- associated eIF3.
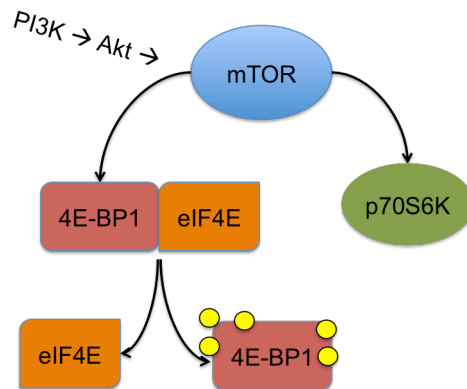
Figure 3.1: Translation effectors downstream of mTOR. The tumor suppressor 4EBP1 negatively regulates the eIF4E oncogene. mTOR hyperphosphorylates 4EBP1, dissociating it from eIF4E, leading to recruitment of the translational initiation complex (eIF4G, eIF4A helicase and eIF4E) to the 5' end of specific mRNAs to regulate cap-dependent translation. The ribosomal protein S6 (rpS6) is phosphorylated by p70S6Ks (p70S6K1 and p70S6K2). Its role in translation control is poorly understood.

Interaction of eIF4E with both the m^7GTP cap and eIF4G is considered to be a rate-limiting step in translation.[43] Regulation of this step occurs through 4E-binding protein (4EBP), which

binds to eIF4E at the 4E-4G-interaction interface to prohibit its participation in the initiation complex.[44] Hypophosphorylated 4EBP binds eIF4E at high affinity, whereas direct phosphorylation by mTOR causes 4EBP to dissociate from eIF4E, allowing eIF4E to participate in the translation initiation complex, leading to an increase in cap-dependent translation (Figure 3.1).[39,45] Importantly, increased protein synthesis is critical for MYC-induced cancers.[15,37] For example, over-expressed MYC leads to augmented protein synthesis.[46] Loss of function of a single ribosomal protein reduces protein synthesis to normal levels, and drastically impaired MYC-induced lymphomagenesis.[37] In addition, overexpression of eIF4E protects cells from MYC-induced apoptosis. Conversely, MYC reverses pathways leading to senescence due to overexpression of eIF4E.[40]

It remains an outstanding question how MYC and mTOR, two of the most frequently deregulated pathways in human cancer, converge on translation control as a mechanism leading to tumor development. For instance, MYC can drive expression of eIF4E, although induction of eIF4E is not sufficient for increased eIF4E activity, as this activity is inhibited by the eIF4E binding protein 4EBP.[33,35] We recently uncovered an unexpected and important link between MYC and mTOR-dependent phosphorylation of 4EBP during MYC-driven tumorigenesis. Employing a genetic approach we showed that mTOR-dependent phosphorylation of 4EBP is essential for cancer cell survival throughout MYC-dependent malignant progression, from tumor initiation to maintenance.[1] Furthermore, we found that hyperphosphorylation of 4EBP, which inactivates its tumor suppressive activity, renders MYC-driven lymphomas and myelomas druggable by a potent new class of mTOR active site inhibitors that are capable of blocking 4EBP phosphorylation.[47] Recent data also show that SHH-induced proliferation of cerebellar granule neural precursors requires eIF4E, whereas S6K is required for their cell cycle exit and differentiation.[48] Thus it is likely that mTOR phosphorylation of 4EBP is a critical process for proliferation in the aggressive MYCN-driven subgroups of medulloblastoma, and that disruption

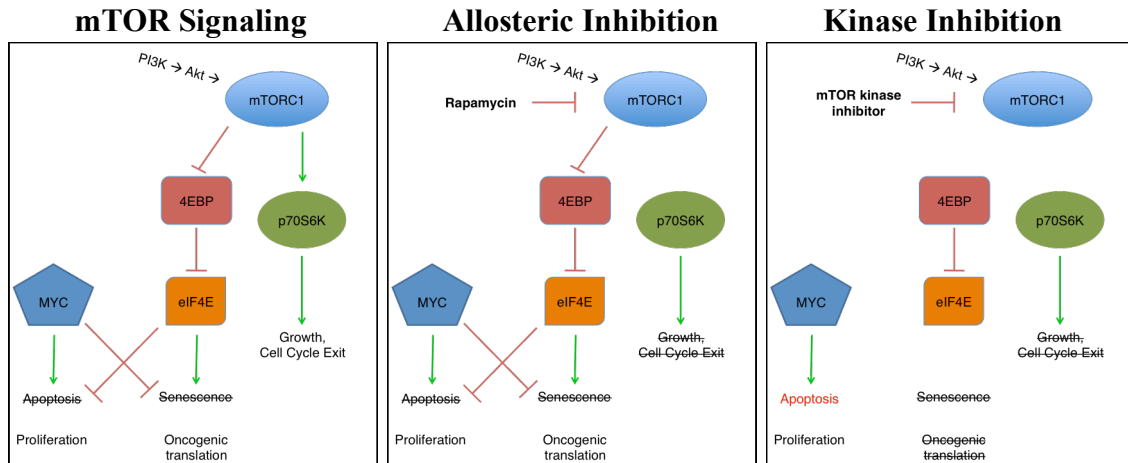of eIF4E through inhibition of mTOR will demonstrate a lethal interaction with MYCN (and MYC) (Figure 3.2).

Figure 3.2: mTOR kinase inhibitors target the cooperation between mTOR signaling and MYC. mTOR regulates the translational machinery through activating p70S6K and inhibiting the translation initiation factor inhibitory subunit 4EBP, which allows eIF4E to cooperate with MYC to drive proliferation. Rapamycin inhibits signaling only through p70S6K, whereas mTOR kinase inhibitors block signaling to both p70S6K and 4EBP, thus disrupting the cooperation between eIF4E and MYC.

New mouse models, pharmacological tools and clinical drugs allow us to explore the differential roles of S6K and 4EBP in the pathogenesis of medulloblastoma. The allosteric mTOR inhibitor rapamycin and analogs abrogate mTOR-dependent phosphorylation of S6K but not phosphorylation of 4EBP. However, the clinical mTOR kinase inhibitor MLN0128 (and other emerging mTOR kinase inhibitors) block mTOR-dependent phosphorylation of both 4EBP and S6K.[39] If activation of cap-dependent translation plays a critical role in MYCN-driven subsets of medulloblastoma, then our studies will provide an important preclinical rationale for targeting the MYCN/mTOR co-dependent translational apparatus with an active site inhibitor of mTOR, in SHH/MYCN and Group 4 MYCN-driven medulloblastoma.

3.3 Results

We have developed a model of SHH-subtype medulloblastoma through transduction of P0 cerebellar neurospheres with $MYCN^{T58A}$.[21] Since only mutationally-stabilized but not wild-type MYCN is capable of transforming these neurospheres, we hypothesized that the increased level of $MYCN^{T58A}$ might itself be responsible for increased signaling through mTOR/4EBP. To this end, we created clonogenic lines from P0 neurospheres harvested from either the cerebellum or forebrain and transformed with $MYCN^{T58A}$. As $MYCN^{T58A}$ is introduced via the RCAS retrovirus, expression of $MYCN^{T58A}$ protein is variable, likely due to differences in insertion sites. We found that the protein level of $MYCN^{T58A}$ correlates well with the level of mTOR signaling through 4EBP (Figure 3.3). Surprisingly, $MYCN^{T58A}$ levels did not correlate with the level of total 4EBP (a known MYC target) or p-rpS6 (another mTOR target). These levels of MYCN also did not correlate with p-Erk. p-Akt, or total levels of any PI3K isoform. These observations are consistent with the idea of MYCN as a promoter of signaling through 4EBP.

If MYCN promotes mTOR-dependent signaling through 4EBP, and if 4EBP and MYCN cooperate in proliferation and evasion of apoptosis, then blocking signaling through 4EBP but not S6K should cause apoptosis in MYCN-dependent medulloblastoma. We thus treated a cell line derived from the GTML transgenic model of MYCN-driven medulloblastoma (GTML5) with increasing doses of the allosteric mTOR inhibitor rapamycin and the mTOR kinase inhibitor MLN0128. While both rapamycin and MLN0128 cause potent loss of rpS6 phosphorylation, only MLN0128 inhibits mTOR phosphorylation of 4EBP (Figure 3.4, immunoblot). Accordingly, only MLN0128 causes a dose-dependent increase in apoptosis as measured by Annexin V staining that was consistent with loss of phosphorylation of 4EBP (Figure 3.4, bar graph). Notably, apoptosis was unrelated to signaling through rpS6 or Akt, consistent with the hypothesis that 4EBP prevents apoptosis in the context of MYCN-driven cancer.
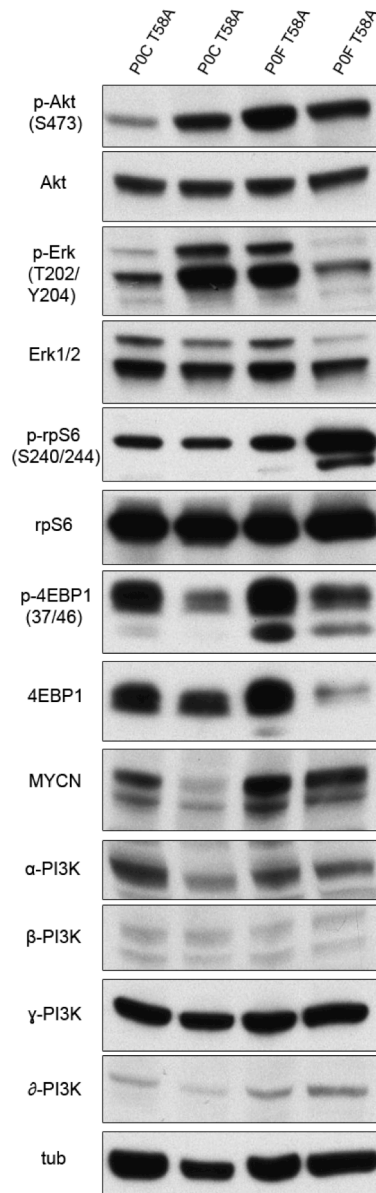
Figure 3.3: MYCN levels in medulloblastoma clones correlate with 4EBP signaling. Postnatal day 0 cerebellar (P0C) and forebrain (P0F) mouse cells transformed with mutationally-stabilized *MYCN* (T58A) probed for MYCN protein levels and activation of mTOR signaling.
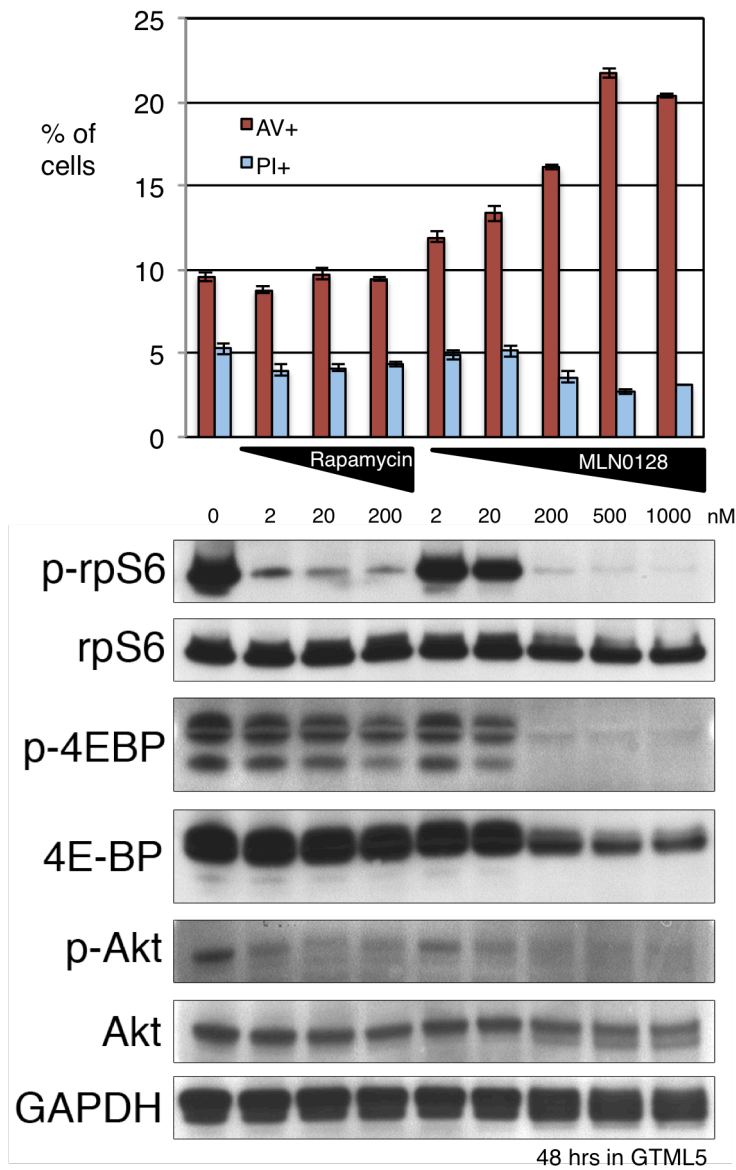
Figure 3.4: Apoptosis driven by inhibitors of mTOR kinase correlates with blockade of p-4EBP rather than p-AKT. Top) MLN0128 induces apoptosis (Annexin V flow cytometry) whereas rapamycin does not, in GTML5 cells derived from a GEMM model for group 4 MYCN-driven medulloblastoma. Bottom) Rapamycin and MLN0128 both reduce rpS6 and Akt phosphorylation in GTML5 cells, whereas only MLN0128 abrogates 4EBP phosphorylation. Reduced levels of p-4EBP correlates with induction of apoptosis. AV – Annexin V; PI – Propidium iodide.

MYCN undergoes a series of post-translational modifications that lead to its eventual ubiquitination and degradation (see Figure 1.1), and one of these steps requires PP2A-dependent dephosphorylation downstream of PI3K signaling. Thus it has been proposed that mTOR inhibition can accelerate degradation of MYCN and thus lead to reduced MYCN protein levels, an alternative explanation to the apoptosis observed due to mTOR kinase but not allosteric inhibition.[49] To test this, we treated GTML5 with rapamycin as well as both PP242 and MLN0128, both kinase inhibitors, and found that while PP242 and MLN0128 both inhibited both phosphorylation of rpS6 and 4EBP, none of these mTOR inhibitors cause any appreciable loss of MYCN protein (Figure 3.5A and B).
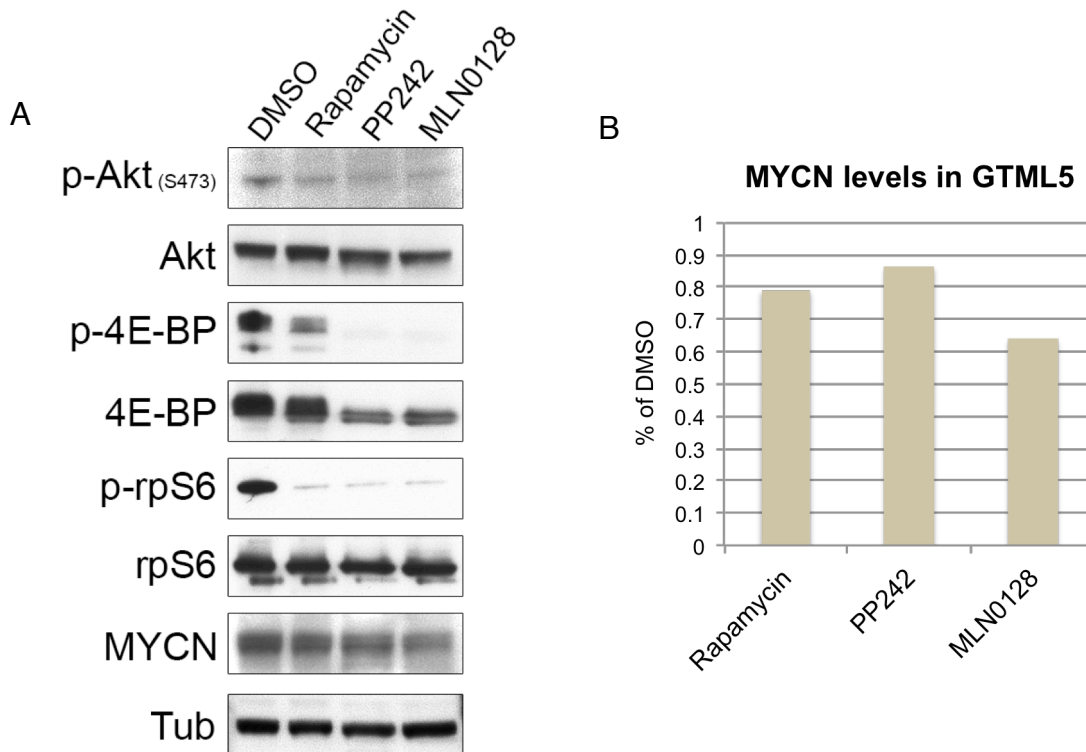

Figure 3.5: mTOR kinase inhibition has minimal effect on MYCN protein level. A) Immunoblot of cell line derived from GTML model of Group 4 MB (GTML5) treated with Rapamycin (50 nM), PP242 (2.5 μM), or MLN0128 (200 nM). B) Quantification showing that MYCN protein level is unaffected by mTOR inhibition.

ATP-competitive inhibitors of mTOR are currently being tested in a variety of adult tumors in clinical trials. However, their utility in pediatric brain tumors such as medulloblastoma is unknown. To test this, we treated transgenic GTML mice with MYCN-driven medulloblastoma (as measured by luciferase imaging) with 1 mg/kg MLN0128 p.o. and assessed for on-target efficacy *in vivo*. Both 1 hour and 24 hours after the last dose, mice treated with MLN0128 had reduced mTOR signaling as measured by p-rpS6 and p-4EBP as compared to vehicle (Figure 3.6). Notably, while p-rpS6 levels were comparable between normal brain and tumor tissue, p-4EBP levels were highly elevated in tumor tissue compared to normal brain. This provides additional evidence *in vivo* that elevated 4EBP signaling but not rpS6 is critical for MYCN-driven medulloblastoma, and provides important evidence that MLN0128 can be used as an effective inhibitor of mTOR signaling in medulloblastoma.

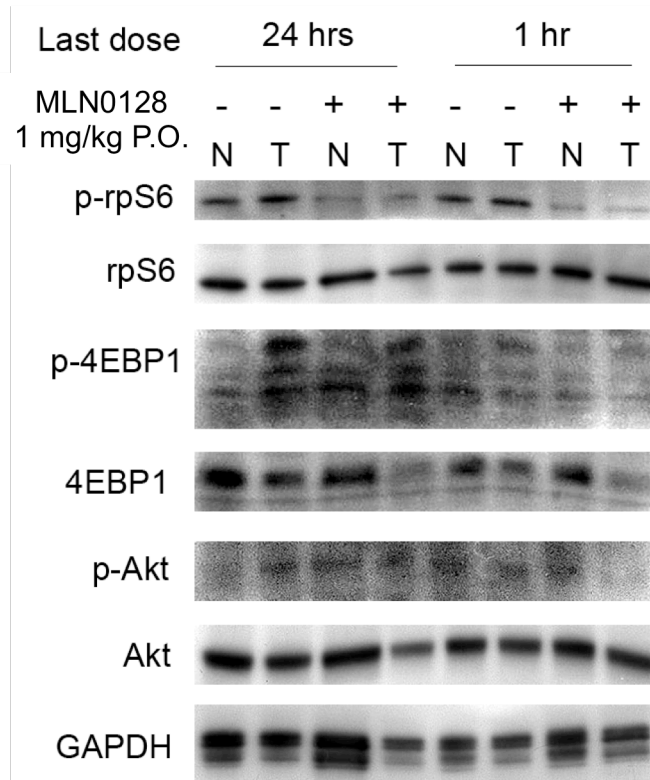

Figure 3.6: MLN0128 inhibits elevated mTOR signaling in GTML model of medulloblastoma. MLN0128 penetrates blood-brain-barrier to inhibit mTOR signaling, evident at both 24 hrs and 1 hr after last dose (1 mg/kg). N – normal, T – tumor tissue.

3.4 Discussion

While rapalogs have shown success in specific contexts such as renal cell carcinoma and endometrial cancers, they have largely failed in trials for glioblastoma. Single-agent rapalog trials have generally shown modest radiographic improvement of disease without significant increase in overall survival or progression-free survival.[50-52] Similarly, combination trials of rapamycin with the chemotherapeutic agent temozolomide,[53] VEGF inhibitor bevacizumab[54,55] or others[56] have shown little to no improvement in progression-free survival and overall survival.

In contrast, ATP-competitive mTOR inhibitors and dual PI3K/mTOR inhibitors have shown activity in preclinical studies and are beginning to enter clinical trials. These agents inhibit both mTORC1 and mTORC2 in an ATP-competitive manner that blocks phosphorylation of both p70S6K and 4E-BPs. The mTOR inhibitors AZD-8055 and WYE-125132 (WYE-132) are effective in preclinical models of glioblastoma, and AZD-8055 is currently in a phase I trial for adults with recurrent gliomas.[57,58] The dual PI3K/mTOR inhibitor XL765 (SAR245409) showed promise as both monotherapy and in combination with temozolomide in xenograft models of glioblastoma and is currently in phase I trials.[59] Another dual PI3K/mTOR inhibitor NVP-BEZ235 has not only shown efficacy as single agent but as an enhancer of radiosensitivity in preclinical trials.[60-62]

Despite these advancements, our understanding of the molecular features that predict sensitivity to mTOR pathway inhibitors is limited. The majority of studies looking for predictors of sensitivity focus on the level of activity in the mTOR pathway, as a proxy for the cancer cell's reliance on this pathway.[63] However, this method has limited utility, as mTOR signaling is still not as strong of an outcome predictor as MYCN protein in MB.[64,65] Here we provide evidence that MYCN and mTOR cooperate in medulloblastoma, and that kinase inhibition of mTOR in the context of MYCN-driven cancer leads to apoptosis. This suggests that MYCN expression is a

critical predictor of sensitivity to mTOR kinase inhibition, providing a path forward for treating the subset of this disease that relies on MYCN and possibly MYC as well.

Questions remain about the mechanism of MYCN cooperation with mTOR, one a master regulator of transcription and the other of translation. One possibility is that MYCN, as a transcriptional amplifier, tips the balance towards oncogenic—and away from anti-oncogenic—gene products in the available pool of mRNA. Thus mTOR would be required for sustained translation of this resulting oncogenic pool of mRNA.

However, a more likely but not mutually exclusive possibility is that signaling through mTOR leads to gene-specific changes in translation rate. Techniques such as ribosome profiling may be able to answer these questions. For example, how do levels of MYCN affect mRNA occupancy by ribosomes? More interestingly, how does mTOR signaling through 4EBP or S6K alone affect gene-specific translation rates? We have generated multiply transgenic mouse strains that express the RCAS virus receptor in GFAP-positive neurospheres, Gtva/GFAP-tTA/4EBP^M and Gtva/rpS6$^{P-/-}$, the latter which cannot signal through 4EBP in the presence of doxycycline and the latter which cannot phosphorylate rpS6. This genetic dissection of mTOR signaling in conjunction with ribosome profiling may give insight into the mRNA-specific role for mTOR signaling in medulloblastomagenesis, and possibly identify new targets critical in medulloblastoma.

3.5 Materials and Methods

Cell culture

Medulloblastoma cells were grown in Neurobasal with Vitamin B27, FGF and EGF. P0 or E16 cerebellar neurospheres were isolated from the cerebellum, and separated from brainstem tissue. They were cultured on ultra low-adhesion conditions with FGF and EGF added every 24 hours for 7 days before transduction with RCAS virus in a 1:1 mix of viral stock (in NB) and existing media. Neurospheres were passaged using Accutase.

Western blotting and inhibitors

Cells were harvested and lysed with Cell Signaling Lysis buffer + 1% SDS, sonicated and supernatants boiled in LDS sample buffer (Invitrogen). Western blots were performed as described previously,[66] with primary antibodies to MYCN (ab24193, Abcam and SC-), GAPDH (Cell Signaling 2118), rpS6 (Cell Signaling 2217), phosphor-Akt Ser473 (Cell Signaling 4060), phospho-rpS6 (Cell Signaling 5364), Akt (Cell Signaling 4691), 4E-BP1 (Cell Signaling 9644), phopsho-4E-BP (Cell Signaling 2855). Western blot quantitation performed with ImageJ software. Rapamycin was obtained from Cell Signaling (9904), and PP242 and MLN0128 were synthesized as described previously.[39]

Flow cytometry

Medulloblastoma cells were treated for the indicated time, trypsinized, washed, stained with Dylight 800 at 0.3 μg/mL (Pierce, 46421), fixed with 1.5% PFA, and permeabilized with 100% methanol. Cells were stained with propidium iodide (BD, 556547) and analyzed on the BD FACSCalibur flow cytometer. Data was gated using Cytobank. Data was analyzed using GraphPad Prism software.

3.6 Chapter 3 References

(1)   Pourdehnad, M.; Truitt, M. L.; Siddiqi, I. N.; Ducker, G. S.; Shokat, K. M.; Ruggero, D. Myc and mTOR Converge on a Common Node in Protein Synthesis Control That Confers Synthetic Lethality in Myc-Driven Cancers. *Proceedings of the National Academy of Sciences* **2013**, *110*, 11988–11993.

(2)   Polkinghorn, W. R.; Tarbell, N. J. Medulloblastoma: Tumorigenesis, Current Clinical Paradigm, and Efforts to Improve Risk Stratification. *Nat Clin Pract Oncol* **2007**, *4*, 295–304.

(3)   Packer, R. J.; Zhou, T.; Holmes, E.; Vezina, G.; Gajjar, A. Survival and Secondary Tumors in Children with Medulloblastoma Receiving Radiotherapy and Adjuvant Chemotherapy: Results of Children's Oncology Group Trial A9961. *Neuro-Oncology* **2013**, *15*, 97–103.

(4)   Palmer, S. L.; Armstrong, C.; Onar-Thomas, A.; Wu, S.; Wallace, D.; Bonner, M. J.; Schreiber, J.; Swain, M.; Chapieski, L.; Mabbott, D.; et al. Processing Speed, Attention, and Working Memory After Treatment for Medulloblastoma: an International, Prospective, and Longitudinal Study. *J. Clin. Oncol.* **2013**, *31*, 3494–3500.

(5)   Jakacki, R. I.; Burger, P. C.; Zhou, T.; Holmes, E. J.; Kocak, M.; Onar, A.; Goldwein, J.; Mehta, M.; Packer, R. J.; Tarbell, N.; et al. Outcome of Children with Metastatic Medulloblastoma Treated with Carboplatin During Craniospinal Radiotherapy: a Children's Oncology Group Phase I/II Study. *J. Clin. Oncol.* **2012**, *30*, 2648–2653.

(6)   Northcott, P. A.; Korshunov, A.; Witt, H.; Hielscher, T.; Eberhart, C. G.; Mack, S.; Bouffet, E.; Clifford, S. C.; Hawkins, C. E.; French, P.; et al. Medulloblastoma Comprises Four Distinct Molecular Variants. *J. Clin. Oncol.* **2011**, *29*, 1408–1414.

(7)   Kool, M.; Koster, J.; Bunt, J.; Hasselt, N. E.; Lakeman, A.; van Sluis, P.; Troost, D.; Meeteren, N. S.-V.; Caron, H. N.; Cloos, J.; et al. Integrated Genomics Identifies Five Medulloblastoma Subtypes with Distinct Genetic Profiles, Pathway Signatures and Clinicopathological Features. *PLoS ONE* **2008**, *3*, e3088.

(8)   Northcott, P. A.; Fernandez-L, A.; Hagan, J. P.; Ellison, D. W.; Grajkowska, W.; Gillespie, Y.; Grundy, R.; Van Meter, T.; Rutka, J. T.; Croce, C. M.; et al. The miR-17/92 Polycistron Is Up-Regulated in Sonic Hedgehog-Driven Medulloblastomas and Induced by N-Myc in Sonic Hedgehog-Treated Cerebellar Neural Precursors. *Cancer Res* **2009**, *69*, 3249–3255.

(9)   Northcott, P. A.; Hielscher, T.; Dubuc, A.; Mack, S.; Shih, D.; Remke, M.; Al-Halabi, H.; Albrecht, S.; Jabado, N.; Eberhart, C. G.; et al. Pediatric and Adult Sonic Hedgehog Medulloblastomas Are Clinically and Molecularly Distinct. *Acta Neuropathol* **2011**.

(10)   Northcott, P. A.; Jones, D. T. W.; Kool, M.; Robinson, G. W.; Gilbertson, R. J.; Cho, Y.-J.; Pomeroy, S. L.; Korshunov, A.; Lichter, P.; Taylor, M. D.; et al. Medulloblastomics: the End of the Beginning. *Nat Rev Cancer* **2012**, *12*, 818–834.

(11)   Buonamici, S.; Williams, J.; Morrissey, M.; Wang, A.; Guo, R.; Vattay, A.; Hsiao, K.; Yuan, J.; Green, J.; Ospina, B.; et al. Interfering with Resistance to Smoothened Antagonists by Inhibition of the PI3K Pathway in Medulloblastoma. *Sci Transl Med* **2010**, *2*, 51ra70.

(12)   Rohner, A.; Spilker, M. E.; Lam, J. L.; Pascual, B.; Bartkowski, D.; Li, Q. J.; Yang, A. H.; Stevens, G.; Xu, M.; Wells, P. A.; et al. Effective Targeting of Hedgehog Signaling in a Medulloblastoma Model with PF-5274857, a Potent and Selective Smoothened Antagonist That Penetrates the Blood-Brain Barrier. *Molecular cancer therapeutics* **2012**, *11*, 57–65.

(13)   Leary, S. E. S.; Olson, J. M. The Molecular Classification of Medulloblastoma: Driving the Next Generation Clinical Trials. *Curr. Opin. Pediatr.* **2012**, *24*, 33–39.

(14) Pfister, S.; Remke, M.; Benner, A.; Mendrzyk, F.; Toedt, G.; Felsberg, J.; Wittmann, A.; Devens, F.; Gerber, N. U.; Joos, S.; et al. Outcome Prediction in Pediatric Medulloblastoma Based on DNA Copy-Number Aberrations of Chromosomes 6q and 17q and the MYC and MYCN Loci. *J. Clin. Oncol.* **2009**, *27*, 1627–1636.

(15) Swartling, F. J.; Grimmer, M. R.; Hackett, C. S.; Northcott, P. A.; Fan, Q.-W.; Goldenberg, D. D.; Lau, J.; Masic, S.; Nguyen, K.; Yakovenko, S.; et al. Pleiotropic Role for MYCN in Medulloblastoma. *Genes Dev* **2010**, *24*, 1059–1072.

(16) Browd, S. R.; Kenney, A. M.; Gottfried, O. N.; Yoon, J. W.; Walterhouse, D.; Pedone, C. A.; Fults, D. W. N-Myc Can Substitute for Insulin-Like Growth Factor Signaling in a Mouse Model of Sonic Hedgehog-Induced Medulloblastoma. *Cancer Res* **2006**, *66*, 2666–2672.

(17) Kim, S. U.; Park, I. H.; Kim, T. H.; Kim, K. S.; Choi, H. B.; Hong, S. H.; Bang, J. H.; Lee, M. A.; Joo, I. S.; Lee, C. S.; et al. Brain Transplantation of Human Neural Stem Cells Transduced with Tyrosine Hydroxylase and GTP Cyclohydrolase 1 Provides Functional Improvement in Animal Models of Parkinson Disease. *Neuropathology* **2006**, *26*, 129–140.

(18) Varlakhanova, N. V.; Cotterman, R. F.; deVries, W. N.; Morgan, J.; Donahue, L. R.; Murray, S.; Knowles, B. B.; Knoepfler, P. S. Myc Maintains Embryonic Stem Cell Pluripotency and Self-Renewal. *Differentiation* **2010**, *80*, 9–19.

(19) Kool, M.; Korshunov, A.; Remke, M.; Jones, D. T. W.; Schlanstein, M.; Northcott, P. A.; Cho, Y.-J.; Koster, J.; Schouten-van Meeteren, A.; van Vuurden, D.; et al. Molecular Subgroups of Medulloblastoma: an International Meta-Analysis of Transcriptome, Genetic Aberrations, and Clinical Data of WNT, SHH, Group 3, and Group 4 Medulloblastomas. *Acta Neuropathol* **2012**.

(20) Wang, J.; Lin, W.; Popko, B.; Campbell, I. L. Inducible Production of Interferon-Γ in the Developing Brain Causes Cerebellar Dysplasia with Activation of the Sonic Hedgehog Pathway. *Molecular and Cellular Neuroscience* **2004**, *27*, 489–496.

(21) Swartling, F. J.; Savov, V.; Persson, A. I.; Chen, J.; Hackett, C. S.; Northcott, P. A.; Grimmer, M. R.; Lau, J.; Chesler, L.; Perry, A.; et al. Distinct Neural Stem Cell Populations Give Rise to Disparate Brain Tumors in Response to N-MYC. *Cancer Cell* **2012**, *21*, 601–613.

(22) Bueren, von, A. O.; Oehler, C.; Shalaby, T.; Hoff, von, K.; Pruschy, M.; Seifert, B.; Gerber, N. U.; Warmuth-Metz, M.; Stearns, D.; Eberhart, C. G.; et al. C-MYC Expression Sensitizes Medulloblastoma Cells to Radio- and Chemotherapy and Has No Impact on Response in Medulloblastoma Patients. *BMC Cancer* **2011**, *11*, 74.

(23) Blackwell, T. K.; Kretzner, L.; Blackwood, E. M.; Eisenman, R. N.; Weintraub, H. Sequence-Specific DNA Binding by the C-Myc Protein. *Science* **1990**, *250*, 1149–1151.

(24) Blackwood, E. M.; Eisenman, R. N. Max: a Helix-Loop-Helix Zipper Protein That Forms a Sequence-Specific DNA-Binding Complex with Myc. *Science* **1991**, *251*, 1211–1217.

(25) Manohar, C. F.; Bray, J. A.; Salwen, H. R.; Madafiglio, J.; Cheng, A.; Flemming, C.; Marshall, G. M.; Norris, M. D.; Haber, M.; Cohn, S. L. MYCN-Mediated Regulation of the MRP1 Promoter in Human Neuroblastoma. *Oncogene* **2004**, *23*, 753–762.

(26) Bell, E.; Lunec, J.; Tweddle, D. A. Cell Cycle Regulation Targets of MYCN Identified by Gene Expression Microarrays. *Cell Cycle* **2007**, *6*, 1249–1256.

(27) Berwanger, B.; Hartmann, O.; Bergmann, E.; Bernard, S.; Nielsen, D.; Krause, M.; Kartal, A.; Flynn, D.; Wiedemeyer, R.; Schwab, M.; et al. Loss of a FYN-Regulated Differentiation and Growth Arrest Pathway in Advanced Stage Neuroblastoma. *Cancer Cell* **2002**, *2*, 377–386.

(28) Gustafson, W. C.; Weiss, W. A. Myc Proteins as Therapeutic Targets. *Oncogene* **2010**, *29*, 1249–1259.

(29)   Coller, H. A.; Grandori, C.; Tamayo, P.; Colbert, T.; Lander, E. S.; Eisenman, R. N.; Golub, T. R. Expression Analysis with Oligonucleotide Microarrays Reveals That MYC Regulates Genes Involved in Growth, Cell Cycle, Signaling, and Adhesion. *Proceedings of the National Academy of Sciences of the United States of America* **2000**, *97*, 3260–3265.

(30)   Greasley, P. J.; Bonnard, C.; Amati, B. Myc Induces the Nucleolin and BN51 Genes: Possible Implications in Ribosome Biogenesis. *Nucleic acids research* **2000**, *28*, 446–453.

(31)   Guo, Q. M.; Malek, R. L.; Kim, S.; Chiao, C.; He, M.; Ruffy, M.; Sanka, K.; Lee, N. H.; Dang, C. V.; Liu, E. T. Identification of C-Myc Responsive Genes Using Rat cDNA Microarray. *Cancer Res* **2000**, *60*, 5922–5928.

(32)   Pajic, A.; Spitkovsky, D.; Christoph, B.; Kempkes, B.; Schuhmacher, M.; Staege, M. S.; Brielmeier, M.; Ellwart, J.; Kohlhuber, F.; Bornkamm, G. W.; et al. Cell Cycle Activation by C-Myc in a Burkitt Lymphoma Model Cell Line. *International journal of cancer Journal international du cancer* **2000**, *87*, 787–793.

(33)   Schuhmacher, M.; Kohlhuber, F.; Hölzel, M.; Kaiser, C.; Burtscher, H.; Jarsch, M.; Bornkamm, G. W.; Laux, G.; Polack, A.; Weidle, U. H.; et al. The Transcriptional Program of a Human B Cell Line in Response to Myc. *Nucleic acids research* **2001**, *29*, 397–406.

(34)   Menssen, A.; Hermeking, H. Characterization of the C-MYC-Regulated Transcriptome by SAGE: Identification and Analysis of C-MYC Target Genes. *Proceedings of the National Academy of Sciences of the United States of America* **2002**, *99*, 6274–6279.

(35)   Ruggero, D. The Role of Myc-Induced Protein Synthesis in Cancer. *Cancer Res* **2009**, *69*, 8839–8843.

(36)   Larsson, O.; Perlman, D. M.; Fan, D.; Reilly, C. S.; Peterson, M.; Dahlgren, C.; Liang, Z.; Li, S.; Polunovsky, V. A.; Wahlestedt, C.; et al. Apoptosis Resistance Downstream of eIF4E: Posttranscriptional Activation of an Anti-Apoptotic Transcript Carrying a Consensus Hairpin Structure. *Nucleic acids research* **2006**, *34*, 4375–4386.

(37)   Barna, M.; Pusic, A.; Zollo, O.; Costa, M.; Kondrashov, N.; Rego, E.; Rao, P. H.; Ruggero, D. Suppression of Myc Oncogenic Activity by Ribosomal Protein Haploinsufficiency. *Nature* **2008**, *456*, 971–975.

(38)   Wendel, H.-G.; Stanchina, E. de; Fridman, J. S.; Malina, A.; Ray, S.; Kogan, S.; Cordon-Cardo, C.; Pelletier, J.; Lowe, S. W. Survival Signalling by Akt and eIF4E in Oncogenesis and Cancer Therapy. *Nature* **2004**, *428*, 332–337.

(39)   Feldman, M. E.; Apsel, B.; Uotila, A.; Loewith, R.; Knight, Z. A.; Ruggero, D.; Shokat, K. M. Active-Site Inhibitors of mTOR Target Rapamycin-Resistant Outputs of mTORC1 and mTORC2. *PLOS Biol* **2009**, *7*, e38.

(40)   Ruggero, D.; Montanaro, L.; Ma, L.; Xu, W.; Londei, P.; Cordon-Cardo, C.; Pandolfi, P. P. The Translation Factor eIF-4E Promotes Tumor Formation and Cooperates with C-Myc in Lymphomagenesis. *Nat Med* **2004**, *10*, 484–486.

(41)   Holz, M. K.; Ballif, B. A.; Gygi, S. P.; Blenis, J. mTOR and S6K1 Mediate Assembly of the Translation Preinitiation Complex Through Dynamic Protein Interchange and Ordered Phosphorylation Events. *Cell* **2005**, *123*, 569–580.

(42)   Dennis, P. B.; Pullen, N.; Kozma, S. C.; Thomas, G. The Principal Rapamycin-Sensitive P70(S6k) Phosphorylation Sites, T-229 and T-389, Are Differentially Regulated by Rapamycin-Insensitive Kinase Kinases. *Mol Cell Biol* **1996**, *16*, 6242–6251.

(43)   Gingras, A. C.; Raught, B.; Sonenberg, N. eIF4 Initiation Factors: Effectors of mRNA Recruitment to Ribosomes and Regulators of Translation. *Annu Rev Biochem* **1999**, *68*, 913–963.

(44)   Haghighat, A.; Sonenberg, N. eIF4G Dramatically Enhances the Binding of eIF4E to the mRNA 5'-Cap Structure. *Journal of Biological Chemistry* **1997**, *272*, 21677–21680.

(45) Hara, K.; Yonezawa, K.; Kozlowski, M. T.; Sugimoto, T.; Andrabi, K.; Weng, Q. P.; Kasuga, M.; Nishimoto, I.; Avruch, J. Regulation of eIF-4E BP1 Phosphorylation by mTOR. *Journal of Biological Chemistry* **1997**, *272*, 26457–26463.

(46) van Riggelen, J.; Yetil, A.; Felsher, D. W. MYC as a Regulator of Ribosome Biogenesis and Protein Synthesis. *Nat Rev Cancer* **2010**, *10*, 301–309.

(47) Hsieh, A. C.; Costa, M.; Zollo, O.; Davis, C.; Feldman, M. E.; Testa, J. R.; Meyuhas, O.; Shokat, K. M.; Ruggero, D. Genetic Dissection of the Oncogenic mTOR Pathway Reveals Druggable Addiction to Translational Control via 4EBP-eIF4E. *Cancer Cell* **2010**, *17*, 249–261.

(48) Mainwaring, L. A.; Kenney, A. M. Divergent Functions for eIF4E and S6 Kinase by Sonic Hedgehog Mitogenic Signaling in the Developing Cerebellum. *Oncogene* **2011**.

(49) Chesler, L.; Schlieve, C.; Goldenberg, D. D.; Kenney, A.; Kim, G.; McMillan, A.; Matthay, K. K.; Rowitch, D.; Weiss, W. A. Inhibition of Phosphatidylinositol 3-Kinase Destabilizes Mycn Protein and Blocks Malignant Progression in Neuroblastoma. *Cancer Res* **2006**, *66*, 8139–8146.

(50) Chang, S. M.; Wen, P.; Cloughesy, T.; Greenberg, H.; Schiff, D.; Conrad, C.; Fink, K.; Robins, H. I.; De Angelis, L.; Raizer, J.; et al. Phase II Study of CCI-779 in Patients with Recurrent Glioblastoma Multiforme. *Invest New Drugs* **2005**, *23*, 357–361.

(51) Faivre, S.; Kroemer, G.; Raymond, E. Current Development of mTOR Inhibitors as Anticancer Agents. *Nat Rev Drug Discov* **2006**, *5*, 671–688.

(52) Galanis, E.; Buckner, J. C.; Maurer, M. J.; Kreisberg, J. I.; Ballman, K.; Boni, J.; Peralba, J. M.; Jenkins, R. B.; Dakhil, S. R.; Morton, R. F.; et al. Phase II Trial of Temsirolimus (CCI-779) in Recurrent Glioblastoma Multiforme: a North Central Cancer Treatment Group Study. *J. Clin. Oncol.* **2005**, *23*, 5294–5304.

(53) Josset, E.; Burckel, H.; Noël, G.; Bischoff, P. The mTOR Inhibitor RAD001 Potentiates Autophagic Cell Death Induced by Temozolomide in a Glioblastoma Cell Line. *Anticancer Res.* **2013**, *33*, 1845–1851.

(54) Hainsworth, J. D.; Shih, K. C.; Shepard, G. C.; Tillinghast, G. W.; Brinker, B. T.; Spigel, D. R. Phase II Study of Concurrent Radiation Therapy, Temozolomide, and Bevacizumab Followed by Bevacizumab/Everolimus as First-Line Treatment for Patients with Glioblastoma. *Clin Adv Hematol Oncol* **2012**, *10*, 240–246.

(55) Lassen, U.; Sorensen, M.; Gaziel, T. B.; Hasselbalch, B.; Poulsen, H. S. Phase II Study of Bevacizumab and Temsirolimus Combination Therapy for Recurrent Glioblastoma Multiforme. *Anticancer Res.* **2013**, *33*, 1657–1660.

(56) Puli, S.; Jain, A.; Lai, J. C. K.; Bhushan, A. Effect of Combination Treatment of Rapamycin and Isoflavones on mTOR Pathway in Human Glioblastoma (U87) Cells. *Neurochem. Res.* **2010**, *35*, 986–993.

(57) Chresta, C. M.; Davies, B. R.; Hickson, I.; Harding, T.; Cosulich, S.; Critchlow, S. E.; Vincent, J. P.; Ellston, R.; Jones, D.; Sini, P.; et al. AZD8055 Is a Potent, Selective, and Orally Bioavailable ATP-Competitive Mammalian Target of Rapamycin Kinase Inhibitor with in Vitro and in Vivo Antitumor Activity. *Cancer Res* **2010**, *70*, 288–298.

(58) Yu, K.; Shi, C.; Toral-Barza, L.; Lucas, J.; Shor, B.; Kim, J. E.; Zhang, W.-G.; Mahoney, R.; Gaydos, C.; Tardio, L.; et al. Beyond Rapalog Therapy: Preclinical Pharmacology and Antitumor Activity of WYE-125132, an ATP-Competitive and Specific Inhibitor of mTORC1 and mTORC2. *Cancer Res* **2010**, *70*, 621–631.

(59) Prasad, G.; Sottero, T.; Yang, X.; Mueller, S.; James, C. D.; Weiss, W. A.; Polley, M.-Y.; Ozawa, T.; Berger, M. S.; Aftab, D. T.; et al. Inhibition of PI3K/mTOR Pathways in Glioblastoma and Implications for Combination Therapy with Temozolomide. *Neuro-Oncology* **2011**, *13*, 384–392.

(60) Cerniglia, G. J.; Karar, J.; Tyagi, S.; Christofidou-Solomidou, M.; Rengan, R.; Koumenis, C.; Maity, A. Inhibition of Autophagy as a Strategy to Augment

Radiosensitization by the Dual Phosphatidylinositol 3-Kinase/Mammalian Target of Rapamycin Inhibitor NVP-BEZ235. *Mol. Pharmacol.* **2012**, *82*, 1230–1240.

(61)   Kuger, S.; Graus, D.; Brendtke, R.; Günther, N.; Katzer, A.; Lutyj, P.; Polat, B.; Chatterjee, M.; Sukhorukov, V. L.; Flentje, M.; et al. Radiosensitization of Glioblastoma Cell Lines by the Dual PI3K and mTOR Inhibitor NVP-BEZ235 Depends on Drug-Irradiation Schedule. *Transl Oncol* **2013**, *6*, 169–179.

(62)   Sunayama, J.; Sato, A.; Matsuda, K.-I.; Tachibana, K.; Suzuki, K.; Narita, Y.; Shibui, S.; Sakurada, K.; Kayama, T.; Tomiyama, A.; et al. Dual Blocking of mTor and PI3K Elicits a Prodifferentiation Effect on Glioblastoma Stem-Like Cells. *Neuro-Oncology* **2010**, *12*, 1205–1219.

(63)   Mueller, S.; Phillips, J.; Onar-Thomas, A.; Romero, E.; Zheng, S.; Wiencke, J. K.; McBride, S. M.; Cowdrey, C.; Prados, M. D.; Weiss, W. A.; et al. PTEN Promoter Methylation and Activation of the PI3K/Akt/mTOR Pathway in Pediatric Gliomas and Influence on Clinical Outcome. *Neuro-Oncology* **2012**, *14*, 1146–1152.

(64)   Ellison, D. W.; Kocak, M.; Dalton, J.; Megahed, H.; Lusher, M. E.; Ryan, S. L.; Zhao, W.; Nicholson, S. L.; Taylor, R. E.; Bailey, S.; et al. Definition of Disease-Risk Stratification Groups in Childhood Medulloblastoma Using Combined Clinical, Pathologic, and Molecular Variables. *J. Clin. Oncol.* **2011**, *29*, 1400–1407.

(65)   Pócza, T.; Sebestyén, A.; Turányi, E.; Krenács, T.; Márk, Á.; Sticz, T. B.; Jakab, Z.; Hauser, P. mTOR Pathway as a Potential Target in a Subset of Human Medulloblastoma. *Pathol. Oncol. Res.* **2014**.

(66)   Chanthery, Y. H.; Gustafson, W. C.; Itsara, M.; Persson, A.; Hackett, C. S.; Grimmer, M.; Charron, E.; Yakovenko, S.; Kim, G.; Matthay, K. K.; et al. Paracrine Signaling Through MYCN Enhances Tumor-Vascular Interactions in Neuroblastoma. *Sci Transl Med* **2012**, *4*, 115ra3.

It is the policy of the University to encourage the distribution of all theses, dissertations, and manuscripts. Copies of all UCSF theses, dissertations, and manuscripts will be routed to the library via the Graduate Division. The library will make all theses, dissertations, and manuscripts accessible to the public and will preserve these to the best of their abilities, in perpetuity.

I hereby grant permission to the Graduate Division of the University of California, San Francisco to release copies of my thesis, dissertation, or manuscript to the Campus Library to provide access and preservation, in whole or in part, in perpetuity.

Author Signature_____ Date __6/5/2014__

92